

Experimental Kinetics Studies of Gas Phase Halogen Reactions Involved in Stratospheric Ozone Depletion

by

Jennifer Beth Lipson

A.B. Chemistry
Harvard University, 1994


Submitted to the Department of Chemistry
in Partial Fulfillment of the Requirements for the Degree of

Doctor of Philosophy in Chemistry
at the
Massachusetts Institute of Technology


June, 1999

© Massachusetts Institute of Technology, 1999. All Rights Reserved.

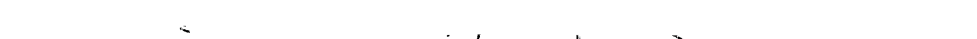
Signature of the Author


Department of Chemistry
May 14, 1999

Certified by


Mario J. Molina
Institute Professor
Thesis Supervisor

Accepted by


Dietmar Seyferth
Chairman
Departmental Committee on Graduate Students

This doctoral thesis has been examined by a Committee of the Department of Chemistry as follows:



Professor Jeffrey I. Steinfeld  _____ Chairman

Professor Mario J. Molina  _____ Thesis Supervisor

Professor Ronald G. Prinn _____
Department of Earth, Atmospheric and Planetary Sciences

Experimental Kinetics Studies of Gas Phase Halogen Reactions Involved in Stratospheric Ozone Depletion

by

Jennifer Beth Lipson

Submitted to the Department of Chemistry on May 14, 1999
in partial fulfillment of the requirements for the
Degree of Doctor of Philosophy in Chemistry

ABSTRACT

The kinetics of several important gas phase halogen reactions involved in stratospheric ozone depletion have been investigated using the turbulent flow tube technique coupled with high pressure chemical ionization mass spectrometry. In order to create accurate models of ozone depletion, it is critical to have accurate measurements of the rate constants of the reactions that control the partitioning of chlorine and bromine in the stratosphere. Attempts to model midlatitude ozone depletion have tended to underestimate ozone depletion below 30 km and overestimate ozone depletion above 35 km. Discrepancies between measured and modeled ozone may be due to uncertainties in the laboratory-measured rate constants or due to missing chemistry in the models.

The $\text{HO}_2 + \text{BrO}$ reaction is a rate-limiting step in an important catalytic cycle involved in stratospheric ozone depletion. A study of the temperature dependence of the overall rate constant of the $\text{HO}_2 + \text{BrO}$ reaction has been conducted at pressures near 100 Torr and at a range of temperatures extending to those found in the lower stratosphere. The $\text{OH} + \text{ClO}$ reaction has long been proposed as a potential source of stratospheric HCl. A study of the kinetics of this reaction has been conducted at pressures between 100 and 200 Torr and at a range of temperatures extending to those found in the lower stratosphere. These experiments provide the first direct evidence of HCl production from the $\text{OH} + \text{ClO}$ reaction, and measurements of the branching ratio demonstrate that this channel is kinetically accessible under stratospheric conditions. These measurements have helped to resolve a long-standing discrepancy between measured and modeled chlorine partitioning in the upper stratosphere. Preliminary work on the $\text{HO}_2 + \text{ClO}$ reaction has also been carried out. Similar to the analogous bromine reaction, this reaction also participates in an important catalytic cycle involved in stratospheric ozone depletion. Overall, the experiments presented in this thesis should help to improve modeling of stratospheric ozone by elucidating some important missing chemistry and by placing more stringent constraints on the partitioning of chlorine and bromine in the stratosphere.

Thesis Supervisor: Mario J. Molina

Title: Institute Professor

Table of Contents

Acknowledgements	6
Chapter 1: Introduction	8
1.1 Research Motivation	8
1.2 Overview of Experimental Technique	11
1.2.1 Turbulent Flow Tube Technique	11
1.2.2 Chemical Ionization Mass Spectrometry	14
1.3 Thesis Outline	15
References for Chapter 1	17
Chapter 2: Kinetics of the HO₂ + BrO Reaction: Measurements of the Overall Rate Constant	19
2.1 Introduction	19
2.2 Experimental Section	22
2.2.1 Radical Production	24
2.2.2 Detection of Reactants and Products	28
2.3 Results and Discussion	30
2.4 Conclusions	38
References for Chapter 2	39
Chapter 3: Kinetics of the OH + ClO Reaction: Measurements of the Overall Rate Constant and Preliminary Branching Ratio Experiments	42
3.1 Introduction	42
3.2 Experimental Section	45
3.2.1 Radical Production: Overall Rate Constant Measurements	47
3.2.2 Radical Production: Branching Ratio Experiments	52
3.2.3 Detection of Reactants and Products	54
3.3 Results and Discussion	56
3.3.1 Overall Rate Constant Measurements	57

3.3.2	Branching Ratio Experiments	65
3.4	Conclusions	76
	References for Chapter 3	77
Chapter 4:	Kinetics of the OH + ClO Reaction: Measurements of the Branching Ratio	81
4.1	Introduction	81
4.2	Experimental Section	83
4.2.1	Radical Production	85
4.2.2	Detection of Reactants and Products	94
4.3	Results and Discussion	96
4.3.1	Branching Ratio Experiments	96
4.3.2	Statistical Rate Theory Calculations	109
4.4	Conclusions	125
	References for Chapter 4	126
Chapter 5:	Kinetics of the HO₂ + ClO Reaction: Current Research	130
5.1	Introduction	130
5.2	Experimental Section	132
5.2.1	Radical Production	134
5.2.2	Detection of Reactants and Products	141
5.3	Preliminary Results and Discussion	142
5.3.1	Overall Rate Constant Measurements.....	142
5.3.2	Branching Ratio Experiments.....	146
5.4	Preliminary Conclusions	149
	References for Chapter 5	150
Chapter 6:	Conclusions and Future Directions	151

Acknowledgements

First, I would like to thank my research advisor, Mario Molina, for his guidance and support during my doctoral research. I have learned a great deal through my interactions with him, and I appreciate his patience and kindness.

I would also like to thank Steven Wofsy, my undergraduate research advisor at Harvard University, for introducing me to the field of atmospheric chemistry. My experience in his laboratory inspired me to apply to graduate school. In lab, I really enjoyed working with Kristie Boering, and I am thankful for her encouragement and advice.

Next, I would like to thank Matt Elrod. I am really grateful that I had the opportunity to work with Matt during my first year in lab at M.I.T. I really benefited from his knowledge and research expertise. He showed me that sweat and hard work will eventually bring back good results. I especially want to thank him for always being willing to answer my questions, even after leaving M.I.T. He is a great researcher, teacher and friend.

In addition to Matt, there are several other people that I have worked with closely during my time at M.I.T.: I would like to thank Thomas Beiderhase for his contributions to the OH + ClO experiments. Thanks also go to Janelle Brown, a very helpful undergraduate research student. Next, I would like to thank Matthias Olzmann for his work on the OH + ClO theoretical calculations. Extra thanks goes to Thomas Beiderhase for initiating this fruitful collaboration. Finally, I would like to thank Raenell Soller for her assistance with the most recent experiments.

Although I didn't have the chance to work with them directly, I would like to thank John Jayne and John Seeley for their pioneering work on the turbulent flow tube technique. I especially want to thank John Seeley for encouraging me to present my research, and John Jayne for his helpful comments before my presentation at the NASA AEAP conference.

Within the Molina group, there are many other people who have been helpful and supportive during the last five years. First, I would like to thank the people who always kept me smiling: In the early days there was Danna Leard, Matt Elrod, Roger Meads and Paul Wooldridge. Thanks especially to Danna for fun times watching TV and playing ice hockey. More recently, there have been people such as Carl Percival, Geoff Smith and Keith Broekhuizen. A special thanks goes to Keith for helping me with my experiments during his first summer in lab. Also, thanks to Keith and Geoff for being faithful lunch buddies, and especially for making me feel "extra special" on my birthday last year. Even though I'm not going very far, I will miss you guys a lot.

There are many other Molina group members who have been friendly and helpful over the years. Thanks especially to Manjula Canagaratna, Ulrich Poschl, Thomas Koop,

Markus Haider, Lukas Gutzwiller, Telma Castro and Dara Salcedo. A special thanks to Martin Hunter for his help and advice during my search for a postdoctoral position. Next, I would like to thank Luisa Molina for all her help over the last five years. Her experience is a great asset to the laboratory. Also, thanks to the many people who have provided administrative and technical support over the years: Linda Kubrick, Mark Pendleton and Leonard Newton, just to name a few.

I would like to thank Professor Jeffrey Steinfeld very much for coordinating the Environmental Chemistry Seminar and Traineeship. I really enjoyed taking part in this seminar, and I am very grateful for the financial support offered by this program. I am also glad that I had the opportunity to work more closely with Professor Steinfeld as a teaching assistant for his courses on atmospheric chemistry and chemical kinetics.

Next, I want to thank Matt Berger for his love and support over my five years at M.I.T. I especially thank him for all the little things like picking me up those many nights at lab and coming to all my ice hockey games. Through the good and the bad, he has been my rock.

Finally, I would like to thank my family. I could not have come this far without the love and encouragement of my mom, dad and sister. Thanks to my mom for being a source of inspiration. Thanks to my sister for her advice and help over the years. Thanks to my dad for encouraging me to achieve my goals. Also, thanks to my grandma and uncle for their support. I am really grateful to have such a caring family.

Chapter 1: Introduction

1.1 Research Motivation

Stratospheric ozone depletion is an important environmental problem and a major area of research in the field of atmospheric chemistry. Stratospheric ozone shields the earth from harmful ultraviolet radiation. The theory that anthropogenic chlorine compounds such as chlorofluorocarbons (CFCs) could cause stratospheric ozone depletion was first proposed by *Molina and Rowland* [1974]. Unlike most pollutants, CFCs are not readily broken down in the troposphere because they are insoluble in water and have slow rates of reaction with OH. As a result, CFCs have very long atmospheric lifetimes on the order of tens to hundreds of years [*Wayne*, 1991]. These extremely stable compounds are eventually transported to the stratosphere, where they are broken down by ultraviolet radiation. The active chlorine atoms released by the CFCs can participate in catalytic cycles that destroy ozone. One chlorine atom can lead to the destruction of hundreds of thousands of ozone molecules. Similar to chlorine, bromine also has the potential to cause significant ozone depletion in the stratosphere. Anthropogenic sources of bromine include methyl bromide, used for agricultural fumigation, and the halons, used for fire retardation.

The most dramatic example of ozone depletion is the annually occurring “ozone hole” over Antarctica during the Austral spring, first reported by *Farman et al.* [1985]. However, significant depletion of ozone, as much as 5% per decade since the mid-1970's, has also been observed over midlatitudes in both the Northern and Southern Hemispheres [*Stolarski et al.*, 1991; *Stolarski et al.*, 1992; *DeLuisi et al.*, 1994; *Tourpali et al.*, 1997]. Although a great deal of progress has been made, there are still many uncertainties about the mechanisms of midlatitude ozone depletion. Attempts to model midlatitude ozone depletion have tended to underestimate ozone depletion below 30 km and overestimate ozone depletion above 35 km [*McElroy and Salawitch*, 1989]. Discrepancies between

measured and modeled ozone may be due to missing chemistry in the models or due to an incomplete understanding of the partitioning of species that destroy stratospheric ozone, such as chlorine and bromine.

In the stratosphere, chlorine and bromine are present in active forms (e.g., Cl, ClO, Br, BrO) that participate in catalytic ozone depletion cycles and inactive forms (e.g., HCl, ClONO₂, HBr, BrONO₂). These inactive forms are relatively stable compounds that serve as temporary reservoirs for chlorine and bromine. HCl and HBr are particularly stable molecules, and so these long-lived species can diffuse back into the troposphere where rain-out creates a permanent sink for stratospheric chlorine or bromine [*Wallace et al.*, 1997]. Chemical reactions that convert active chlorine or bromine into inactive forms are chain-terminating steps in catalytic ozone depletion cycles.

Attempts to model stratospheric ozone levels have consistently overestimated the amount of active chlorine and bromine in the upper stratosphere. The models have also tended to overpredict ozone loss rates above 35 km [e.g., *Brasseur et al.*, 1985; *McElroy and Salawitch*, 1989]. This long-standing “ozone deficit” problem may be the result of errors in the calculated halogen partitioning. A number of studies have suggested that discrepancies between measured and calculated halogen partitioning are due to missing chemistry in the models. These studies propose that reactions such as OH + ClO, HO₂ + ClO, OH + BrO and HO₂ + BrO could have thermodynamically feasible minor channels that produce HCl or HBr [e.g., *Toumi and Bekki*, 1993; *Chance et al.*, 1996; *Chartrand and McConnell*, 1998]. The formation of HCl or HBr is a chain-terminating step in catalytic ozone depletion cycles. Therefore, even relatively small branching ratios could have a large impact on modeled halogen partitioning. Unfortunately, laboratory measurements have been unable to definitively measure HCl or HBr production from these reactions due to limitations of the experimental techniques used or due to large uncertainties in the results.

In order to create accurate models of stratospheric ozone depletion, it is critical to have accurate measurements of the rates of the reactions that control the partitioning of chlorine and bromine in the stratosphere. As pointed out by *Wennberg et al.* [1994] and *Fish and Burton* [1997], the interpretation of field measurements and the development of atmospheric models have been hindered by uncertainties in the laboratory-measured rate constants. These uncertainties are largely due to the fact that many of the studies have not been conducted under pressure and temperature conditions characteristic of the stratosphere. Many important atmospheric reactions have only been investigated at moderate temperatures and low pressures due to limitations inherent in the conventional discharge laminar flow tube technique. As a result, it has been necessary to use extrapolations to predict the behavior of these reactions under stratospheric conditions. However, recent discoveries have shown that many gas phase bimolecular reactions involving free radicals exhibit complex dependencies on temperature and pressure. Reactions such as $\text{HO}_2 + \text{BrO}$ and $\text{OH} + \text{ClO}$ are believed to proceed through the formation of an intermediate complex that is stabilized at low temperatures. Intermediate complex formation can also be collisionally stabilized at high pressures. Thus, many of these bimolecular reactions have a negative activation energy and a dependence on total pressure [*Mozurkewich and Benson*, 1984; *Troe*, 1994]. In some reactions, new product channels may become accessible under temperature and pressure conditions that favor complex formation.

This thesis will present experimental kinetics studies of several important gas phase halogen reactions involved in stratospheric ozone depletion. The experiments have been conducted under pressure and temperature conditions characteristic of the stratosphere using the turbulent flow tube technique coupled with chemical ionization mass spectrometry detection. These studies should help to improve modeling of stratospheric ozone by elucidating some important missing chemistry and by placing more stringent constraints on the partitioning of chlorine and bromine in the stratosphere.

1.2 Overview of Experimental Technique

1.2.1 Turbulent Flow Tube Technique

Previous work done in our laboratory has demonstrated that the turbulent flow tube technique can be used to determine the rate constants of gas phase bimolecular reactions under a wide range of pressures and temperatures [Seeley *et al.*, 1993; Seeley, 1994; Seeley *et al.*, 1996a]. Previous work has further shown that coupling the turbulent flow technique with high pressure chemical ionization mass spectrometry detection is an excellent method for studying radical-radical reactions with high sensitivity [Seeley *et al.*, 1996b].

The general principle of the flow tube technique is that the chemical removal of reactants is equally balanced by reactant transport, such that the concentrations of all the species are at steady state. (For a general review of flow tube techniques, see for example Howard, [1979].) A schematic diagram of a flow tube system is presented in Figure 1.

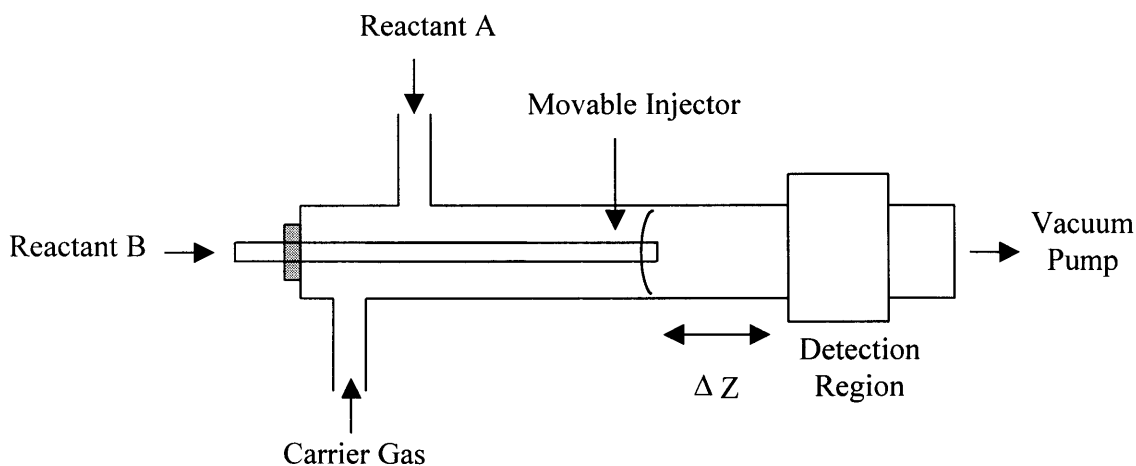


Figure 1. Schematic diagram of a discharge flow system for the study of the general reaction $A + B \rightarrow \text{products}$.

In a typical flow tube experiment, one reactant is introduced through a side arm, and the other is introduced through a movable injector. The main flow of carrier gas, usually N₂, He or Ar, is injected at the rear of the flow tube, and a vacuum pump at the front of the flow tube creates the motion of the gases. Because the system is at steady state, kinetic information can be obtained by changing the reaction time between reactants by changing the position of the movable injector. In order to accurately define the reaction time, the velocity profile of the gas must be known. If the velocity profile is flat, it can be assumed that every molecule travels at the average velocity (u_{ave}) of the gas. This condition is called plug flow, and it greatly simplifies the procedure for determining the rate constant. For a bimolecular reaction under plug flow and pseudo-first-order conditions, the continuity equation for the limiting reagent (A) becomes:

$$-u_{ave} (d[A]/dz) - k^1[A] = 0$$

As a result, the rate constant of the reaction can be determined by following the decay of the limiting reagent as a function of axial injector position (z). The concentration of the excess reagent must be known, and the experiment must be repeated for several different excess reagent concentrations.

Most kinetic flow tube experiments have been performed under laminar flow conditions. (For a general review of fluid dynamics, see for example *Fahien*, [1983].) Laminar flow is characterized by a Reynolds number less than 2000. The Reynolds number is defined as:

$$\text{Re} = \frac{2 a u_{ave} \rho}{\mu}$$

where a is the internal radius of the flow tube, u_{ave} is the average velocity of the gas, ρ is the density of the gas, and μ is the viscosity of the gas. However, the plug flow condition places strong constraints on the temperature and pressure conditions accessible by the conventional discharge laminar flow tube technique. The plug flow requirement limits conventional laminar flow tube studies to pressures lower than 10 Torr [Howard, 1979]. This limitation is due to the fact that laminar flow has a very peaked velocity profile. Within the laminar flow regime, molecular diffusion is the sole mechanism for reactant mixing. The rate of transport via molecular diffusion is essentially inversely proportional to the total pressure. At low pressures, molecular diffusion is rapid enough that each molecule samples many different radial positions. As a result, each molecule effectively travels at the average velocity, and therefore the plug flow approximation is valid for low pressure laminar flow conditions. However, increased molecular diffusion at low pressures also leads to increased diffusion to the walls of the flow tube. For low pressure laminar flow, the loss of reactive species, such as radicals, to the flow tube walls becomes prohibitive at temperatures below 230 K. In theory, kinetics experiments can be conducted under high pressure laminar flow conditions if u_{ave} and $[A]$ (limiting reagent) can be determined experimentally as functions of radial and axial position. Rate constants can then be determined by plugging u_{ave} and $[A]$ into the continuity equation and numerically solving for k . This approach to experimental flow tube kinetics has been developed by Abbott *et al.* [1990], although the complexity of this technique may limit its applicability.

Development work done in our laboratory has shown that turbulent flow is a feasible technique for kinetics flow tube studies [Seeley *et al.*, 1993; Seeley, 1994]. Turbulent flow is generally characterized by a Reynolds number greater than 2000. Under turbulent flow conditions, mixing occurs mainly by eddy diffusion. Turbulent flow is characterized by the development of a turbulent core and a laminar sublayer near the walls of the flow tube. Within the turbulent core, the velocity profile of the gas is

essentially flat, and the plug flow approximation is found to be valid to within ~10%. At high pressures, the rate of molecular diffusion across the laminar sublayer at the flow tube walls is slow. As a result, wall reactions in high pressure turbulent flow are greatly reduced compared to low pressure laminar flow. The reduction of wall loss greatly extends the temperature range accessible by turbulent flow tube studies. The high pressure turbulent flow tube technique can be used to study atmospheric reactions at pressures ranging from 50 to 760 Torr and at temperatures as low as 180 K.

1.2.2 Chemical Ionization Mass Spectrometry

Many kinetics studies of atmospheric reactions have used electron impact mass spectrometry (EIMS) for the detection of reactants and products. In general, mass spectrometry has the advantage of being able to detect a wide range of species compared to other commonly used optical detection techniques such as laser induced fluorescence. However, EIMS does not have as good sensitivity as some of these other techniques. Furthermore, the high energy electrons used for ionization in EIMS can also cause fragmentation, resulting in non-unique mass peaks.

Development work done in our laboratory has shown that high pressure chemical ionization does not cause fragmentation and greatly improves detection sensitivity compared to EIMS (by as much as 3 orders of magnitude) [Seeley *et al.*, 1996b]. The improved sensitivity is due to the fact that chemical ionization is possible at high pressures, whereas high vacuum conditions are necessary for electron impact ionization. The advantage of ionizing at high pressure is that the ions can be focused by electrostatic lenses at each pumping stage. Therefore, the ion content of the gas is enriched at each pumping stage as the gas enters the quadrupole mass spectrometer. SF_6^- was chosen as a reagent ion because it has fast rates of reaction with a wide range of atmospherically relevant molecules. Chemical ionization of neutrals by SF_6^- usually occurs through either charge-transfer reactions or fluoride ion-transfer reactions.

The versatility and high sensitivity of chemical ionization make it an excellent detection technique for searching for possible minor product channels from reactions such as OH + ClO. Chemical ionization mass spectrometry coupled with the turbulent flow technique is a powerful tool for studying the kinetics of atmospheric reactions over a wide range of pressures and temperatures, including conditions characteristic of the stratosphere.

1.3 Thesis Outline

This thesis will present experimental kinetics studies of several important gas phase halogen reactions involved in stratospheric ozone depletion. Chapter 2 describes measurements of the temperature dependence of the overall rate constant for the HO₂ + BrO reaction. This reaction is a rate-limiting step in one of the important ozone depletion catalytic cycles. Uncertainties in previous rate constant measurements for the HO₂ + BrO reaction are a significant source of error in the modeling of midlatitude stratospheric ozone depletion [*Fish and Burton, 1997*].

Chapter 3 describes the results of kinetics experiments on the OH + ClO reaction. This reaction has long been proposed as a potential source of missing HCl in stratospheric models [e.g., *Toumi and Bekki, 1993; Chance et al., 1996*]. However, previous branching ratio studies have been unable to positively establish the existence of a minor channel to form HCl. In Chapter 3, measurements of the overall rate constant for the OH + ClO reaction are reported, and initial branching ratio experiments are presented. The preliminary branching ratio experiments were conducted using OD instead of OH, due to the large experimental background of HCl in the system. These measurements provide the first direct evidence of a minor channel to form DCl.

Chapter 4 discusses efforts to reduce the HCl background level in the system and describes improvements to the experimental set-up. HCl production from the minor channel of the OH + ClO reaction is positively identified, and measurements of the

branching ratio are reported. The temperature and pressure dependencies of the branching ratio are also investigated. The experimental results are compared with statistical rate theory calculations for the OH + ClO reaction. The implications of the results for models of stratospheric ozone depletion are also discussed.

Chapter 5 presents preliminary results from current research on the HO₂ + ClO reaction. Similar to the analogous bromine reaction, the HO₂ + ClO reaction is a rate-limiting step in one of the important catalytic cycles involved in ozone depletion. The temperature dependence of the rate constant for this reaction is not well known.

The experimental kinetics studies presented in this thesis should help to improve modeling of stratospheric ozone by elucidating some important missing chemistry and by placing more stringent constraints on the partitioning of chlorine and bromine in the stratosphere. Hopefully, these studies will contribute not only to a better understanding of the homogeneous mechanisms of ozone depletion, but also to a better understanding of complex-mode radical reactions.

References for Chapter 1

Abbatt, J. P. D., K. L. Demerjian, and J. G. Anderson, A new approach to free radical kinetics: radially and axially resolved high-pressure discharge flow with results for OH + C₂H₆, C₃H₈, n-C₄H₁₀, n-C₅H₁₂ → products at 297 K, *J. Phys. Chem.*, *94*, 4566, 1990.

Brasseur, G., A. De Rudder, and C. Tricot, Stratospheric response to chemical perturbations, *J. Atmos. Chem.*, *3*, 261, 1985.

Chance, K. V., W. A. Traub, D. G. Johnson, K. W. Jucks, P. Ciarpallini, R. A. Stachnik, R. J. Salawitch, and H. A. Michelsen, Simultaneous measurements of stratospheric HO_x, NO_x, and Cl_x: Comparison with a photochemical model, *J. Geophys. Res.*, *101*, 9031, 1996.

Chartrand, D. J., and J. C. McConnell, Evidence for HBr production due to minor channel branching at mid-latitudes, *Geophys. Res. Lett.*, *25*, 55, 1998.

DeLuisi, J. J., C. L. Mateer, D. Theisen, P. K. Bhartia, D. Longenecker, and B. Chu, Northern middle-latitude ozone profile features and trends observed by SBUV and Umkehr, 1979-1990, *J. Geophys. Res.*, *99*, 18901, 1994.

Fahien, R. W., *Fundamentals of Transport Phenomena*, McGraw-Hill, New York, 1983.

Farman, J. C., B. G. Gardiner, and J. D. Shanklin, Large losses of total ozone in Antarctic reveal seasonal ClO_x/NO_x interaction, *Nature*, *315*, 207, 1985.

Fish, D. J., and M. R. Burton, The effect of uncertainties in kinetic and photochemical data on model predictions of stratospheric ozone depletion, *J. Geophys. Res.*, *102*, 25537, 1997.

Howard, C. J., Kinetic measurements using flow tubes, *J. Phys. Chem.*, *83*, 3, 1979.

McElroy, M. B., and R. J. Salawitch, Changing composition of the global stratosphere, *Science*, *243*, 763, 1989.

Molina, M. J., and F. S. Rowland, Stratospheric sink for chlorofluoromethanes: Chlorine atom-catalysed destruction of ozone, *Nature*, *249*, 810, 1974.

Mozurkewich, M., and S. W. Benson, Negative activation energies and curved Arrhenius plots. 1. Theory of reactions over potential wells, *J. Phys. Chem.*, *88*, 6429, 1984.

Seeley, J. V., J. T. Jayne, and M. J. Molina, High pressure fast-flow technique for gas phase kinetics studies, *Int. J. Chem. Kinet.*, *25*, 571, 1993.

Seeley, J. V., *Experimental Studies of Gas Phase Reactions Using the Turbulent Flow Tube Technique*, Ph. D. Thesis, Massachusetts Institute of Technology, 1994.

Seeley, J. V., J. T. Jayne, and M. J. Molina, Kinetic studies of chlorine atom reactions using the turbulent flow tube technique, *J. Phys. Chem.*, *100*, 4019, 1996a.

Seeley, J. V., R. F. Meads, M. J. Elrod, and M. J. Molina, Temperature and pressure dependence of the rate constant for the HO₂ + NO reaction, *J. Phys. Chem.*, *100*, 4026, 1996b.

Stolarski, R. S., P. Bloomfield, R. D. McPeters, and J. R. Herman, Total ozone trends deduced from Nimbus 7 TOMS data, *Geophys. Res. Lett.*, *18*, 1015, 1991.

Stolarski, R. S., R. Bojkov, L. Bishop, C. Zerefos, J. Staehelin, and J. Zawodny, Measured trends in stratospheric ozone, *Science*, *256*, 342, 1992.

Toumi, R., and S. Bekki, The importance of the reactions between OH and ClO for stratospheric ozone, *Geophys. Res. Lett.*, *20*, 2447, 1993.

Tourpali, K., X. X. Tie, C. S. Zerefos, and G. Brasseur, Decadal evolution of total ozone decline: Observations and model results, *J. Geophys. Res.*, *102*, 23955, 1997.

Troe, J., The colourful world of complex-forming bimolecular reactions, *J. Chem. Soc., Faraday Trans.*, *90*, 2303, 1994.

Wallace, L., W. Livingston, and D. N. B. Hall, A twenty-five year record of stratospheric hydrogen chloride, *Geophys. Res. Lett.*, *24*, 2363, 1997.

Wayne, R. P., *Chemistry of Atmospheres*, 2nd ed., Oxford University Press, New York, 1991.

Wennberg, P. O., R. C. Cohen, R. M. Stimpfle, J. P. Koplw, J. G. Anderson, R. J. Salawitch, D. W. Fahey, E. L. Woodbridge, E. R. Keim, R. S. Gao, C. R. Webster, R. D. May, D. W. Toohey, L. M. Avallone, M. H. Proffitt, M. Loewenstein, J. R. Podolske, K. R. Chan, and S. C. Wofsy, Removal of stratospheric O₃ by radicals: In situ measurements of OH, HO₂, NO, NO₂, ClO and BrO, *Science*, *266*, 398, 1994.

Chapter 2: Kinetics of the HO₂ + BrO Reaction: Measurements of the Overall Rate Constant

2.1 Introduction

Similar to chlorine, bromine can participate in catalytic cycles that deplete stratospheric ozone. Anthropogenic sources of bromine include methyl bromide (CH₃Br), used for agricultural fumigation, and the halons (CBrF₃, CBrClF₂, C₂Br₂F₄), used for fire retardation. Despite an international ban on the production and sale of halons in developed nations in 1994, tropospheric concentrations of many halons have continued to increase in recent years [Butler *et al.*, 1998]. The increase in emissions suggests that halon reserves are continuing to be used, presumably due to a lack of suitable alternative fire extinguishants. Production of methyl bromide in developed nations is due to be phased out by the year 2005, although current legislation in the United States allows for continued production of small amounts of methyl bromide after 2005 for critical agricultural uses.

Increased loading of bromine in the atmosphere is a significant concern because of the very high efficiency of bromine in destroying stratospheric ozone. Although bromine is approximately 2 orders of magnitude less abundant than chlorine in the stratosphere, bromine is believed to be up to 80 times more efficient than chlorine on a per atom basis in catalyzing ozone depletion. The greater efficiency of bromine is due to the fact that the bromine reservoir species (HBr, BrONO₂) are less stable than the analogous chlorine reservoir species [McElroy and Salawitch, 1989]. As a result, bromine is much more likely to be present in its active forms (Br, BrO) than chlorine. For example, Lary [1996] estimates that BrO makes up 40% of inorganic bromine at 20 km and as much as 75% of inorganic bromine at 40 km. The increased efficiency of bromine compared to chlorine is also due to the fact that bromine is capable of extracting hydrogen from only a few minor stratospheric species such as HO₂ and CH₂O [Wofsy *et al.*, 1975]. Hydrogen extraction to

form HBr or HCl is an important chain-terminating step in catalytic ozone depletion cycles. In contrast to bromine, chlorine readily reacts with atmospherically abundant CH₄ to produce HCl. The rate constant for the reaction of Cl with CH₄ is more than 10 orders of magnitude greater than the rate constant for the reaction of Br with CH₄ [*DeMore et al.*, 1997; *Mallard et al.*, 1994].

In 1980, *Yung et al.* proposed that the power of bromine compounds to destroy ozone could be enhanced by the following synergistic cycle with chlorine:



It has been estimated that such chemistry involving bromine species is responsible for ~25% of the ozone loss observed during the Antarctic ozone hole event [*Anderson et al.*, 1991], and up to 40% of the loss over the Arctic in winter [*Salawitch et al.*, 1990].

In 1980, another catalytic cycle involving bromine was also proposed:



This cycle was originally dismissed as unimportant because the rate constant for reaction 4 (based on the first kinetic study of that reaction by *Cox and Sheppard* [1982]) was too slow in the atmosphere to contribute significantly to ozone depletion [*Yung et al.*, 1980]. However, more recent experimental results have suggested that reaction 4 proceeds at a substantially faster rate than had been indicated by previous measurements, and may indeed play a major role in bromine-catalyzed ozone depletion chemistry [*Poulet et al.*, 1992; *Hayman et al.*, 1992; *Bridier et al.*, 1993; *Larichev et al.*, 1995; *Li et al.*, 1997; *Cronkhite et al.*, 1998]. For example, model calculations performed by *Poulet et al.* indicated an increase from 1.14 to 1.45% column ozone loss at midlatitudes from bromine compounds alone when they included their faster rate constant measurement in the model. However, a consensus has not yet been achieved for the room temperature rate constant or the temperature dependence of the rate constant for the HO₂ + BrO reaction. Uncertainties in previous rate constant measurements for the HO₂ + BrO reaction are a significant source of error in the modeling of midlatitude stratospheric ozone depletion [*Fish and Burton*, 1997].

Although the main products of the HO₂ + BrO reaction are HOBr and O₂, reaction 4 might also proceed via a second channel which is thermodynamically feasible ($\Delta H = -7.7$ kcal mol⁻¹):



The only two laboratory studies of reaction 4b have placed small upper limits (< 2%) on this channel [*Mellouki et al.*, 1994; *Larichev et al.*, 1995]. However, since reaction 4b is a chain-terminating step, even a relatively small branching ratio would have a large impact on stratospheric bromine partitioning. A recent modeling study by *Lary* [1996] proposed that a branching ratio of only 1% would make reaction 4b the dominant source

of HBr in the lower stratosphere. Another recent modeling study by *Chartrand and McConnell* [1998] found that including a 1-2% branching ratio for the $\text{HO}_2 + \text{BrO}$ reaction significantly improved the agreement between measured and calculated mixing ratios of HBr at northern midlatitudes. Although reaction 4b represents a possible missing source of HBr in current models, other solutions have also been proposed. For example, the $\text{OH} + \text{BrO}$ reaction could also have a thermodynamically feasible minor channel to produce HBr. A modeling study by *Chipperfield et al.* [1997] found that including a 1-2% branching ratio for the $\text{OH} + \text{BrO}$ reaction improved the agreement between measured and calculated mixing ratios of HBr at northern midlatitudes. The $\text{OH} + \text{BrO}$ reaction will be mentioned in more detail in Chapter 4 when branching ratio experiments for the $\text{OH} + \text{ClO}$ reaction are discussed.

In this chapter, a study of the temperature dependence of the overall rate constant for the $\text{HO}_2 + \text{BrO}$ reaction will be presented. These experiments were conducted at pressures near 100 Torr and at a range of temperatures extending to those found in the lower stratosphere using a turbulent flow tube coupled to a high pressure chemical ionization mass spectrometer. Previous experiments in our laboratory have shown that the turbulent flow tube technique can be used to accurately determine the rate constants of reactions at pressures ranging from 50 to 760 Torr and at temperatures as low as 180 K [*Seeley et al.*, 1993; *Seeley et al.*, 1996a]. Similar to the previous study of $\text{HO}_2 + \text{NO}$ from our laboratory [*Seeley et al.*, 1996b], high pressure chemical ionization mass spectrometry was used to detect many species relevant to the $\text{HO}_2 + \text{BrO}$ reaction with high sensitivity.

2.2 Experimental Section

A schematic diagram of the experimental apparatus is presented in Figure 1. The flow tube was constructed with 2.2 cm i.d. Pyrex tubing, coated with Halocarbon wax, and was 120 cm in total length. A large flow of nitrogen carrier gas ($\sim 50 \text{ STP L min}^{-1}$)

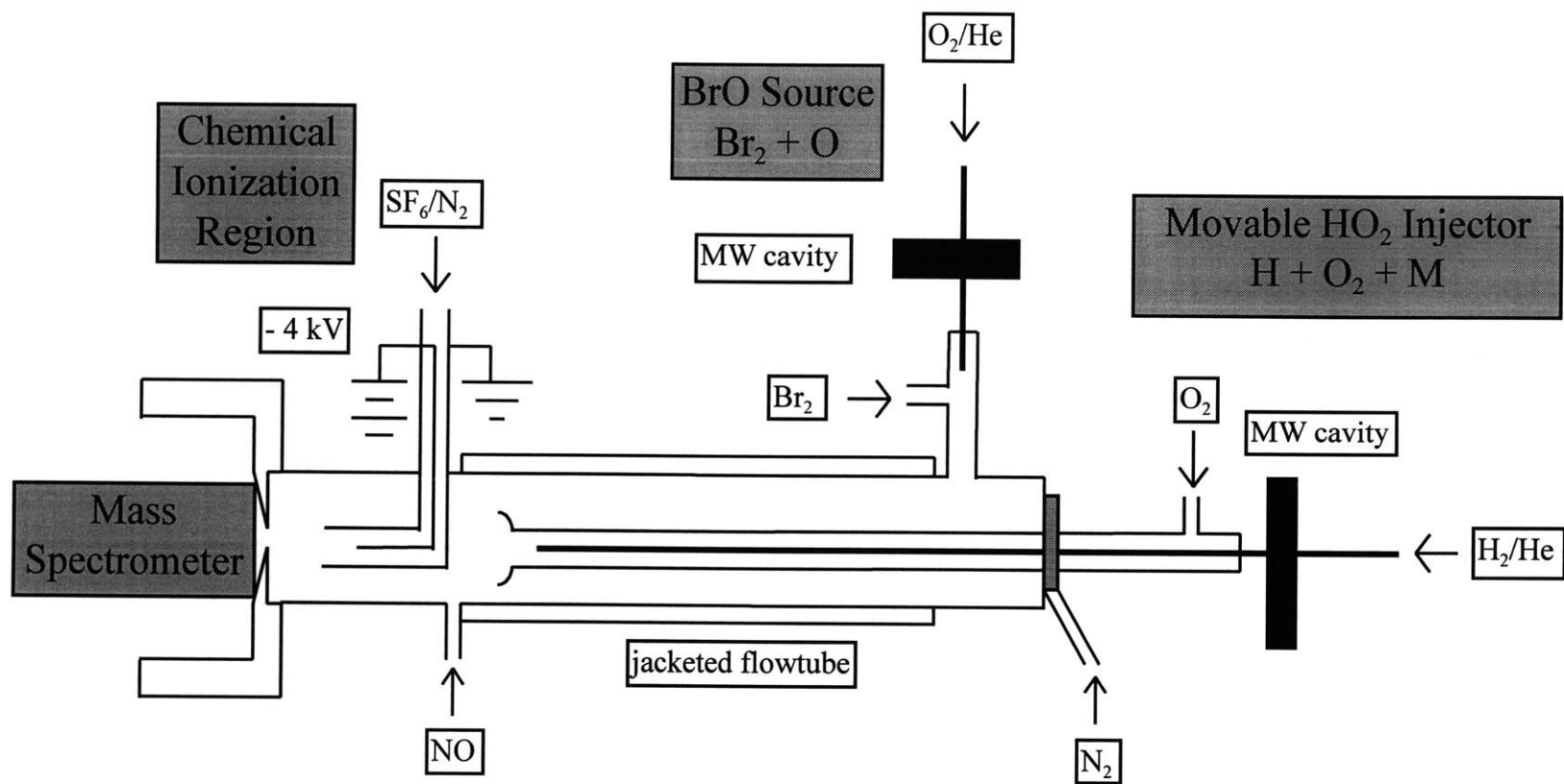


Figure 1. Schematic diagram of experimental apparatus

was injected at the rear of the flow tube. The gases necessary to generate BrO were introduced through a 10 cm long, 12.5 mm diameter sidearm located at the rear of the flow tube. HO₂ was generated in a triple-nested movable injector. The outer encasement (made from corrugated Teflon tubing) was used so that the injector could be moved to various injector positions without breaking any vacuum seals, as well as to prevent ambient gases from condensing on cold portions of the injector. A fan-shaped Teflon device was placed at the end of the injector in order to enhance turbulent mixing. The corona ion source was placed between the temperature regulated flow tube and the inlet to the quadrupole mass spectrometer. All gas flows were monitored with calibrated mass flow meters. The flow tube pressure was measured upstream of the corona ion source using a 0-1000 Torr capacitance manometer. For the low temperature studies, HCFC-123 was used as a coolant for the jacketed flow tube, and the nitrogen carrier gas was also precooled by passing it through a copper coil immersed in either a HCFC-123 or a liquid N₂ reservoir followed by resistive heating. The temperature was determined at both the entrance and exit points of the temperature regulated region of the flow tube using Cu-constantan thermocouples. The temperature was controlled in the reaction region to within 1 K.

2.2.1 Radical Production

BrO was generated using the following reaction:



($k_7 = 2.0 \times 10^{-11} \text{ cm}^3 \text{ molecule}^{-1} \text{ s}^{-1}$ [Mallard *et al.*, 1994]). Oxygen atoms were produced by combining a 0.5 STP L min⁻¹ flow of helium (99.999 %), which had passed through a silica gel trap immersed in liquid nitrogen, with a 0.1-0.5 STP mL min⁻¹ flow of a 1 % O₂ (99.995 %)/He mixture which then passed through a microwave discharge produced by a

Beenakker cavity operating at 50 W. To generate BrO, the oxygen atoms were then injected into a sidearm and mixed with an excess of Br₂ (~ 10¹² molecule cm⁻³) in order to ensure that no oxygen atoms were introduced into the main flow. The simultaneous generation of bromine atoms resulted in insignificant loss of HO₂ through reaction 8



($k_8 = 2.0 \times 10^{-12} \text{ cm}^3 \text{ molecule}^{-1} \text{ s}^{-1}$ [DeMore *et al.*, 1997]) and did not affect the values of the measured BrO pseudo-first-order decays. However, this secondary reaction did lead to higher background levels of HBr. Absolute BrO concentrations were periodically determined by the titration reaction



($k_9 = 2.1 \times 10^{-11} \text{ cm}^3 \text{ molecule}^{-1} \text{ s}^{-1}$ [DeMore *et al.*, 1997]) and subsequent calibration of the NO₂ mass spectrometer signal. Purified NO/N₂ mixtures were passed through a silica gel trap immersed in a dry ice/ethanol bath to further reduce the background NO₂ contribution. For this study, BrO concentrations ranged from 0.25 to 1.0 x 10¹¹ molecule cm⁻³.

HO₂ was generated by the following reaction:



The rate constant for reaction 10 at 100 Torr is 1.7 x 10⁻¹³ cm³ molecule⁻¹ s⁻¹ [DeMore *et al.*, 1997]. Because HO₂ was introduced through a movable injector where the corresponding concentrations are ~ 30 times higher than in the main flow tube, the disproportionation reaction



($k_{11} = 1.9 \times 10^{-12} \text{ cm}^3 \text{ molecule}^{-1} \text{ s}^{-1}$ at 100 Torr [DeMore *et al.*, 1997]) was a concern in the production of large quantities of HO_2 . By taking advantage of the long lifetime of H atoms, this difficulty was surmounted by using a nested injector which kept the hydrogen atoms (entrained in the inner 3 mm Pyrex tube) and oxygen molecules (entrained in the outer 6 mm Pyrex tube) separate throughout all but the last 1 cm of the injector. The hydrogen atoms were allowed to mix with a very large excess of O_2 ($5 \times 10^{17} \text{ molecule cm}^{-3}$ inside the injector) for only about 1 ms, allowing reaction 10 to virtually go to completion, but preventing significant recombination of HO_2 . Hydrogen atoms were generated by combining a 2.5 STP L min^{-1} flow of helium (99.999 %) with a 0.2 - 5.0 STP mL min^{-1} flow of a 2 % H_2 (99.999 %)/He mixture which then passed through a molecular sieve trap immersed in liquid nitrogen and finally through a microwave discharge produced by a Beenakker cavity operating at 70 W. Some OH was generated by this source, but it was adequately removed by the excess of Br_2 present in the flow tube.

For reasons of convenience, absolute HO_2 concentrations were routinely determined by the titration of H atoms



($k_{12} = 1.6 \times 10^{-10} \text{ cm}^3 \text{ molecule}^{-1} \text{ s}^{-1}$ [Mallard *et al.*, 1994]) and the modeling of reaction 10 and competing side reactions to determine actual HO_2 concentrations. For all conditions used in this study, HO_2 concentrations were found to be at least 90 % of the titrated H atom concentrations. Direct titrations of HO_2



($k_{13} = 8.0 \times 10^{-12} \text{ cm}^3 \text{ molecule}^{-1} \text{ s}^{-1}$ [Seeley *et al.*, 1996b]) were periodically performed (in a manner similar to that described for BrO) to verify the accuracy of the H + Br₂ method. Although the HO₂ concentrations used in this study were low enough to avoid significant homogeneous recombination of HO₂ (usually less than 10 % loss over the entire reaction zone [$\sim 25 \text{ ms}$]), HO₂ losses as high as 40 % (at 210 K) were observed at the lowest temperatures achieved in this study. Using the extrapolated value [DeMore *et al.*, 1997] for k_{11} at 210 K and the highest HO₂ concentration ($10^{12} \text{ molecule cm}^{-3}$) used at that temperature, the loss of HO₂ from homogeneous recombination is predicted to be only 17 %. Some of the unexpectedly high observed loss might be due to wall reactions. However, considering that the HO₂ recombination is a complex-mode reaction, extrapolation to low temperatures could well underestimate the actual rate constant value. In any case, we used the *mean* HO₂ concentration present in the reaction zone to determine the bimolecular rate coefficient. For conditions typical of our experiments, modeling indicates that this approximation results in values accurate to within 5 % of the true rate constant. The mean HO₂ concentrations were determined as follows: Since the HO₂ concentrations, which were routinely titrated, were determined at the time = initial position of the reaction zone, the actual average HO₂ concentrations were lower. To correct for this, the time = final and time = initial mass spectrometer signals for HO₂ were used to scale the titrated HO₂ concentrations. In the low pressure studies of Larichev *et al.* [1995] higher HO₂ concentrations ($5 \times 10^{12} \text{ molecule cm}^{-3}$) were used and similar scaling methods were applied. Li *et al.* [1997] used even higher HO₂ concentrations ($8 \times 10^{12} \text{ molecule cm}^{-3}$) and also used some sort of scaling method. HO₂ concentrations used in this study ranged from 0.5 to $2.0 \times 10^{12} \text{ molecule cm}^{-3}$. In order to insure pseudo-first-order kinetic conditions, [BrO] was kept at most one-tenth as large as [HO₂].

2.2.2 Detection of Reactants and Products

Most of the chemical species relevant to this study (HO_2 , BrO , HOBr , NO_2 , Br_2 , and HBr) were chemically ionized with the SF_6^- reagent ion and then detected with the quadrupole mass spectrometer. A schematic diagram of the ion source and mass spectrometer is presented in Figure 2. SF_6^- was produced in the ion source by passing approximately 5×10^{12} molecule cm^{-3} of SF_6 mixed with a large N_2 flow (10 STP L min^{-1}) over the corona discharge. The corona ion source consisted of a steel needle held at an electric potential of -4 kV and a grounded 6 mm stainless steel tube counterelectrode, which (with a ballast resistor of 100 M Ω) resulted in a discharge current of about 30 μA . The needle body was electrically isolated from the counterelectrode with a piece of Pyrex tubing. In order to confine the corona ionization process to SF_6 alone and to control the ion-molecule reaction time, another piece of Pyrex tubing (of variable length) was used to direct the SF_6^- downstream into the main flow tube effluent.

Ions were detected with a quadrupole mass spectrometer housed in a two-stage differentially pumped vacuum chamber. Flow tube gases (neutrals and ions) were drawn into the front chamber through a 0.1 mm aperture, which was held at a potential of ~ -130 V. The ions were focused by three lenses constructed from 3.8 cm i.d., 4.8 cm o.d copper gaskets. The front chamber was pumped by a 6 inch 2400 L s^{-1} diffusion pump. The gases entered the rear chamber through a skimmer cone with a 1.2 mm orifice (held at ~ -20 V) which was placed approximately 5 cm from the front aperture. The rear chamber was pumped by a 500 L s^{-1} turbomolecular pump. Once the ions passed through the skimmer cone, they were mass filtered and detected with a quadrupole mass spectrometer.

In the chemical ionization scheme employed here, BrO , Br_2 , and NO_2 were detected as their parent negative ions by charge-transfer reactions with SF_6^- :



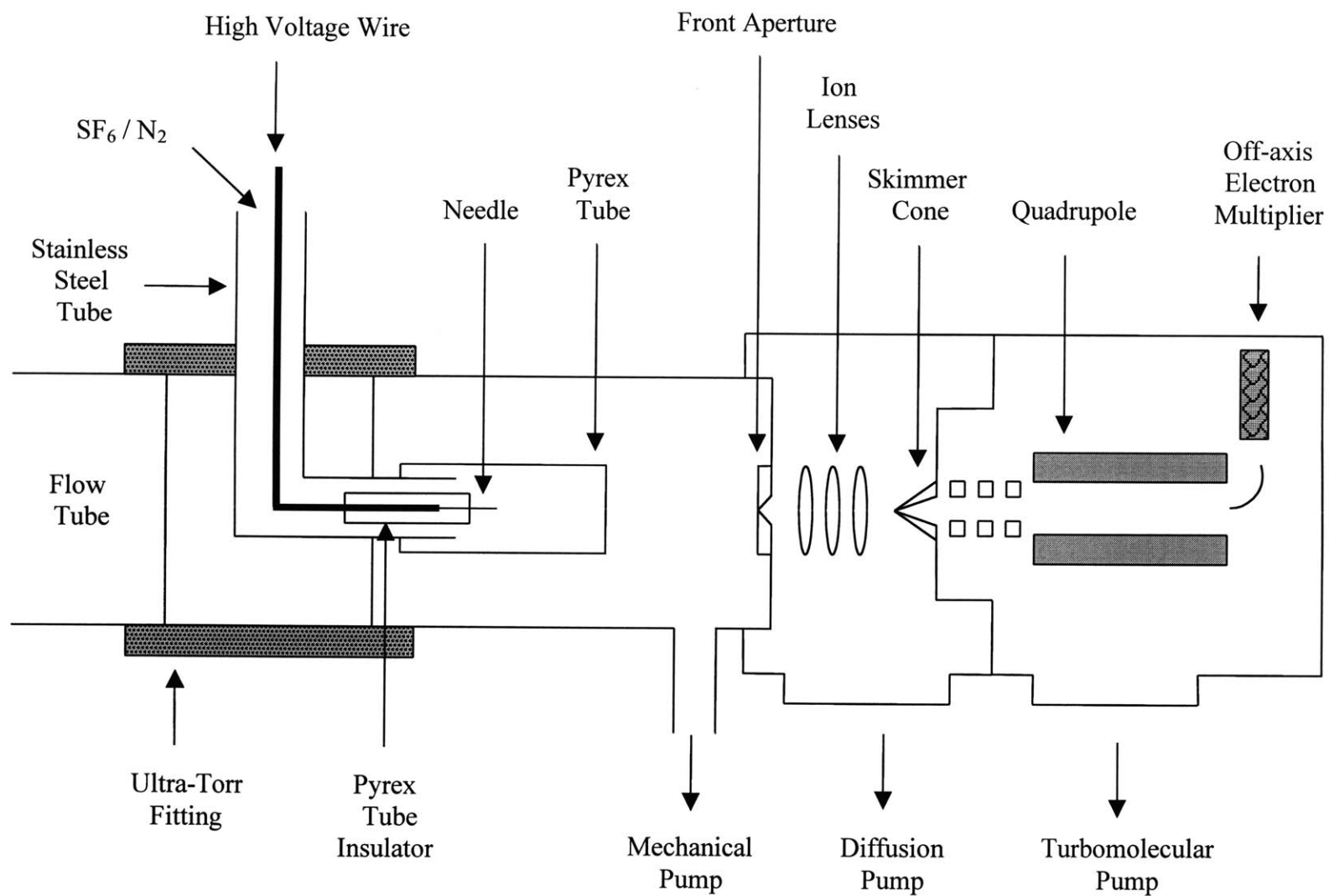


Figure 2. Schematic diagram of chemical ionization mass spectrometer



The rate constant for reaction 14 has not been measured, while the rate coefficients for reactions 15 and 16 are 5.1×10^{-10} and $1.3 \times 10^{-10} \text{ cm}^3 \text{ molecule}^{-1} \text{ s}^{-1}$, respectively [Streit, 1982]. HBr was detected as FHB r^- through a fluoride-transfer reaction with SF $_6^-$:



The rate constant for reaction 17 is $5.0 \times 10^{-10} \text{ cm}^3 \text{ molecule}^{-1} \text{ s}^{-1}$ [Streit, 1982]. HOBr was detected as SF $_5\text{O}^-$ [Huey *et al.*, 1995], and HO $_2$ was detected as SF $_4\text{O}_2^-$, presumably through multi-step pathways.

2.3 Results and Discussion

In the earlier study of HO $_2$ + NO from our laboratory, we reported that our chemical ionization detection scheme resulted in sensitivities of 100, 200, and 1000 ppt (at 100 Torr) for NO $_2$, HO $_2$, and OH, respectively [Seeley *et al.*, 1996b]. Although we did not carry out formal calibrations of the mass spectrometer for the bromine species detected with this method (Br $_2$, BrO, HBr, HOBr), it was apparent that these species could be detected with a similar sensitivity to that obtained for NO $_2$. The mass spectrometer signals for these compounds were found to be linear over the range of concentrations used in this work. The stated sensitivity was more than adequate for the present work; actually, it was necessary to degrade the sensitivity of the spectrometer (by decreasing the ion-molecule reaction time) to allow the introduction of greater amounts of reactants without inducing complications from secondary ion-molecule processes.

Bimolecular rate constants were obtained via the usual pseudo-first-order approximation method, using HO $_2$ as the excess reagent. Typical BrO decay curves as a

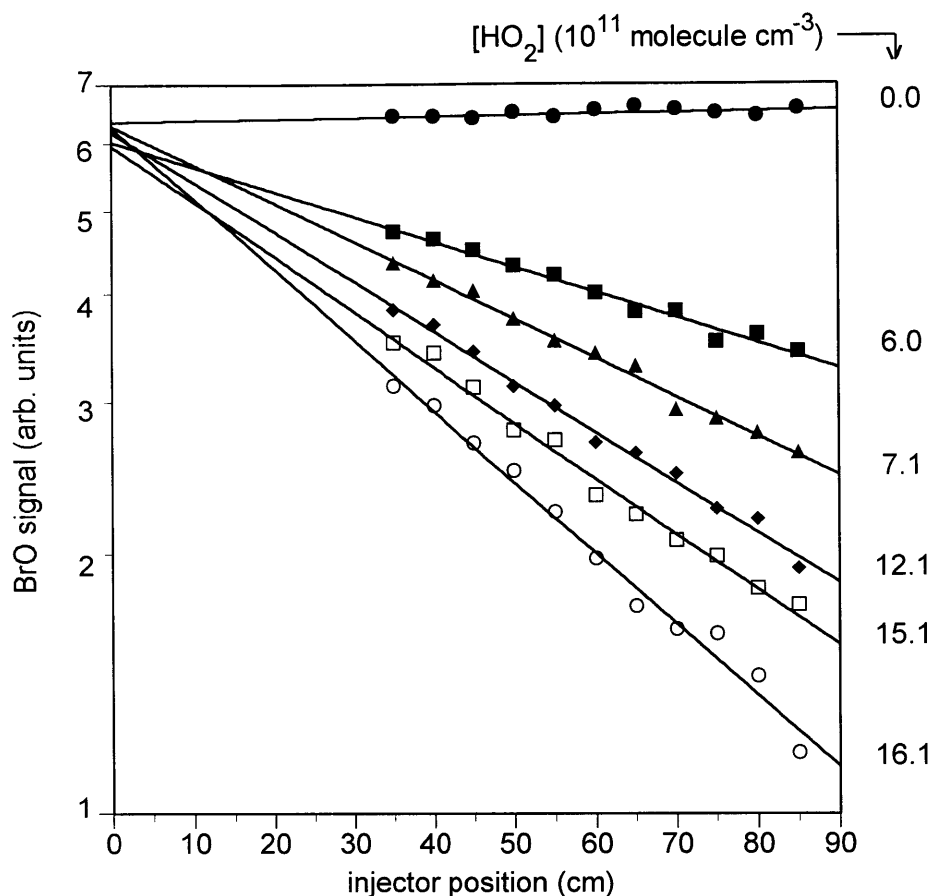


Figure 3. Typical set of BrO signals as a function of injector distance. This data set was obtained under the following conditions: $P = 100$ Torr; $T = 298$ K; average velocity = 1375 cm s^{-1} ; Reynolds number = 2600.

function of injector distance are shown in Figure 3. The first-order rate constants obtained from fitting the BrO decay curves were plotted against $[\text{HO}_2]$ in order to determine the bimolecular rate constant, as shown in Figure 4. This approach for determining bimolecular rate constants assumes that deviations from the plug flow approximation are negligible. Under the conditions present in our turbulent flow tube, *Seeley et al.* [1996b] estimated that these deviations result in apparent rate constants which are at most 8 % below the actual values. Hence, the flow corrections were

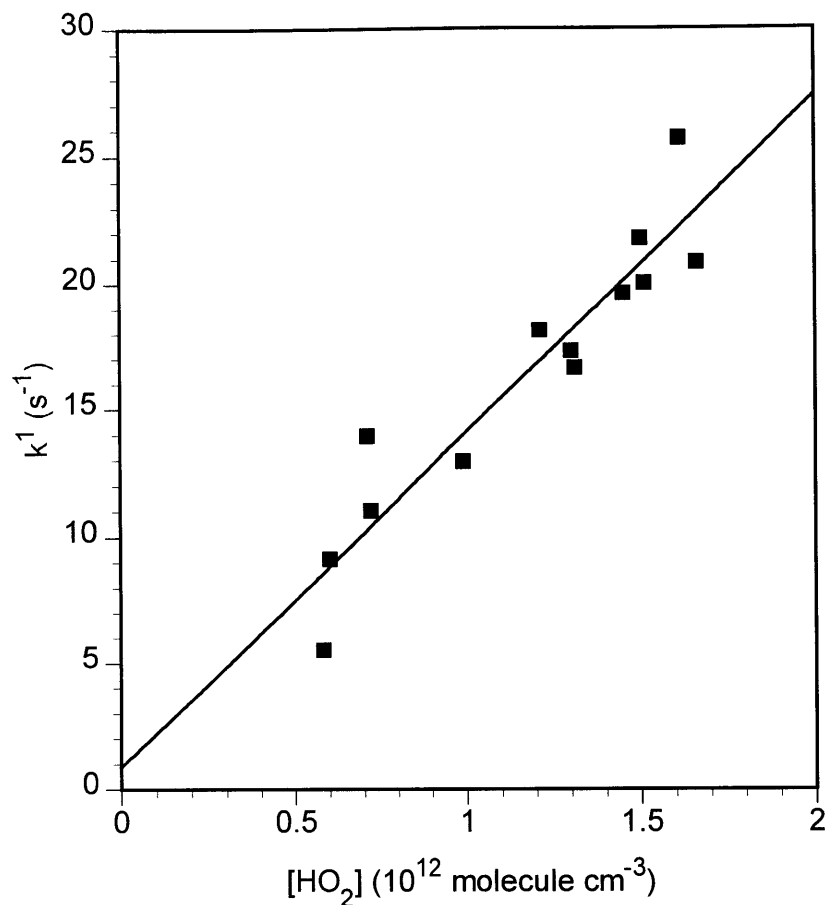


Figure 4. Typical plot of k^1 as a function of $[\text{HO}_2]$. This plot was obtained under the same conditions as listed in Figure 3.

neglected as they are smaller than the sum of the other likely systematic errors in the measurements of gas flows, temperature, detector signal, pressure and absolute HO_2 concentrations. Indeed, we consider the major source of error in our experiments to arise from the determination of $[\text{HO}_2]$ from the titration and scaling procedures outlined above. Considering such sources of error, we estimate that rate constants can be determined with an accuracy of $\pm 30\%$ (2σ).

We performed four separate determinations of the rate constant at 298 K (see Table 1 for a complete list of experimental conditions and measured rate constants) and arrived at

Table 1. Summary of Experimental Conditions and Measured Rate Constants for the HO₂ + BrO Reaction

T (K)	P (Torr)	velocity (cm s ⁻¹)	Reynolds Number	$k \pm 2\sigma$ (10 ⁻¹¹ cm ³ molecule ⁻¹ s ⁻¹)
298	100	1375	2600	1.32 ± 0.30
298	97	1800	3300	1.38 ± 0.24
298	99	1500	2750	1.44 ± 0.30
298	95	1675	2700	1.50 ± 0.28
283	92	1450	2850	1.68 ± 0.34
273	95	1425	2970	1.64 ± 0.32
270	90	1570	3120	1.69 ± 0.32
263	98	1570	3400	1.66 ± 0.22
260	92	1900	4250	2.09 ± 0.36
253	92	1575	3600	2.01 ± 0.32
253	107	1420	3820	2.10 ± 0.40
249	93	1850	4350	2.33 ± 0.56
243	94	1740	4420	1.99 ± 0.40
230	91	1550	4100	2.63 ± 0.81
220	92	1260	3600	2.67 ± 0.46
216	90	1680	4970	2.55 ± 0.94
210	94	1500	4900	2.95 ± 0.92

the mean value of $k = (1.4 \pm 0.3) \times 10^{-11} \text{ cm}^3 \text{ molecule}^{-1} \text{ s}^{-1}$; the uncertainty represents the two standard deviation statistical error in the data and is not an estimate of systematic errors. Table 2 contains a comparison of all reported rate constants for the HO₂ + BrO reaction near room temperature. Although our value indicates a significantly faster rate constant than was determined in the original study of *Cox and Sheppard* [1982], our result is about a factor of two lower than some of the other recent studies [*Poulet et al.*, 1992; *Hayman et al.*, 1992; *Bridier et al.*, 1993; *Larichev et al.*, 1995]. However, the very recent measurements of *Li et al.* [1997] and *Cronkhite et al.* [1998] are in better agreement with our findings.

Table 2. Comparison of Measured Rate Constants Near Room Temperature for the HO₂ + BrO Reaction

Technique	P (Torr)	k (10 ⁻¹¹ cm ³ molecule ⁻¹ s ⁻¹)	Reference
MM/UV	760	0.5 ± $\begin{matrix} 0.5 \\ 0.3 \end{matrix}$	Cox and Sheppard [1982]
DF-LF/EIMS	1	3.3 ± 0.5	Poulet et al. [1992]
LP/UV	760	3.0 ± 2.0	Hayman et al. [1992]
FP/UV	760	3.4 ± 1.0	Bridier et al. [1993]
DF-LF/EIMS	1	3.3 ± 0.5	Larichev et al. [1995]
DF-LF/EIMS	1-3	1.73 ± 0.61* 2.05 ± 0.64&	Li et al. [1997]
LP/UV-TDL	12, 25	2.0 ± 0.6	Cronkhite et al. [1998]
DF-TF/CIMS	100	1.4 ± 0.3	This work Elrod et al. [1996]

* with HO₂ as excess reagent.

& with BrO as excess reagent.

MM: molecular modulation; LP: laser photolysis; FP: flash photolysis; DF: discharge flow; LF: laminar flow; TF: turbulent flow; UV: ultraviolet spectroscopy detection; TDL: tunable diode laser spectroscopy detection; EIMS: electron impact mass spectrometry detection; CIMS: chemical ionization mass spectrometry detection.

We performed several measurements at temperatures between 210 and 298 K in order to establish the temperature dependence of the rate constant for conditions relevant to the lower stratosphere. The rate constant approximately doubled as the temperature was lowered over this range. From the data listed in Table 1 and plotted in Figure 5, we obtain the Arrhenius expression $k(T) = (2.5 \pm 0.8) \times 10^{-12} \exp [(520 \pm 80) / T] \text{ cm}^3 \text{ molecule}^{-1} \text{ s}^{-1}$. The mechanism of the HO₂ + BrO reaction is not well known. However, the observed negative activation energy may be an indication that the HO₂ + BrO reaction

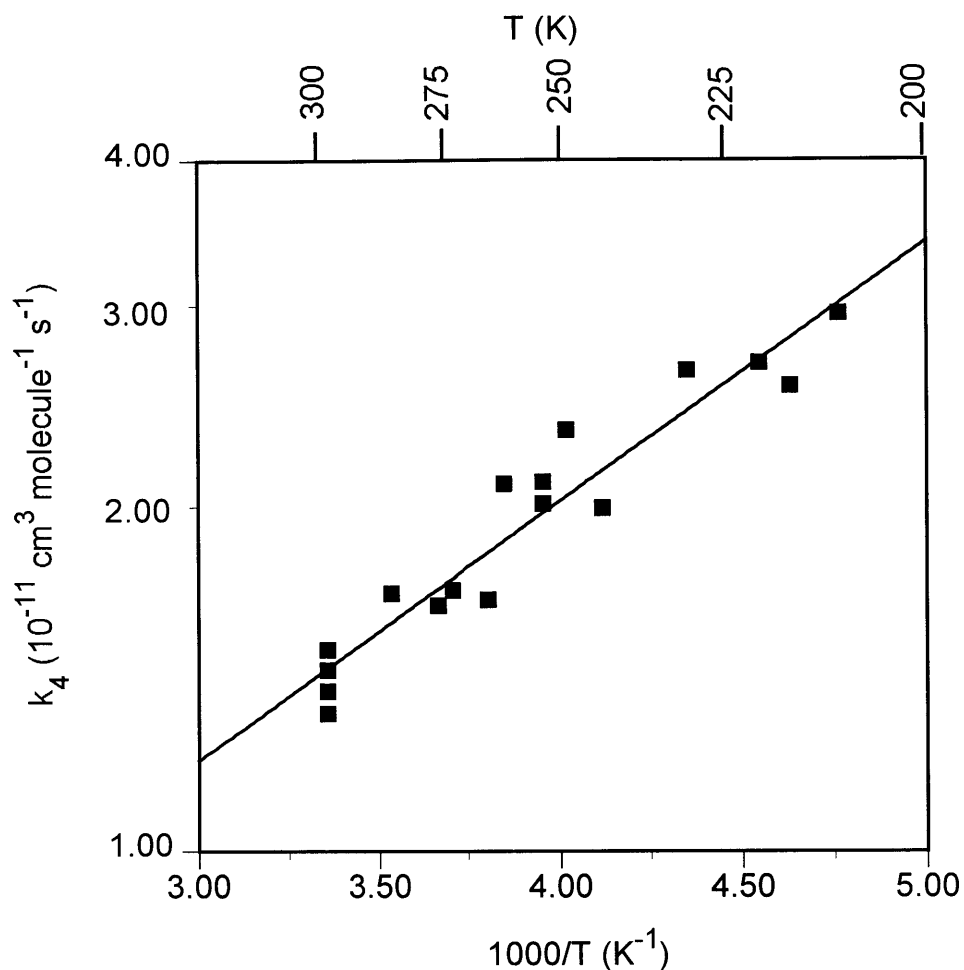


Figure 5. Arrhenius plot for the reaction $\text{HO}_2 + \text{BrO}$; the least-squares fit to the data yields the expression $k(T) = (2.5 \pm 0.8) \times 10^{-12} \exp[(520 \pm 80)/T] \text{ cm}^3 \text{ molecule}^{-1} \text{ s}^{-1}$.

proceeds through the formation of an intermediate complex that is stabilized at low temperatures [e.g., Mozurkewich and Benson, 1984]. In a recent *ab initio* study, Guha and Francisco [1998] investigated the structures and energetics of possible intermediate complexes. They found that the enthalpies of formation of the complexes increased in the order $\text{HOBrO}_2 < \text{HOOOBr} < \text{HOOBrO} < \text{HBrO}_3$, with all of the isomers except HBrO_3 lying lower in energy than $\text{HO}_2 + \text{BrO}$. Although HOBrO_2 is the most stable

isomer, it is unlikely that the HO₂ + BrO reaction proceeds through this intermediate because of the high energy barrier for rearrangement. A more likely mechanism is the formation of the HOOBrO isomer, followed by the formation of a cyclic intermediate and then decomposition to form HOBr and O₂ [Cronkhite *et al.*, 1998]. A possible pathway for the minor channel (reaction 4b) is the production of HOOOBr followed by cyclization and then elimination of HBr and O₃. However, the small experimental upper limit for this channel (< 2%) [Larichev *et al.*, 1995] suggests that there is a significant reaction energy barrier.

Only two other temperature dependence studies have been conducted, and a comparison of our results with the work of Larichev *et al.* [1995] and Li *et al.* [1997] is presented in Table 3. The activation energies reported in the two other studies are in excellent agreement with our value. The pre-exponential factor of Li *et al.* is also in good agreement with our result. However, the pre-exponential factor of Larichev *et al.* is almost a factor of two larger than our measurement. The current JPL recommendation

Table 3. Comparison of Temperature Dependence Studies for the HO₂ + BrO Reaction

Technique	T (K)	P (Torr)	k(T) (cm ³ molecule ⁻¹ s ⁻¹)	Reference
DF-LF/EIMS	233-344	1	$(4.8 \pm 0.3) \times 10^{-12}$ $\exp[(580 \pm 100) / T]$	Larichev <i>et al.</i> [1995]
DF-LF/EIMS	233-348	1	$(3.1 \pm 0.3) \times 10^{-12}$ $\exp[(540 \pm 210) / T]$	Li <i>et al.</i> [1997]
DF-TF/CIMS	210-298	100	$(2.5 \pm 0.8) \times 10^{-12}$ $\exp[(520 \pm 80) / T]$	This work Elrod <i>et al.</i> [1996]

DF: discharge flow; LF: laminar flow; TF: turbulent flow; EIMS: electron impact mass spectrometry detection; CIMS: chemical ionization mass spectrometry detection.

[DeMore *et al.*, 1997] for the temperature dependence of the rate constant for the HO₂ + BrO reaction is: $k(T) = 3.4 \times 10^{-12} \exp[540 / T] \text{ cm}^3 \text{ molecule}^{-1} \text{ s}^{-1}$ based on an average of the results from this study [Elrod *et al.*, 1996] and the results from the studies by Larichev *et al.* and Li *et al.*

The Arrhenius expression reported by Larichev *et al.* is based on their rate constant measurements between 243 and 344 K. At 233 K, the lowest temperature attained in their study, Larichev *et al.* reported the existence of a reproducible, non-Arrhenius data point. However, we found no such anomalous behavior in the rate constant for temperatures as low as 210 K as shown in Figure 5. Similar to our findings, Li *et al.* also obtained an Arrhenius plot that was linear over their entire temperature range (233-348 K). The studies by Larichev *et al.* and Li *et al.* were both conducted using the low pressure laminar flow tube technique. Both studies reported that wall loss became prohibitive at temperatures below 233 K. In contrast, our rate constant measurements extend to temperatures as low as 210 K. As discussed in Chapter 1, the turbulent flow tube technique used in this study has significantly reduced wall loss effects compared to the conventional low pressure laminar flow tube technique. In fact, Larichev *et al.* acknowledged that increased reactant wall loss of BrO (limiting reagent) may have been the cause of their anomalously high rate constant measurement at 233 K. This is an important point since the significant departure from Arrhenius behavior observed by Larichev *et al.* beginning at 233 K is suggestive of a nearly collision-limited rate constant at stratospherically relevant temperatures. A study by Cohen *et al.* [1994] attempted to constrain the rate constant for the HO₂ + BrO reaction using simultaneous field measurements of the OH/HO₂ ratio and BrO concentrations in the lower stratosphere from the Stratospheric Photochemistry, Aerosols and Dynamics Expedition (SPADE). The very fast rate constant measurement at 233 K by Larichev *et al.* is outside the range of rate constants found to be consistent with the field data in the study by Cohen *et al.* In contrast, our measurement of the rate constant for HO₂ + BrO at 210 K is easily within

the range of possible rate constants proposed to be consistent with the interpretation of the field measurements.

In this study, we were unable to address the importance (or existence) of the secondary product channel (reaction 4b) for the $\text{HO}_2 + \text{BrO}$ reaction using our current radical generation and detection scheme, because of problems with the sensitive detection of O_3 and HBr in the presence of the other reactants. With the large quantities of O_2 required for the production of HO_2 , the SF_6^+ chemical ionization scheme yielded small amounts of O_3^+ , thus preventing the sensitive detection of ozone in the presence of oxygen. In addition, the BrO source produced high levels of bromine atoms which reacted with HO_2 and the flow tube walls to create relatively high background HBr signals. However, these problems can potentially be circumvented by employing different synthetic schemes. Nonetheless, mass spectral scans were taken at each temperature to search for possible changes in the product distribution, but we were unable to establish limits on the generation of reaction 4 products other than HOBr .

2.4 Conclusions

The results presented here extend the measurements of the rate constant for $\text{HO}_2 + \text{BrO}$ to conditions representative of the lower stratosphere. This study has shown that the turbulent flow tube technique coupled with high pressure chemical ionization mass spectrometry is an excellent method for studying the kinetics of radical-radical reactions under conditions relevant to the atmosphere. While our room temperature results do not agree with several other previous measurements, they are in better agreement with the most recent studies by *Li et al.* [1997] and *Cronkhite et al.* [1998]. Also, we did not find evidence for non-Arrhenius behavior below 243 K, as suggested in the previous temperature dependence study by *Larichev et al.* [1995]. Our direct results should place more stringent constraints on the partitioning of bromine species in the stratosphere and on the ozone depletion potentials of compounds such as methyl bromide.

References for Chapter 2

- Anderson, J. G., D. W. Toohey, and W. H. Brune, Free radicals within the Antarctic vortex: The role of CFCs in Antarctic ozone loss, *Science*, *251*, 39, 1991.
- Bridier, I., B. Veyret, and R. Lesclaux, Flash photolysis kinetic study of reactions of the BrO radical with BrO and HO₂, *Chem. Phys. Lett.*, *201*, 563, 1993.
- Butler, J. H., S. A. Montzka, A. D. Clarke, J. M. Lobert, and J. W. Elkins, Growth and distribution of halons in the atmosphere, *J. Geophys. Res.*, *103*, 1503, 1998.
- Chartrand, D. J., and J. C. McConnell, Evidence for HBr production due to minor channel branching at mid-latitudes, *Geophys. Res. Lett.*, *25*, 55, 1998.
- Chipperfield, M. P., D. E. Shallcross, and D. J. Lary, A model study of the potential role of the reaction BrO + OH in the production of stratospheric HBr, *Geophys. Res. Lett.*, *24*, 3025, 1997.
- Cohen, R. C., P. O. Wennberg, R. M. Stimpfle, J. Koplw, J. G. Anderson, D. W. Fahey, E. L. Woodbridge, E. R. Keim, R. Gao, M. H. Proffitt, M. Loewenstein, and K. R. Chan, Are models of catalytic removal of O₃ by HO_x accurate? Constraints from *in situ* measurements of the OH to HO₂ ratio, *Geophys. Res. Lett.*, *21*, 2539, 1994.
- Cox, R. A., and D. W. Sheppard, Rate coefficient for the reaction of BrO with HO₂ at 303 K, *J. Chem. Soc., Faraday Trans. 2*, *78*, 1383, 1982.
- Cronkrite, J. M., R. E. Stickel, J. M. Nicovich, and P. H. Wine, Laser flash photolysis studies of radical-radical reaction kinetics: The HO₂ + BrO reaction, *J. Phys. Chem. A*, *102*, 6651, 1998.
- DeMore, W. B., S. P. Sander, C. J. Howard, A. R. Ravishankara, D. M. Golden, C. E. Kolb, R. F. Hampson, M. J. Kurylo, and M. J. Molina, *Chemical Kinetics and Photochemical Data for Use in Stratospheric Modeling*, JPL Publication 97-4, Jet Propulsion Laboratory, Pasadena, CA, 1997.
- Elrod, M. J., R. F. Meads, J. B. Lipson, J. V. Seeley, and M. J. Molina, Temperature dependence of the rate constant for the HO₂ + BrO reaction, *J. Phys. Chem.*, *100*, 5808, 1996.
- Fish, D. J., and M. R. Burton, The effect of uncertainties in kinetic and photochemical data on model predictions of stratospheric ozone depletion, *J. Geophys. Res.*, *102*, 25537, 1997.

- Guha, S., and J. S. Francisco, Structures, vibrational spectra and relative energetics of HBrO₃ isomers, *J. Phys. Chem. A*, *102*, 2072, 1998.
- Hayman, G. D., F. Danis, and D. A. Thomas, Kinetic study of the reactions BrO + BrO and BrO + HO₂, *Air Pollution Research Report 45*, Commission on European Communities, Luxemburg, ed. J. Peeters, 303, 1992.
- Huey, L. G., D. R. Hanson, and C. J. Howard, Reactions of SF₆⁻ and I⁻ with atmospheric trace gases, *J. Phys. Chem.*, *99*, 5001, 1995.
- Larichev, M., F. Maguin, G. Le Bras, and G. Poulet, Kinetics and mechanism of the BrO + HO₂ reaction, *J. Phys. Chem.*, *99*, 15911, 1995.
- Lary, D. J., Gas phase atmospheric bromine photochemistry, *J. Geophys. Res.*, *101*, 1505, 1996.
- Li, Z., R. R. Friedl, and S. P. Sander, Kinetics of the HO₂ + BrO reaction over the temperature range 233-348 K, *J. Chem. Soc., Faraday Trans.*, *93*, 2683, 1997.
- Mallard, W. G., F. Westley, J. T. Herron, and R. F. Hampson, *NIST Chemical Kinetics Database Version 6.0*, NIST Standard Reference Data, Gaithersberg, MD, 1994.
- McElroy, M. B., and R. J. Salawitch, Changing composition of the global stratosphere, *Science*, *243*, 763, 1989.
- Mellouki, A., R. K. Talukdar, and C. J. Howard, Kinetics of the reactions of HBr with O₃ and HO₂: The yield of HBr from HO₂ + BrO, *J. Geophys. Res.*, *99*, 22949, 1994.
- Mozurkewich, M., and S. W. Benson, Negative activation energies and curved Arrhenius plots. 1. Theory of reactions over potential wells, *J. Phys. Chem.*, *88*, 6429, 1984.
- Poulet, G., M. Pirre, F. Maguin, R. Ramaroson, and G. Le Bras, Role of the BrO + HO₂ reaction in the stratospheric chemistry of bromine, *Geophys. Res. Lett.*, *19*, 2305, 1992.
- Salawitch, R. J., M. B. McElroy, J. H. Yatteau, S. C. Wofsy, M. R. Schoeberl, L. R. Lait, P. A. Newman, K. R. Chan, M. Loewenstein, J. R. Podolske, S. E. Strahan, and M. H. Proffitt, Loss of ozone in the Arctic vortex for the winter of 1989, *Geophys. Res. Lett.*, *17*, 561, 1990.
- Seeley, J. V., J. T. Jayne, and M. J. Molina, High pressure fast-flow technique for gas phase kinetics studies, *Int. J. Chem. Kinet.*, *25*, 571, 1993.
- Seeley, J. V., J. T. Jayne, and M. J. Molina, Kinetic studies of chlorine atom reactions using the turbulent flow tube technique, *J. Phys. Chem.*, *100*, 4019, 1996a.

Seeley, J. V., R. F. Meads, M. J. Elrod, and M. J. Molina, Temperature and pressure dependence of the rate constant for the $\text{HO}_2 + \text{NO}$ reaction, *J. Phys. Chem.*, *100*, 4026, 1996b.

Streit, G. E., Negative ion chemistry and the electron affinity of SF_6 , *J. Chem. Phys.*, *77*, 826, 1982.

Wofsy, S. C., M. B. McElroy, and Y. L. Yung, The chemistry of atmospheric bromine, *Geophys. Res. Lett.*, *2*, 215, 1975.

Yung, Y. L., J. P. Pinto, R. T. Watson, and S. P. Sander, Atmospheric bromine and ozone perturbations in the lower stratosphere, *J. Atmos. Sci.*, *37*, 339, 1980.

Chapter 3: Kinetics of the OH + ClO Reaction: Measurements of the Overall Rate Constant and Preliminary Branching Ratio Experiments

3.1 Introduction

One of the long-standing problems in modeling the chemistry of the upper stratosphere has been the inability of models to correctly predict ozone concentrations above ~35 km. Between 35 and 75 km, the lifetime of ozone is short relative to the time-scale for transport, and so ozone is expected to be in photochemical equilibrium. However, models have consistently failed to reproduce the expected balance between production and loss of odd oxygen ($O + O_3$). Attempts to model ozone levels in the upper stratosphere and lower mesosphere have resulted in an overprediction of ozone loss rates by as much as 35% near 40 km [e.g., *Brasseur et al.*, 1985; *McElroy and Salawitch*, 1989; *Eluszkiewicz and Allen*, 1993; *Siskind et al.*, 1995; *Khosravi et al.*, 1998]. This “ozone deficit” problem has been partially attributed to the failure of models to correctly reproduce the observed partitioning of chlorine in the upper atmosphere. The models tend to overestimate the amount of active chlorine (e.g., ClO) relative to the amount of stable chlorine (e.g., HCl) by as much as a factor of 2 [e.g., *Allen and Delitsky*, 1991; *Stachnik et al.*, 1992; *Toumi and Bekki*, 1993; *Chance et al.*, 1996; *Dessler et al.*, 1996]. Since calculated O_3 levels are very sensitive to the partitioning of chlorine, an overprediction of active chlorine will lead to an underestimation of O_3 , particularly near 40 km where the chlorine cycle has its maximum contribution to the odd oxygen loss rate [*Osterman et al.*, 1997]. Many studies have proposed that discrepancies between measured and calculated chlorine partitioning could be resolved by including an additional source of HCl in the models.

The reaction of OH with ClO has long been suggested as a possible source of HCl production in the upper stratosphere [e.g., *Brasseur et al.*, 1985; *Natarajan and Callis*,

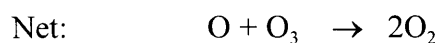
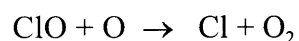
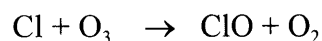
1991; Chandra *et al.*, 1993; Toumi and Bekki, 1993; Chance *et al.*, 1996]. Although the major products of the OH + ClO reaction are HO₂ and Cl ($\Delta H^\circ_{298\text{ K}} = -1.3 \text{ kcal mol}^{-1}$),



the reaction may have a minor channel that produces HCl and O₂ ($\Delta H^\circ_{298\text{ K}} = -55.8 \text{ kcal mol}^{-1}$):



Reaction 1b is thermodynamically feasible, but kinetically unfavorable because two bonds must be broken almost simultaneously; it most likely proceeds through a four-centered transition state. The conversion of ClO to Cl in reaction 1a is a chain-propagating step in catalytic ozone depletion cycles because ClO and Cl are both active forms of chlorine. For example, Cl and ClO participate in the ozone depletion cycle:



However, reaction 1b converts an active form of chlorine (ClO) into a more stable reservoir species (HCl). Since reaction 1b is a chain-terminating step, even a relatively small branching ratio may lead to substantially less ozone depletion by chlorine-containing compounds.

Several recent modeling studies of the upper stratosphere have shown that including a small branching ratio for the OH + ClO reaction has a dramatic effect on the partitioning of chlorine in their simulations. In fact, a very recent sensitivity analysis by *Dubey et al.* [1998] found that reaction 1b is the most important source of uncertainty in modeled chlorine partitioning. In most of the modeling studies, including a branching ratio of ~5-10% essentially eliminated the discrepancies between measured and modeled chlorine partitioning [e.g., *Natarajan and Callis*, 1991; *Toumi and Bekki*, 1993; *Eckman et al.*, 1995; *Chance et al.*, 1996; *Khosravi et al.*, 1998; *Ruhnke et al.*, 1999]. In a recent study, *Michelsen et al.* [1996] found that including a 7% branching ratio in their model resulted in agreement between measured and modeled profiles of [HCl], [ClONO₂] and [ClO] at nearly all altitudes and latitudes. Furthermore, *Michelsen et al.* concluded that uncertainties in the rate constants of other important reactions involving HCl such as Cl + CH₄ → HCl + CH₃ and OH + HCl → Cl + H₂O cannot fully account for the observed errors in calculated chlorine partitioning. In many modeling studies, the addition of reaction 1b also helped to reduce the disagreement between measured and modeled ozone concentrations, especially near 40 km where the chlorine cycle has its maximum contribution to the odd oxygen loss rate [e.g., *Chandra et al.*, 1993; *Siskind et al.*, 1995; *Jucks et al.*, 1996; *Osterman et al.*, 1997]. However, above 45 km (where the HOx cycle is the dominant loss process), the models continue to overestimate ozone loss rates, possibly indicating a problem with calculated HOx partitioning [e.g., *Siskind et al.*, 1995; *Sandor et al.*, 1997; *Summers et al.*, 1997; *Khosravi et al.*, 1998].

Previous attempts to measure the branching ratio of the OH + ClO reaction have been unable to rule out an HCl yield of zero for the minor channel due to uncertainties in the results. The laboratory studies were not able to directly observe a product from reaction 1b due to either the inability to detect HCl and O₂ [*Leu and Lin*, 1979; *Burrows et al.*, 1984; *Hills and Howard*, 1984] or due to insufficient sensitivity for HCl [*Poulet et al.*, 1986]. Because of the indirect methods used in the studies of *Leu and Lin* and *Burrows*

et al. and the large uncertainties in all of the measurements of the branching ratio, no consensus had been reached on the existence of channel 1b. As a result, most atmospheric models have not included this channel in their reaction set.

Some discrepancies also exist in the previous studies of the temperature dependence of the overall rate constant for the OH + ClO reaction [Leu and Lin, 1979; Ravishankara *et al.*, 1983; Burrows *et al.*, 1984; Hills and Howard, 1984; Poulet *et al.*, 1986]. Hills and Howard report a slight negative temperature dependence, but two other studies by Burrows *et al.* and Ravishankara *et al.* found that the rate constant was independent of temperature. All previous studies of the rate constant and the branching ratio were conducted at low pressure (~1 Torr) due to the limitations inherent in the conventional discharge laminar flow tube technique. As pointed out by Wennberg *et al.* [1994], the interpretation of field measurements of important atmospheric species is hindered by uncertainties in the laboratory-measured rate constants due to the fact that many of the studies have not been carried out under pressure and temperature conditions characteristic of the stratosphere.

In this chapter, measurements of the temperature dependence of the overall rate constant for the OH + ClO reaction will be presented. A preliminary investigation of the branching ratio will also be presented. Because of the large background of HCl produced by the ClO source, OD was used instead of OH in the branching ratio experiments. These studies were conducted at pressures near 100 Torr and at a range of temperatures extending to those found in the lower stratosphere using a turbulent flow tube coupled to a high pressure chemical ionization mass spectrometer.

3.2 Experimental Section

A schematic diagram of the experimental apparatus is presented in Figure 1 and is similar to that used in our previous study of the HO₂ + BrO reaction (Chapter 2). The flow tube (2.2 cm i.d., 120 cm long) was constructed of Pyrex tubing and coated with

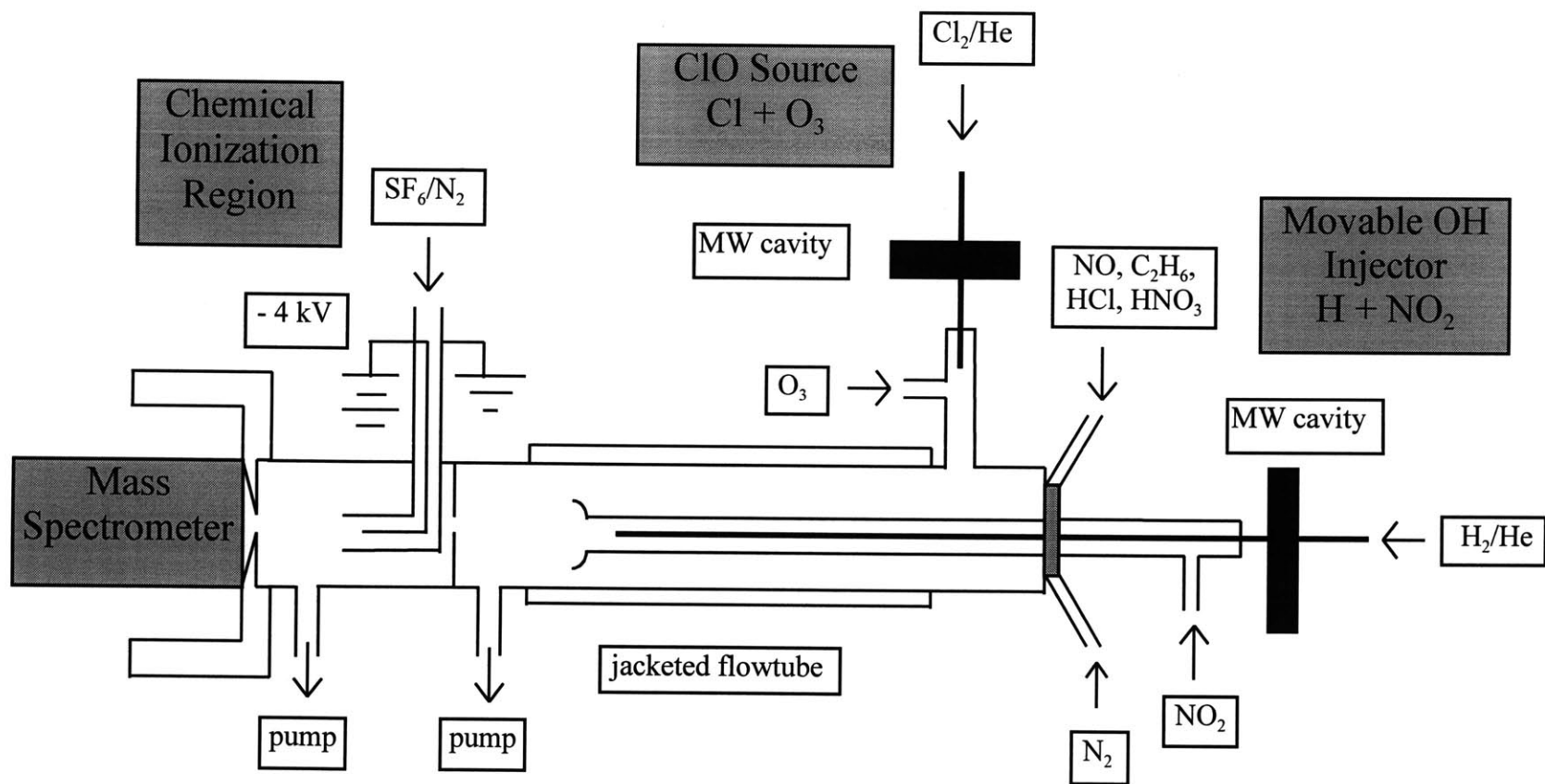


Figure 1. Schematic diagram of experimental apparatus

Halocarbon wax. A large flow of nitrogen carrier gas (~ 50 STP L min^{-1}) was injected at the rear of the flow tube. For the kinetics experiments, the gases necessary to generate ClO were introduced through a sidearm (10 cm long, 12.5 mm diameter) located at the rear of the flow tube. OH(D) was generated in a triple-nested movable injector which consisted of an inner 3 mm Pyrex tube, a middle 6 mm Pyrex tube and an outer encasement made from corrugated Teflon tubing. The outer encasement was used so that the injector could be moved to various injector positions without breaking any vacuum seals, as well as to prevent ambient gases from condensing on cold portions of the injector. A fan-shaped Teflon device was placed at the end of the injector in order to enhance turbulent mixing. For the branching ratio experiments the OH(D) was generated in the side arm and the ClO was generated in the injector. The electric discharge ion source was placed between the temperature regulated flow tube and the inlet to the quadrupole mass spectrometer. A 1.7 mm aperture between the flow tube and the ion-molecule region created a pressure drop from 100 Torr in the flow tube to 15 Torr in the ion-molecule region. The pressures in the two regions were measured using MKS capacitance manometers (1000 Torr full scale). All gas flows were monitored with calibrated Tylan General mass flow meters. For the low temperature studies, HCFC-123 was used as a coolant for the jacketed flow tube, and the nitrogen carrier gas was also precooled by passing it through a copper coil immersed in either an ice-water or a liquid N_2 reservoir followed by resistive heating. The temperature was determined at both the entrance and exit points of the temperature regulated region of the flow tube using copper-constantan thermocouples. The temperature was controlled in the reaction region to within 1 K.

3.2.1 Radical Production: Overall Rate Constant Measurements

Bimolecular rate constants were measured using the pseudo-first-order approximation method with ClO as the excess reagent. ClO was generated using the

following reaction:



($k_2 = 1.2 \times 10^{-11} \text{ cm}^3 \text{ molecule}^{-1} \text{ s}^{-1}$ [DeMore *et al.*, 1997]). Chlorine atoms were produced by combining a 2.0 STP L min⁻¹ flow of helium (99.999 %), which had passed through a molecular sieve trap immersed in liquid nitrogen, with a 0.3-3.0 STP mL min⁻¹ flow of a 5 % Cl₂ (>99.9 %)/He mixture which then passed through a microwave discharge produced by a Beenakker cavity operating at 70 W. To generate ClO, the chlorine atoms were then injected into a 20 cm long piece of 6 mm Teflon tubing connected to the side arm and mixed with an excess of O₃ ($\sim 10^{13} \text{ molecule cm}^{-3}$) in order to ensure that only negligible amounts of chlorine atoms were introduced into the main flow. The large excess of O₃ also helped to scavenge Cl atoms produced by the main channel of the OH(D) + ClO reaction, and therefore helped to minimize the reverse reaction:



($k_3 = 9.1 \times 10^{-12} \text{ cm}^3 \text{ molecule}^{-1} \text{ s}^{-1}$ [DeMore *et al.*, 1997]) which could have affected the pseudo-first-order decays of OH(D). The O₃ was generated by passing O₂ (99.994%) through an OREC ozonator, and then the O₃ was stored in a silica gel trap immersed in a dry ice/ethanol bath. O₃ was introduced into the system by passing a 5.0-20.0 STP mL min⁻¹ flow of N₂ through the trap. Ozone partial pressures were determined by UV absorbance at 253.7 nm (Penray Hg lamp) in a 0.98 cm flow-through quartz cell.

Absolute ClO concentrations were determined by the titration reaction:



($k_4 = 1.7 \times 10^{-11} \text{ cm}^3 \text{ molecule}^{-1} \text{ s}^{-1}$ [DeMore *et al.*, 1997]) and subsequent calibration of the NO_2 mass spectrometer signal. In order to reduce the background NO_2 contribution, the NO used in these experiments was first purified by the following process: The NO (CP grade) was condensed in a cold finger using liquid nitrogen, and then the resulting crystals were evacuated to remove volatile impurities such as N_2 and O_2 . After a couple of minutes of pumping, the cold finger was isolated from the pump and placed in a dry ice/ethanol bath, which vaporized the NO while leaving NO_2 in the condensed phase. The desired amount of NO was then mixed with N_2 (99.999%) and stored in a stainless steel cylinder.

In the titration reaction (4), the production of Cl atoms was a concern because the excess O_3 used in the experiments could lead to regeneration of ClO via reaction 2. Furthermore, the additional ClO created by regeneration could then go on to react with any excess NO in the flow tube to create more Cl atoms, resulting in a significant overestimation of the ClO concentration. In principle, the titration chemistry could have been modeled to account for the ClO regeneration. However, the extreme non-linearity of the chemistry made the modeling procedure very sensitive to small errors in the input parameters such as reaction time and initial concentrations. Instead, an excess of ethane ($\sim 5 \times 10^{13} \text{ molecule cm}^{-3}$) injected at the rear of the flow tube was used to scavenge the Cl atoms during the ClO titrations:



($k_5 = 5.7 \times 10^{-11} \text{ cm}^3 \text{ molecule}^{-1} \text{ s}^{-1}$ [DeMore *et al.*, 1997]). Ethane was chosen as a scavenger because of its relatively fast rate of reaction with Cl (almost 5 times faster than the $\text{O}_3 + \text{Cl}$ reaction). The HCl product of reaction 5 is stable and did not interfere with the titration chemistry. However, the C_2H_5 product reacts with NO_2 :



($k_6 = 4.5 \times 10^{-11} \text{ cm}^3 \text{ molecule}^{-1} \text{ s}^{-1}$ [Mallard *et al.*, 1994]) which resulted in a slight underestimation of the ClO concentration. Modeling of the titration reaction system was used to correct for this underestimation, and in almost all cases the correction factor was less than 15%. In principle, the following side reaction also could have affected the titration chemistry:



($k_7 = 1.8 \times 10^{-14} \text{ cm}^3 \text{ molecule}^{-1} \text{ s}^{-1}$ [DeMore *et al.*, 1997]). However, the rate of this reaction is relatively slow. Nonetheless, reaction 7 was included in the model of the titration chemistry, and so any small effect of reaction 7 on the observed NO_2 signal was taken into account in the modeling procedure. Overall, the modeling procedure used for the ClO titration was found to be relatively insensitive to small errors in the input parameters. A sample ClO calibration curve is shown in Figure 2. For this study, ClO concentrations ranged from 0.5 to $3.0 \times 10^{12} \text{ molecule cm}^{-3}$.

OH(D) was generated by the following reaction:



($k_8 = 1.3 \times 10^{-10} \text{ cm}^3 \text{ molecule}^{-1} \text{ s}^{-1}$ [DeMore *et al.*, 1997]). Because OH(D) was introduced through a movable injector where the corresponding concentrations are ~ 40 times higher than in the main flow tube, the reaction of OH(D) with NO_2 :



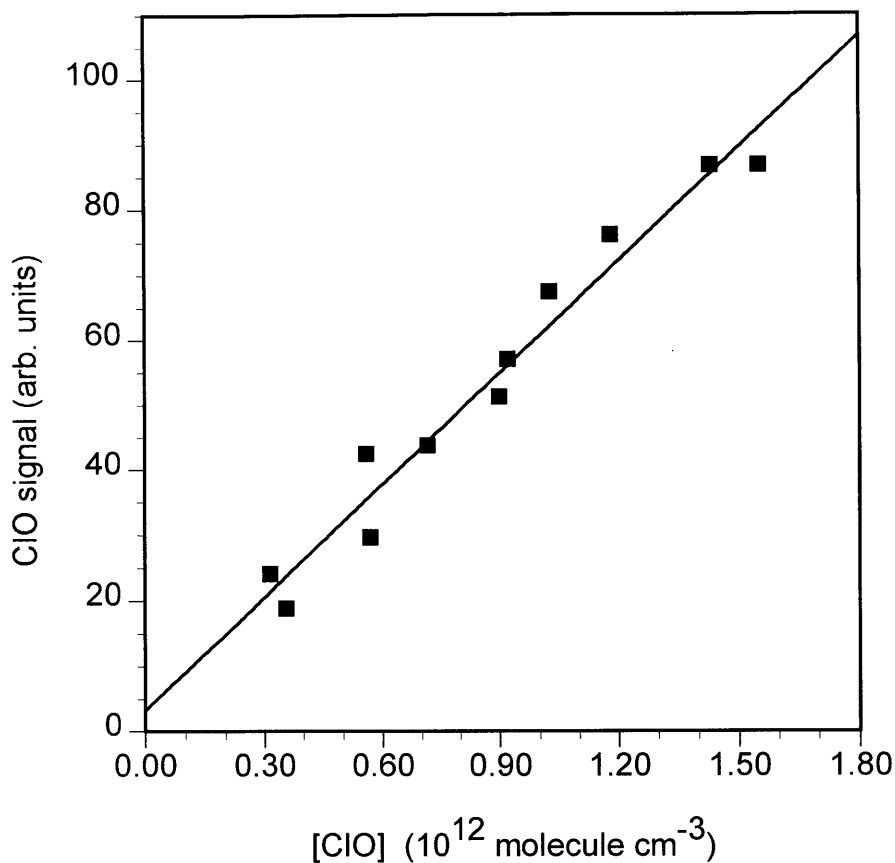


Figure 2. ClO calibration plot

($k_9 = 3.4 \times 10^{-12}$ cm^3 molecule $^{-1}$ s $^{-1}$ at 100 Torr [DeMore *et al.*, 1997]) was a concern in the production of OH(D) by reaction 8. By taking advantage of the long lifetime of H(D) atoms, this difficulty was surmounted by using a nested injector, which kept the H(D) atoms (entrained in the inner 3 mm Pyrex tube) and NO₂ molecules (entrained in the outer 6 mm Pyrex tube) separate throughout all but the last 1 cm of the injector. The H(D) atoms were allowed to mix with an excess of NO₂ ($\sim 10^{13}$ molecule cm^{-3} inside the injector) for only about 1 ms, allowing reaction 8 to virtually go to completion, but preventing significant loss of OH(D) due to reaction 9. H(D) atoms were generated by combining a 1.0 STP L min $^{-1}$ flow of helium (99.999 %) with a 0.1-0.4 STP mL min $^{-1}$

flow of a 2 % H₂ (99.999 %) or D₂ (99.995%)/He mixture which then passed through a molecular sieve trap immersed in liquid nitrogen and finally through a microwave discharge produced by a Beenakker cavity operating at 70 W.

Although reaction 9 was minimized in the production of OH(D), this reaction proved to be a convenient titration method for determining absolute concentrations of OH(D). An excess of NO₂ was used to convert all of the OH(D) into H(D)NO₃ followed by calibration of the H(D)NO₃ mass spectrometer signal using a bubbler containing 60% HNO₃ solution by weight, immersed in an ice-water bath. In determining the absolute concentrations of OD, it was assumed that the DNO₃ and HNO₃ mass spectrometer signals had the same sensitivity. The HNO₃ solution from the bubbler was periodically titrated with NaOH to confirm the long-term stability of the solution. Even after several months of use, the bubbler solution was found to have the same composition as the original stock solution. A sample OH calibration curve is shown in Figure 3. OH(D) concentrations used in this study ranged from 0.5 to 2.0 x 10¹¹ molecule cm⁻³. In order to insure pseudo-first-order kinetic conditions, [OH(D)] was kept at most one-tenth as large as [ClO].

3.2.2 Radical Production: Branching Ratio Experiments

Due to the large background of HCl produced by the ClO source, OD was used instead of OH in the branching ratio experiments. For the branching ratio studies, ClO was generated by reaction 2 in a double-nested movable injector. For these experiments, the chlorine atoms were produced by combining a 4.0 STP L min⁻¹ flow of helium (99.999 %), which had passed through a molecular sieve trap immersed in liquid nitrogen, with a 0.3-1.0 STP mL min⁻¹ flow of a 5 % Cl₂ (>99.9 %)/He mixture which then passed through a microwave discharge produced by a Beenakker cavity operating at 70 W. To generate ClO, the chlorine atoms were mixed with an excess of O₃ (~ 10¹³ molecule cm⁻³) throughout the whole length of the movable injector to ensure minimal

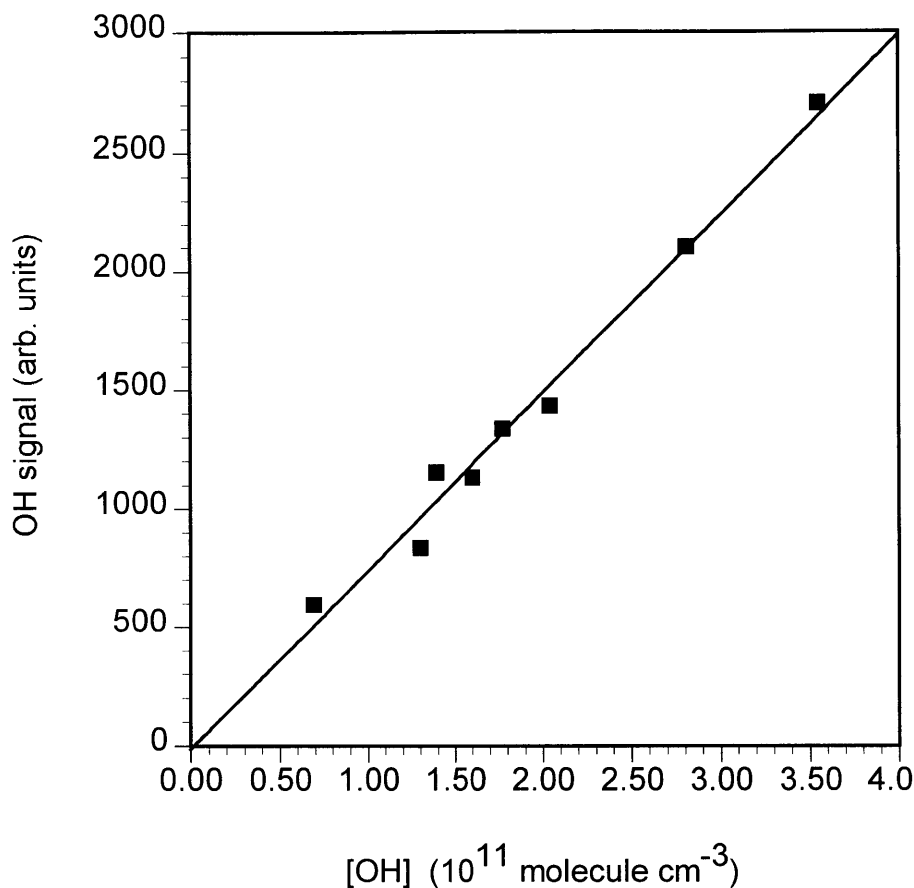


Figure 3. OH calibration plot

concentrations of chlorine atoms in the main flow. The large excess of O_3 also helped to scavenge Cl atoms produced by the main channel of reaction 1, and therefore helped to minimize production of background DCl due to the reaction:



($k_{10} = 3.2 \times 10^{-11} \text{ cm}^3 \text{ molecule}^{-1} \text{ s}^{-1}$ [DeMore *et al.*, 1997]). Since reaction 10 is relatively fast, and DO_2 and Cl are the major products of reaction 1, reaction 10 was found to be the largest potential source of DCl background. Absolute ClO concentrations were measured

using the technique described earlier.

For the branching ratio studies, OD was generated by reaction 8 in the side arm of the flow tube. D atoms were generated by combining a 0.2 STP L min⁻¹ flow of helium (99.999 %) with a 0.1-0.4 STP mL min⁻¹ flow of a 2 % D₂ (99.995%)/He mixture which then passed through a molecular sieve trap immersed in liquid nitrogen and finally through a microwave discharge produced by a Beenakker cavity operating at 70 W. The D atoms were then mixed with an excess of NO₂ to ensure that practically no deuterium atoms were introduced into the main flow. The experimental conditions were optimized in order to minimize background DCl production from the reaction:



($k_{11} = 1.4 \times 10^{-11} \text{ cm}^3 \text{ molecule}^{-1} \text{ s}^{-1}$ [Mallard *et al.*, 1994]). Absolute DCl concentrations were determined by calibration of the DCl mass spectrometer signal using a bubbler containing 20% DCl/D₂O solution by weight, immersed in an ice-water bath. The vapor pressure of HCl for a 20% HCl/H₂O solution by weight at 0° C is 0.038 Torr [Fritz and Fuget, 1956]. For the DCl calibration it was assumed that the 20% DCl solution had the same vapor pressure as the 20% HCl solution. An intercomparison of two bubblers, one containing a 20% DCl solution and the other containing a 20% HCl solution, showed that the DCl and HCl mass spectrometer signals were in very good agreement for the same nitrogen flow. At low temperatures the DCl from the bubbler took a long time to equilibrate. For reasons of convenience, calibrations of the DCl signal at low temperatures were also made by reacting an excess of D atoms with a known amount of Cl₂. The two methods of DCl calibration were in very good agreement.

3.2.3 Detection of Reactants and Products

Most of the chemical species relevant to this study (OH(D), ClO, H(D)O₂, H(D)Cl,

Cl₂, O₃, NO₂, and H(D)NO₃) were chemically ionized with the SF₆⁻ reagent ion and then detected with the quadrupole mass spectrometer. The ion source, ion focusing lenses, pumps and quadrupole mass spectrometer were very similar to the set-up used for the HO₂ + BrO experiments, described in detail in Chapter 2. SF₆⁻ was produced in the ion source by combining a 2.5 STP L min⁻¹ flow of nitrogen with a 0.4 STP mL min⁻¹ flow of a 5 % SF₆/N₂ mixture which then passed over the electric discharge. In the chemical ionization scheme employed here, OH(D), ClO, Cl₂, O₃ and NO₂ were detected as their parent negative ions by charge-transfer reactions with SF₆⁻:



The rate constant for reaction 12 has been estimated by *Lovejoy et al.* [1990] to be $2 \times 10^{-9} \text{ cm}^3 \text{ molecule}^{-1} \text{ s}^{-1}$. The rate constant for reaction 13 has not been measured. The rate constants for reactions 14, 15 and 16 are 1.1×10^{-10} , 1.2×10^{-9} and $1.4 \times 10^{-10} \text{ cm}^3 \text{ molecule}^{-1} \text{ s}^{-1}$, respectively [*Huey et al.*, 1995]. H(D)Cl and H(D)NO₃ were detected as FH(D)Cl⁻ and FH(D)NO₃⁻ through fluoride-transfer reactions with SF₆⁻:



The rate constants for reactions 17 and 18 are 1.5×10^{-9} and $2.0 \times 10^{-9} \text{ cm}^3 \text{ molecule}^{-1} \text{ s}^{-1}$, respectively [*Huey et al.*, 1995]. H(D)O₂ was detected as SF₄O₂⁻, generated presumably through a multi-step pathway.

The ion-molecule region was kept at a lower pressure (15 Torr) than the neutral flow tube (100 Torr). The drop in pressure lowered the concentrations of the neutrals in the ion-molecule region, thus decreasing the rates of potential ion-molecule side reactions. In the previous study of $\text{HO}_2 + \text{NO}$ from our laboratory [Seeley *et al.*, 1996], it was reported that the OH^- mass spectrometer signal was not proportional to $[\text{OH}]$ possibly due to secondary reactions. It is likely that those secondary reactions were taking place in the ion-molecule region, which was kept at the same pressure as the neutral flow tube (70-190 Torr). In this study, we found that the OH(D)^- signal was proportional to $[\text{OH(D)}]$ as determined by titration with NO_2 and subsequent calibration of the H(D)NO_3 mass spectrometer signal. Presumably, the lower concentrations of neutrals in the ion-molecule region helped to decrease secondary reactions involving OH^- , therefore making it possible to use this signal for detection of OH. The lower neutral concentrations in the ion-molecule region also helped to prevent depletion of the SF_6^- reagent ions due to reaction with species in large excess, such as O_3 .

3.3 Results and Discussion

In the earlier study of $\text{HO}_2 + \text{NO}$ from our laboratory, it was reported that our chemical ionization detection scheme resulted in sensitivities of 100, 200 and 1000 ppt (at 100 Torr) for NO_2 , HO_2 , and OH, respectively [Seeley *et al.*, 1996]. Although we did not carry out formal calibrations of the mass spectrometer for all of the chlorine species (e.g., Cl_2 , ClO), it was apparent that these species could be detected with a similar sensitivity to that obtained for NO_2 . The mass spectrometer signals for these compounds were found to be linear over the range of concentrations used in this work. The stated sensitivity was more than adequate for the present work; actually, it was necessary to degrade the sensitivity of the spectrometer (by decreasing the ion-molecule reaction time) to allow the introduction of greater amounts of reactants without depleting the SF_6^- reagent ions or inducing complications from secondary ion-molecule processes.

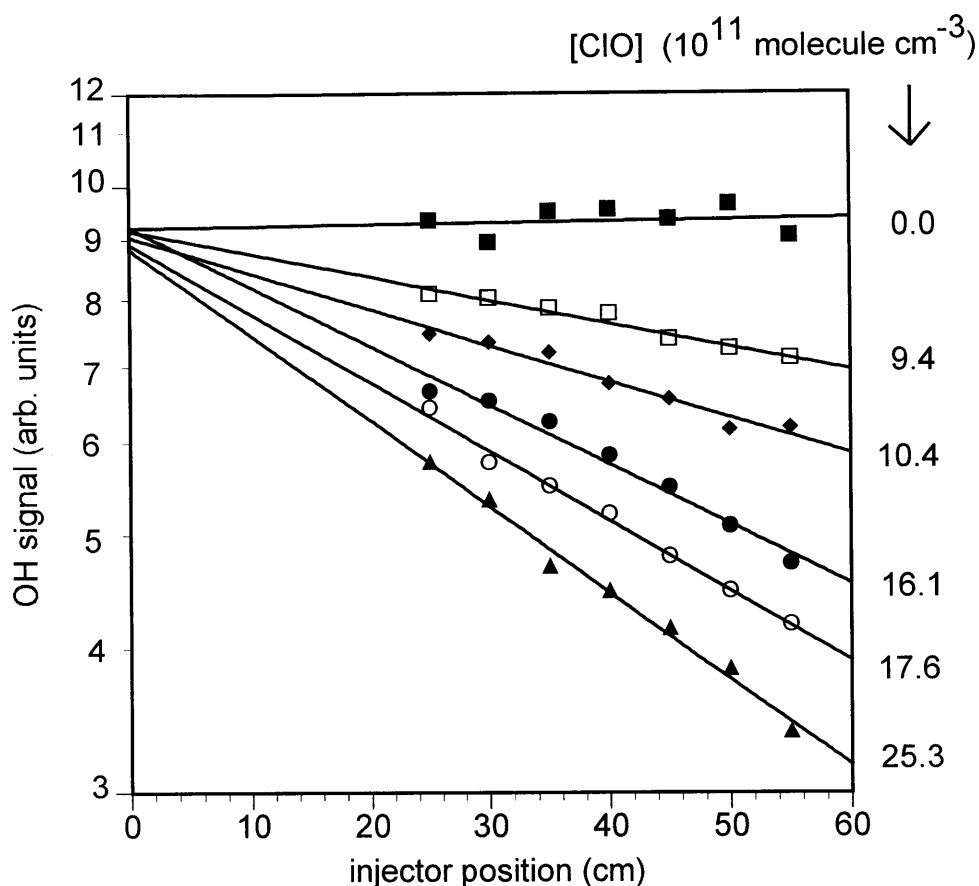


Figure 4. Typical set of OH signals as a function of injector distance. This data set was obtained under the following conditions: $P = 100$ Torr; $T = 298$ K; average velocity = 2100 cm s^{-1} ; Reynolds number = 4010.

3.3.1 Overall Rate Constant Measurements

Bimolecular rate constants were obtained via the usual pseudo-first-order approximation method, using ClO as the excess reagent. Typical OH decay curves as a function of injector distance are shown in Figure 4. The first-order rate constants obtained from fitting the OH decay curves were plotted against [ClO] in order to determine the bimolecular rate constant, as shown in Figure 5. This approach for determining bimolecular rate constants assumes that deviations from the plug flow

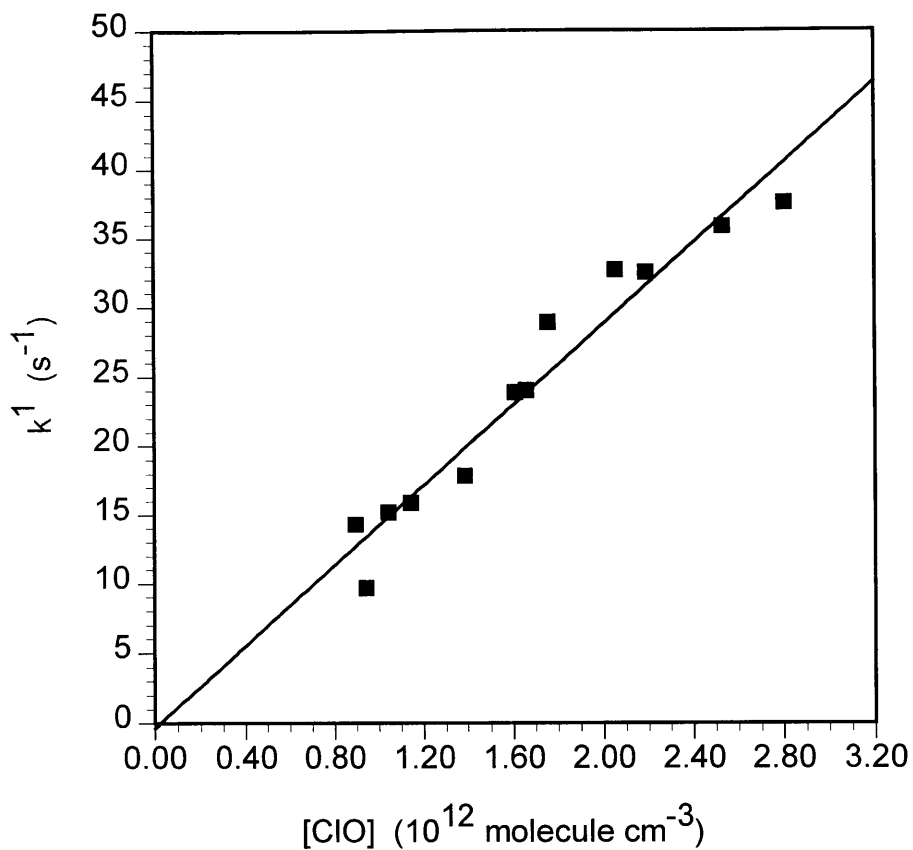


Figure 5. Typical plot of k^1 as a function of [ClO]. This plot was obtained under the same conditions as listed in Figure 4.

approximation are negligible. Under the conditions present in our turbulent flow tube, *Seeley et al.* [1996] estimated that these deviations result in apparent rate constants which are at most 8 % below the actual values. Hence, the flow corrections were neglected as they are smaller than the sum of the other likely systematic errors in the measurements of gas flows, temperature, detector signal, pressure and absolute ClO concentrations. Indeed, we consider the major source of error in our experiments to arise from the determination of [ClO] from the titration procedure outlined above. Considering such sources of error, we estimate that rate constants can be determined with an accuracy of $\pm 30\%$ (2σ).

Table 1. Summary of Experimental Conditions and Measured Overall Rate Constants for the OH + ClO Reaction

T (K)	P (Torr)	Velocity (cm s ⁻¹)	Reynolds number	k ± 2σ (10 ⁻¹¹ cm ³ molecule ⁻¹ s ⁻¹)
298	97	2120	3910	1.36 ± 0.32
298	100	2100	4010	1.46 ± 0.22
298	91	2060	3510	1.47 ± 0.24
298	93	1950	3510	1.53 ± 0.12
280	92	2140	4100	1.72 ± 0.34
252	93	2080	4880	1.58 ± 0.46
247	90	1980	4600	1.80 ± 1.06
243	95	1960	5100	1.66 ± 0.80
234	96	2090	5750	1.90 ± 0.32
224	94	1920	5600	1.91 ± 0.56
224	93	2070	5980	2.15 ± 0.32
215	94	2025	6450	2.26 ± 0.38
214	92	1980	6200	1.97 ± 0.54
208	93	2050	7020	2.38 ± 0.62

A complete list of experimental conditions and measured rate constants is presented in Table 1. We performed four separate determinations of the overall rate constant for OH + ClO at 298 K and arrived at the mean value of $k_1 = (1.46 \pm 0.23) \times 10^{-11} \text{ cm}^3 \text{ molecule}^{-1} \text{ s}^{-1}$; the uncertainty represents the two standard deviation statistical error in the data and is not an estimate of systematic errors. Table 2 contains a comparison of all reported rate constants for the OH + ClO reaction. Our value lies roughly in the middle of the range of reported rate constants at 298 K, and the overlap of uncertainty ranges makes our work consistent with all previous measurements except the lowest value reported by *Leu and Lin* [1979]. However, as *Hills and Howard* [1984] have pointed out, the reported values of *Leu and Lin* are probably too low because these authors did not correct their results for the effect of OH regeneration by reaction 3. A correction is necessary because *Leu and Lin* used an excess of Cl in their production of ClO by

Table 2. Comparison of Measured Overall Rate Constants for the OH + ClO Reaction

Technique	T (K)	P (Torr)	$K_{298\text{K}}$ (10^{-11} cm ³ molecule ⁻¹ s ⁻¹)	Ea/R (K)	Reference
DF-LF/RF	298	1.0-3.5	0.91 ± 0.13	—	Leu and Lin [1979]
DF-LF/RF	248-335	1.0	1.17 ± 0.33	-66	Ravishankara et al. [1983]
DF-LF/RF	243-298	1.0-5.0	1.19 ± 0.32	—	Burrows et al. [1984]
DF-LF/LMR	219-373	1.0	1.75 ± 0.31	-235	Hills and Howard [1984]
DF-LF/LIF	298	0.5-0.9	1.94 ± 0.38	—	Poulet et al. [1986]
DF-TF/CIMS	208-298	100	1.46 ± 0.23	-292	This work: Lipson et al. [1997]

DF, discharge flow; LF, laminar flow; TF, turbulent flow; RF, resonance fluorescence detection; LMR, laser magnetic resonance detection; LIF, laser-induced fluorescence detection; CIMS, chemical ionization mass spectrometry detection.

reaction 2 or by the reaction $\text{Cl} + \text{Cl}_2\text{O} \rightarrow \text{ClO} + \text{Cl}_2$. *Ravishankara et al.* [1983] also used an excess of Cl in the production of ClO, and they reported a 26% correction factor due to OH regeneration. The regeneration of OH was not a concern in our experiments because the excess of O₃ used to produce ClO in our system effectively scavenged Cl atoms, including those produced by reaction 1a. A second reason why the value of *Leu and Lin* may be too low is that they did not perform absolute titrations of ClO. *Leu and Lin* and also *Ravishankara et al.* assumed that the concentrations of ClO produced were equal to the initial concentrations of O₃ or Cl₂O as determined by optical absorption. However, neither study took into account possible loss mechanisms for ClO, such as self-reaction or wall loss. The loss of ClO in a small diameter inlet has been observed to be as large as 50% [*Poulet et al.*, 1986]. An overestimation of ClO concentrations will lead to an underestimation of the rate constant. In our experiments the ClO concentrations were

determined directly by absolute titration, as described in the Experimental Section. The good agreement between our reported rate constant at 100 Torr and previous measurements made at low pressure (~1 Torr) suggests that the overall rate of reaction 1 does not have a significant pressure dependence.

We performed several measurements of the overall rate constant for OH + ClO at temperatures between 208 and 298 K in order to establish the temperature dependence of the rate constant for conditions relevant to the stratosphere. From the data listed in Table 1 and plotted in Figure 6, we obtain the Arrhenius expression $k(T) = (5.5 \pm 1.6) \times 10^{-12} \exp[(292 \pm 72) / T] \text{ cm}^3 \text{ molecule}^{-1} \text{ s}^{-1}$. Compared to the results of *Hills and Howard* [1984], our calculated negative activation energy is ~25% larger and our pre-exponential factor is ~30% smaller. However, these differences result in only a ~10% difference in the rate constant at stratospheric temperatures, compared to the value of *Hills and Howard*. Given the range of uncertainties, the agreement is very good. The two other temperature dependence studies of the OH + ClO reaction reported that the overall rate constant was independent of temperature [*Ravishankara et al.*, 1983; *Burrows et al.*, 1984]. *Ravishankara et al.* did measure a small negative temperature dependence, but they chose to report that k_1 was temperature independent because their temperature coefficient was not statistically significant due to the large uncertainty. The current JPL recommendation [*DeMore et al.*, 1997] for the temperature dependence of the overall rate constant for OH + ClO is: $k(T) = 1.1 \times 10^{-11} \exp[120 / T] \text{ cm}^3 \text{ molecule}^{-1} \text{ s}^{-1}$ based on the results of *Hills and Howard*, *Burrows et al.* and *Poulet et al.* The results of *Leu and Lin* and *Ravishankara et al.* were not used in deriving the recommended value because the concentration of ClO (excess reagent) was not determined directly in these studies.

The research group of A. R. Ravishankara has very recently completed another study of the temperature dependence of the overall rate constant for the OH + ClO reaction [*Kegley-Owen et al.*]. In this study, conducted at pressures ranging from 5 to 15 Torr and at temperatures ranging from 234 to 356 K, decays of OH were detected by laser induced

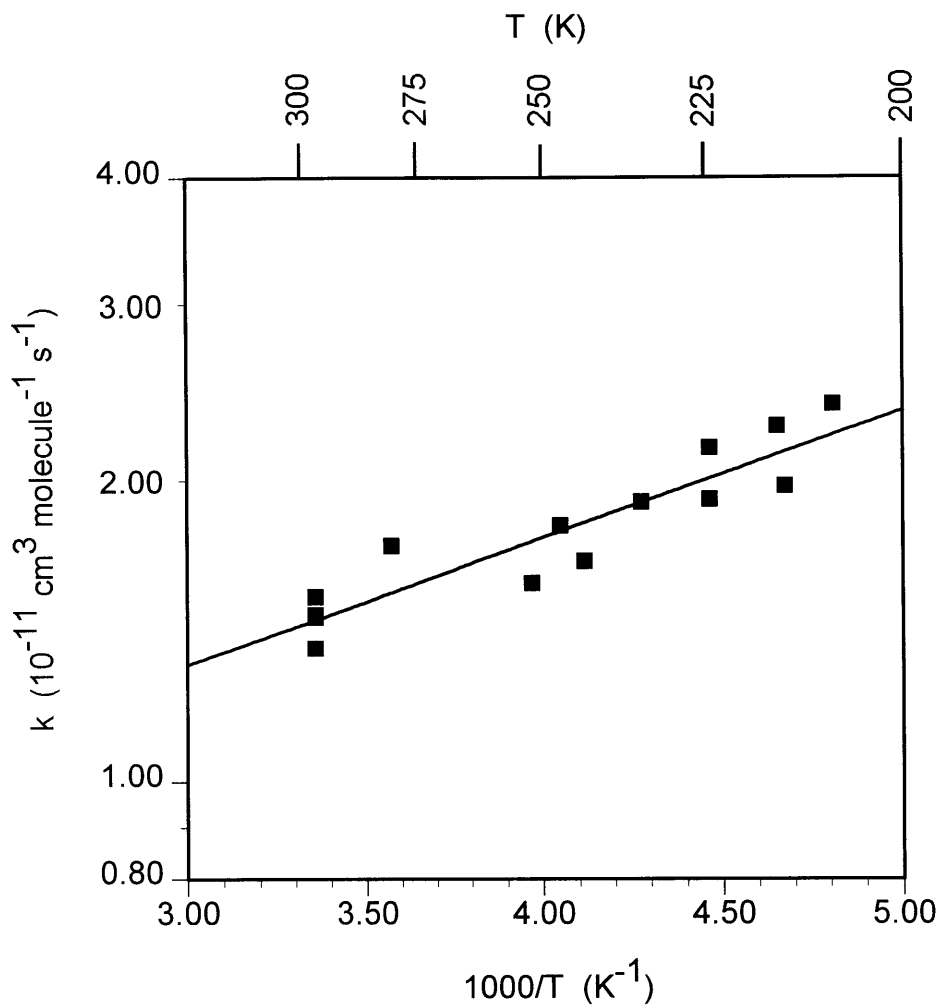


Figure 6. Arrhenius plot for the overall reaction OH + ClO; the least-squares fit to the data yields the expression $k(T) = (5.5 \pm 1.6) \times 10^{-12} \exp[(292 \pm 72)/T]$ cm³ molecule⁻¹ s⁻¹.

Table 3. Summary of Experimental Conditions and Measured Overall Rate Constants for the OD + ClO Reaction

T (K)	P (Torr)	Velocity (cm s ⁻¹)	Reynolds number	k ± 2σ (10 ⁻¹¹ cm ³ molecule ⁻¹ s ⁻¹)
298	99	1840	3460	0.91 ± 0.22
298	90	1920	3200	1.09 ± 0.26
298	91	2000	3540	1.17 ± 0.20
262	98	2090	4770	1.45 ± 0.28
252	94	2090	4910	1.21 ± 0.34
242	90	1800	4250	1.29 ± 0.24
233	90	2045	5290	1.48 ± 0.44
224	91	2080	5870	1.31 ± 0.20
223	92	2050	5700	1.54 ± 0.16
212	91	1840	5800	1.47 ± 0.28
204	90	2060	6820	1.75 ± 0.14

fluorescence in the presence of excess ClO. Absolute ClO concentrations were determined by UV/Visible absorption spectroscopy. Our measured rate constants are approximately 40% lower than the results of *Kegley-Owen et al.* at all temperatures; our pre-exponential factor is about 40% lower, but our calculated negative activation energy is in excellent agreement with the results of this recent study.

We also measured the overall rate constant for the OD + ClO reaction at temperatures between 204 and 298 K, using the same method as described above for the OH + ClO reaction. Table 3 contains a complete list of experimental conditions and measured rate constants for the OD + ClO reaction. From the data listed in Table 3 and plotted in Figure 7, we obtain the Arrhenius expression $k(T) = (4.2 \pm 2.0) \times 10^{-12} \exp [(280 \pm 114) / T] \text{ cm}^3 \text{ molecule}^{-1} \text{ s}^{-1}$. There have been no previous studies of this reaction. The Arrhenius expressions for OH + ClO and OD + ClO are similar, indicating that the isotope effect on the overall rate of reaction 1 is small.

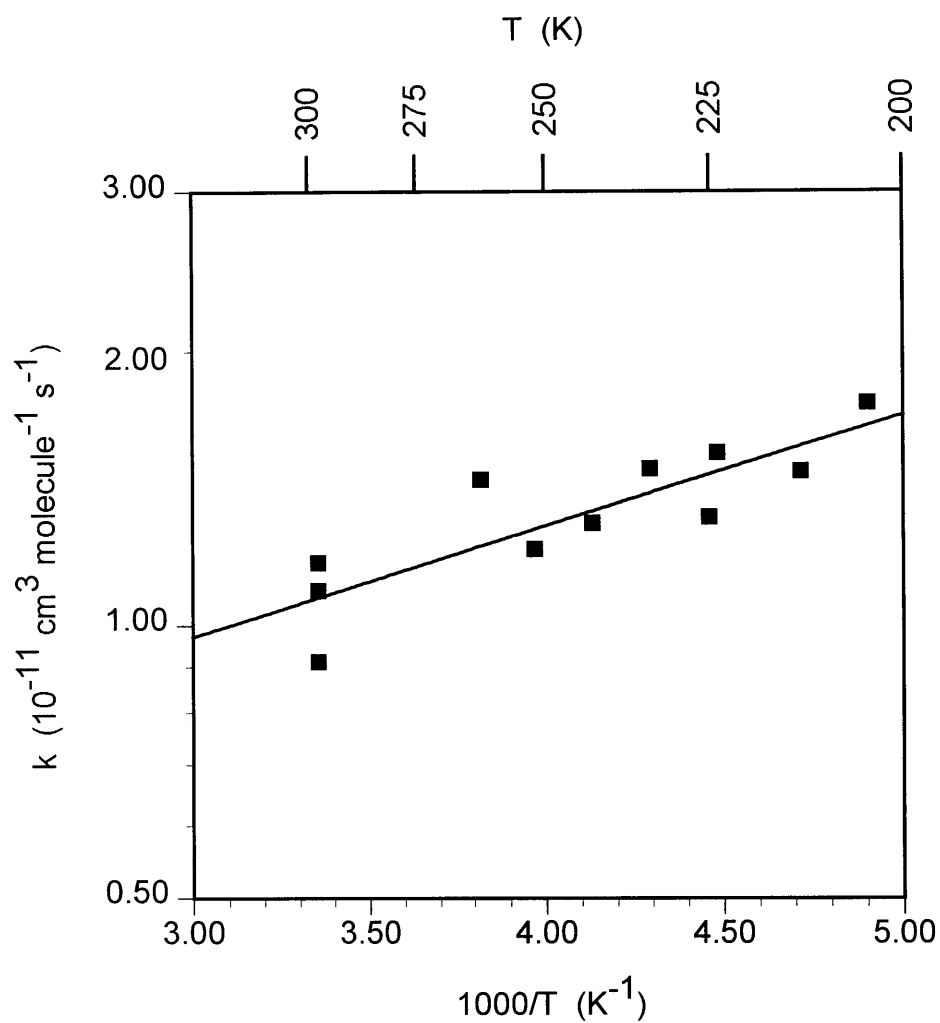


Figure 7. Arrhenius plot for the overall reaction $\text{OD} + \text{ClO}$; the least-squares fit to the data yields the expression $k(T) = (4.2 \pm 2.0) \times 10^{-12} \exp[(280 \pm 114)/T] \text{ cm}^3 \text{ molecule}^{-1} \text{ s}^{-1}$

3.3.2 Branching Ratio Experiments

The large background level of HCl ($\sim 10^{11}$ molecule cm^{-3}) from the ClO source made it difficult to detect small amounts of HCl produced by reaction 1b over the experimental reaction time. The HCl background in our system was most likely due to trace impurities of H_2 in the helium sweep gas used to flush Cl_2 through the microwave discharge in the ClO source. Although 99.999 % pure helium was used, the manufacturer specifications indicate levels of H_2 up to 1 ppm. Before mixing with Cl_2 , the helium was first sent through a molecular sieve trap immersed in liquid nitrogen in order to remove impurities. Unfortunately, molecular hydrogen cannot be trapped out at liquid nitrogen temperatures. If 1 ppm of H_2 ($\sim 10^{12}$ molecule cm^{-3}) was present and sent through the microwave discharge in the presence of chlorine, it could certainly have produced enough H atoms to create background HCl levels on the order of 10^{11} molecule cm^{-3} . In theory, this problem could be solved by using a thermal dissociation source for chlorine instead of a microwave discharge source. Efforts to reduce the HCl background level produced by the ClO source will be discussed in Chapter 4.

Because of the uncertainty created by a large HCl background, we used OD instead of OH for the branching ratio experiments. Since there was almost no DCl background from the ClO source, we were able to observe production of very small concentrations of DCl ($\sim 10^9$ molecule cm^{-3}) over the reaction time (~ 20 ms) which we have positively identified as coming from reaction 1b. Figure 8 shows that the rise of DCl is easily observed above the small background noise. In Figure 8, the DCl rise (black squares) has been overlaid on the background DCl signal (open squares) in order to demonstrate that the DCl rise is much larger than the $\pm 2\sigma$ level of the background noise. Under the optimal experimental conditions ($[\text{ClO}] \sim 1 \times 10^{12}$ molecule cm^{-3} and $[\text{OD}] \sim 1 \times 10^{11}$ molecule cm^{-3}), modeling shows that side reactions can only produce concentrations of DCl ($\sim 10^8$ molecule cm^{-3}) that are less than the detection limit of the instrument (~ 50 ppt). Table 4 contains a list of the reactions used in the modeling. The following side

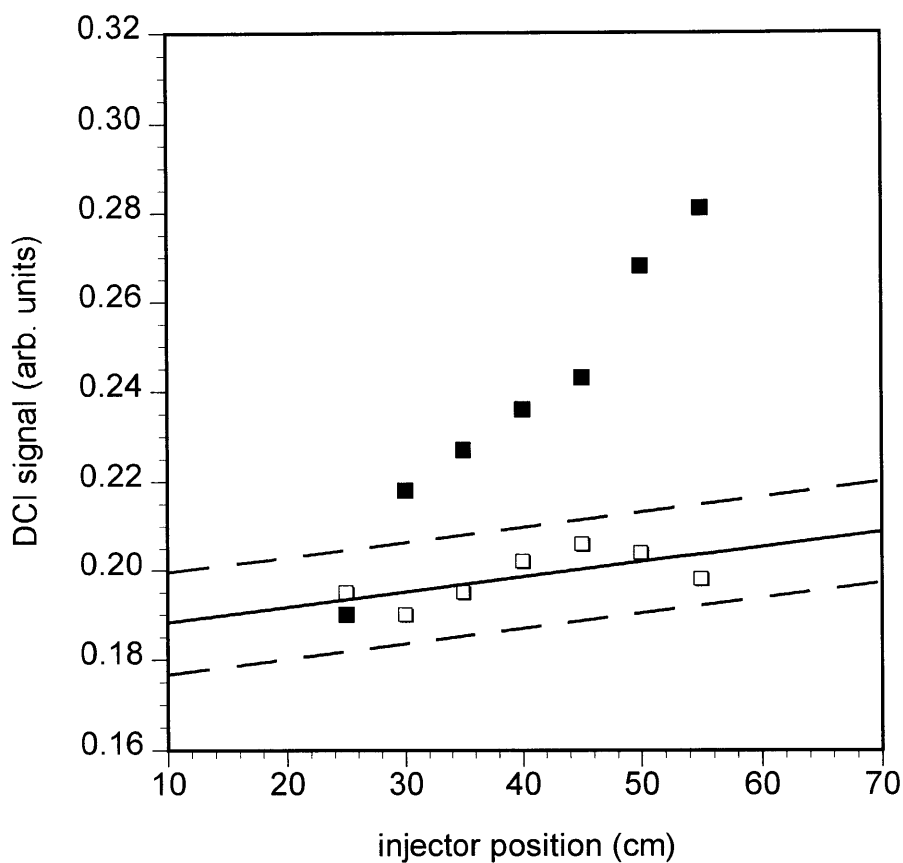


Figure 8. Observed production of DCI ($[\text{DCI}] = 1.4 \times 10^9 \text{ molecule cm}^{-3}$) from reaction 1b (■) above the small DCI background level (□) as a function of injector distance. A least-squares fit to the DCI background data was performed, and the dotted lines represent the $\pm 2\sigma$ level. This data set was obtained under the following conditions: $P = 96 \text{ Torr}$; $T = 298 \text{ K}$; average velocity = 1975 cm s^{-1} ; Reynolds number = 3350; $[\text{OD}]_0 = 1.4 \times 10^{11} \text{ molecule cm}^{-3}$; $[\text{ClO}]_0 = 8.3 \times 10^{11} \text{ molecule cm}^{-3}$.

Table 4. Chemical Reactions Used in Computer Simulations for the Branching Ratio Studies of the OD + ClO Reaction

Reaction	k (cm ³ molecule ⁻¹ s ⁻¹)
OD + ClO → DO ₂ + Cl	1.1 x 10 ⁻¹¹
OD + ClO → DCl + O ₂	see text
Cl + DO ₂ → DCl + O ₂	3.2 x 10 ⁻¹¹
Cl + DO ₂ → OD + ClO	9.1 x 10 ⁻¹²
Cl + O ₃ → ClO + O ₂	1.2 x 10 ⁻¹¹
Cl + D ₂ → DCl + D	1.6 x 10 ⁻¹⁴
Cl + NO ₂ + M → ClONO + M	3.3 x 10 ⁻¹²
D + Cl ₂ → DCl + Cl	1.4 x 10 ⁻¹¹
D + O ₃ → OD + O ₂	2.9 x 10 ⁻¹¹
D + NO ₂ → OD + NO	1.3 x 10 ⁻¹⁰
OD + O ₃ → DO ₂ + O ₂	6.8 x 10 ⁻¹⁴
OD + Cl ₂ → DOCl + Cl	6.7 x 10 ⁻¹⁴
OD + OD → D ₂ O + O	1.5 x 10 ⁻¹²
OD + OD + M → D ₂ O ₂ + M	1.4 x 10 ⁻¹²
OD + DO ₂ → D ₂ O + O ₂	1.1 x 10 ⁻¹⁰
OD + NO ₂ + M → DNO ₃ + M	3.4 x 10 ⁻¹²
OD + NO + M → DONO + M	1.7 x 10 ⁻¹²
OD + DCl → D ₂ O + Cl	1.3 x 10 ⁻¹³
ClO + ClO → products	7.7 x 10 ⁻¹⁴
ClO + DO ₂ → DOCl + O ₂	5.0 x 10 ⁻¹²
ClO + NO → NO ₂ + Cl	1.7 x 10 ⁻¹¹
ClO + NO ₂ + M → ClONO ₂ + M	4.6 x 10 ⁻¹³
DO ₂ + DO ₂ → D ₂ O ₂ + O ₂	6.0 x 10 ⁻¹³
DO ₂ + NO ₂ + M → DO ₂ NO ₂ + M	3.8 x 10 ⁻¹³
DO ₂ + NO → NO ₂ + OD	1.1 x 10 ⁻¹¹

Rate constants are from *DeMore et al.* [1997] and *Mallard et al.* [1994], at 298 K and 100 Torr.

reactions can produce DCl in our system:



In our experiments, the source conditions for OD and ClO were optimized in order to prevent stray D and Cl atoms from entering the main flow tube. Modeling of the OD source shows that the concentration of D atoms was small enough that reaction 11 was negligible as a source of DCl. Furthermore, reaction 19 is too slow to be important in our reaction system ($k_{19} = 1.6 \times 10^{-14} \text{ cm}^3 \text{ molecule}^{-1} \text{ s}^{-1}$ [Mallard *et al.*, 1994]). Reactions 11 and 19 combined to produce DCl concentrations far below the detection limit of the instrument. Reaction 10 was more difficult to avoid because DO_2 and Cl are the products of reaction 1a, the main channel of the OD + ClO reaction. However, modeling shows that the large excess of O_3 , used to generate ClO, was efficient in scavenging Cl atoms produced in the main flow tube. Under optimal experimental conditions, reaction 10 produced levels of DCl ($\sim 10^8 \text{ molecule cm}^{-3}$) that were below the detection limit of the instrument.

Computer modeling was used to extract a rate constant for reaction 1b by fitting the observed DCl production. The model input included the initial concentrations of ClO, OD and of all precursors. Table 5 contains a list of the initial conditions and calculated rate constants (k_{1b}) for the branching ratio experiments. The observed DCl signal was found to increase linearly over the experimental reaction time as can be seen in Figure 8. Modeling confirms that the DCl signal is practically linear and does not approach its equilibrium level under typical experimental conditions and reaction times. The branching ratio for the OD + ClO reaction was measured at room temperature and at a pressure of 100 Torr under a variety of conditions to ensure that the results were

Table 5. Summary of Experimental Conditions and Calculated Rate Constants (k_{1b}) for the Branching Ratio Studies of the OD + ClO Reaction

Expt. #	T (K)	P (Torr)	[OD] ₀ (10^{11} molecule cm^{-3})	[ClO] ₀ (10^{11} molecule cm^{-3})	k_{1b} (10^{-13} cm^3 molecule ⁻¹ s ⁻¹)	Branching Ratio (k_{1b}/k_1)
1	298	94	1.0	8.8	5.3	0.049
2	298	94	3.6	8.6	5.6	0.052
3	298	93	1.4	12.4	5.8	0.054
4	298	96	1.4	8.3	5.9	0.055
5*	298	93	1.9	11.9	5.4	0.050
6	298	180	2.2	6.7	7.3	0.068
7	285	97	1.0	4.4	6.0	0.054
8	262	91	2.9	10.2	6.8	0.056
9	250	92	2.0	13.2	7.6	0.059
10	235	92	2.8	10.9	8.4	0.061
11	227	181	1.7	8.8	11.6	0.080
12	224	93	1.8	11.1	8.2	0.056
13	223	93	2.1	8.4	8.6	0.058
14	211	92	1.6	8.0	9.1	0.058

*Experiment 5 was conducted using an uncoated flow tube. For all other experiments the flow tube was coated with Halocarbon wax.

independent of the initial concentrations. The fitting procedure used to calculate k_{1b} is obviously sensitive to the initial concentrations of OD and ClO and to the observed concentration of DCl produced over a specific reaction time. These concentrations were measured to better than 30% accuracy; we found that these errors propagate linearly into the calculated branching ratio. In experiment 1, the optimal initial concentrations for OD and ClO were used, such that the observed DCl production was due to reaction 1b only. In experiment 2, the initial OD concentration was more than tripled compared to experiment 1. Under these conditions, modeling shows that ~20% of the observed DCl production was due to the side reaction $\text{DO}_2 + \text{Cl}$. Despite the very different initial conditions and the differing amounts of DCl production from side reactions, experiments

1 and 2 yielded very similar rate constants (5.3×10^{-13} and $5.6 \times 10^{-13} \text{ cm}^3 \text{ molecule}^{-1} \text{ s}^{-1}$, respectively). Therefore, the modeling approach appears to correctly simulate the chemistry in our system, yielding branching ratio results which are independent of the initial conditions.

Although modeling shows that for optimal initial conditions the observed DCI production cannot be due to homogeneous side reactions, the possibility exists that the DCI could be a result of heterogeneous reactions on the wall of the flow tube. Several experiments were performed that indicated that the observed DCI production was not due to heterogeneous processes. For most of the branching ratio studies a flow tube coated with Halocarbon wax was used in order to minimize OD wall loss. To check for a heterogeneous source of DCI, we performed one branching ratio experiment using an uncoated flow tube. If the DCI was being produced by heterogeneous reactions, an uncoated flow tube should lead to more observed DCI production, and therefore a larger calculated rate constant for reaction 1b. However, the results from experiment 5 for the uncoated flow tube show that the calculated rate constant ($5.4 \times 10^{-13} \text{ cm}^3 \text{ molecule}^{-1} \text{ s}^{-1}$) is well within the range of rate constants for the coated flow tube experiments. The excellent agreement between the coated and uncoated flow tube experiments indicates that the observed DCI production was not due to heterogeneous reactions on the wall of the flow tube.

A second experiment was performed to investigate the possibility of heterogeneous DCI production, in which we increased the total pressure in the flow tube by almost a factor of two. The molecular diffusion rate across the laminar sublayer at the walls of the flow tube decreases with increasing pressure [*Seeley et al.*, 1993]. Therefore, the effects of heterogeneous processes are reduced at higher pressures. However, as shown in Table 5, the measured rate constant for reaction 1b actually increased by ~35% at the higher pressure (180 vs. 95 Torr), at 298 and at 227 K, indicating that the observed DCI production over the experimental reaction time was not due to heterogeneous reactions.

The pressure dependence of the branching ratio will be investigated in more detail in Chapter 4.

We performed several measurements of the branching ratio for OD + ClO at temperatures between 211 and 298 K in order to establish the temperature dependence of the rate constant k_{1b} for conditions relevant to the stratosphere. From the data listed in Table 5 (for 100 Torr pressure) and plotted in Figure 9, we obtain the Arrhenius expression $k_{1b}(T) = (1.7 \pm 0.3) \times 10^{-13} \exp [(363 \pm 50) / T] \text{ cm}^3 \text{ molecule}^{-1} \text{ s}^{-1}$. The uncertainty represents the two standard deviation statistical error in the data and is not an estimate of systematic errors. The branching ratios (k_{1b}/k_1) reported in Table 5 were calculated using the measured Arrhenius expression for the overall rate constant of the OD + ClO reaction. As shown in Figure 10, the branching ratio (at 100 Torr pressure) ranges from 0.05 ± 0.02 at 298 K to 0.06 ± 0.02 at 211 K. The reported error for the branching ratio is an estimate of the systematic error and the uncertainty of the model fitting procedure based on a sensitivity analysis. The negative temperature dependence of k_{1b} possibly indicates that reaction 1b proceeds through an intermediate complex that is stabilized at low temperatures [e.g., *Mozurkewich and Benson*, 1984; *Smith*, 1991]. Mass spectral scans were recorded to investigate the possible presence of an intermediate complex, but we were unable to positively establish the existence of such a complex.

Our results for the branching ratio of reaction 1 are consistent with the results of previous studies, which are listed in Table 6. However, previous attempts to measure the branching ratio were unsuccessful in ruling out an HCl yield of zero for the minor channel, due to uncertainties in the results. *Leu and Lin* [1979] and *Burrows et al.* [1984] used chemical titration to convert the HO₂ formed by reaction 1a back into OH, which was then detected by resonance fluorescence. The ratio of [HO₂] formed (determined by the regeneration of OH) to [OH] lost was used to calculate the branching ratio. A problem with this indirect method is that the ratio of HO₂ formed to OH lost is not exactly equal to the branching ratio due to additional loss mechanisms for HO₂, such as

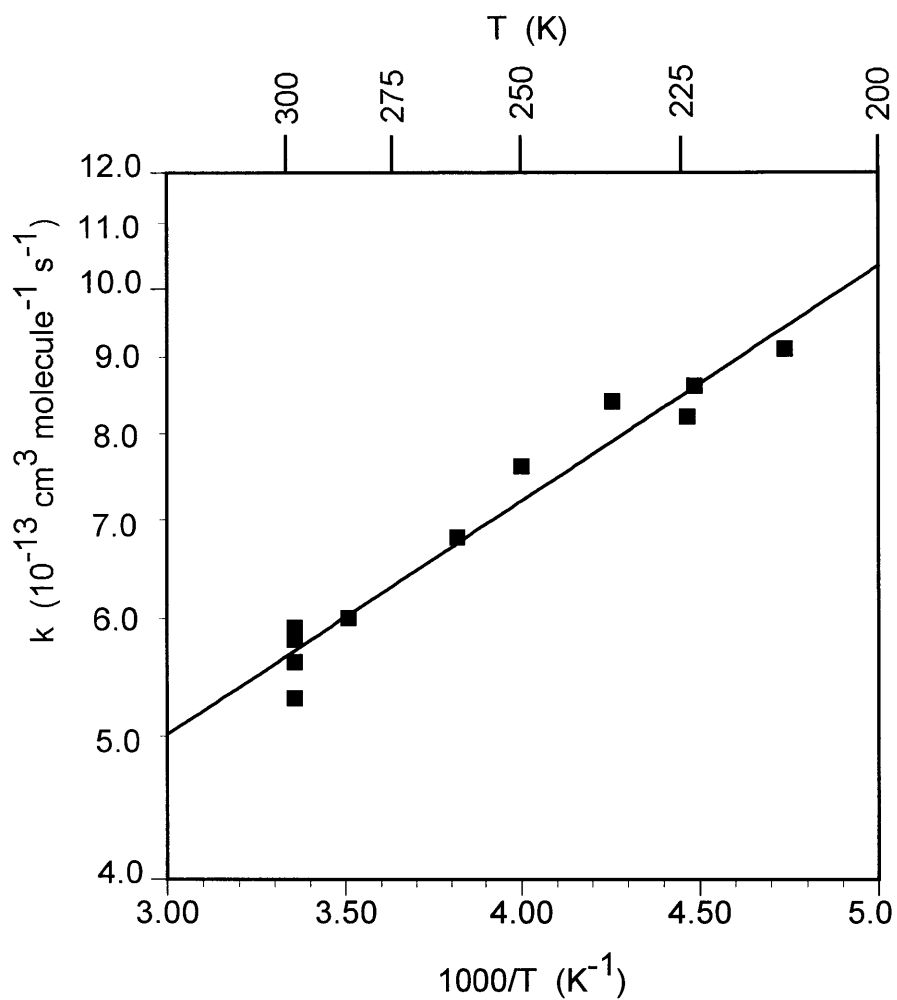


Figure 9. Arrhenius plot for the reaction $\text{OD} + \text{ClO} \rightarrow \text{DCl} + \text{O}_2$; the least-squares fit to the data yields the expression: $k_{1b}(T) = (1.7 \pm 0.3) \times 10^{-13} \exp[(363 \pm 50)/T] \text{ cm}^3 \text{ molecule}^{-1} \text{ s}^{-1}$.

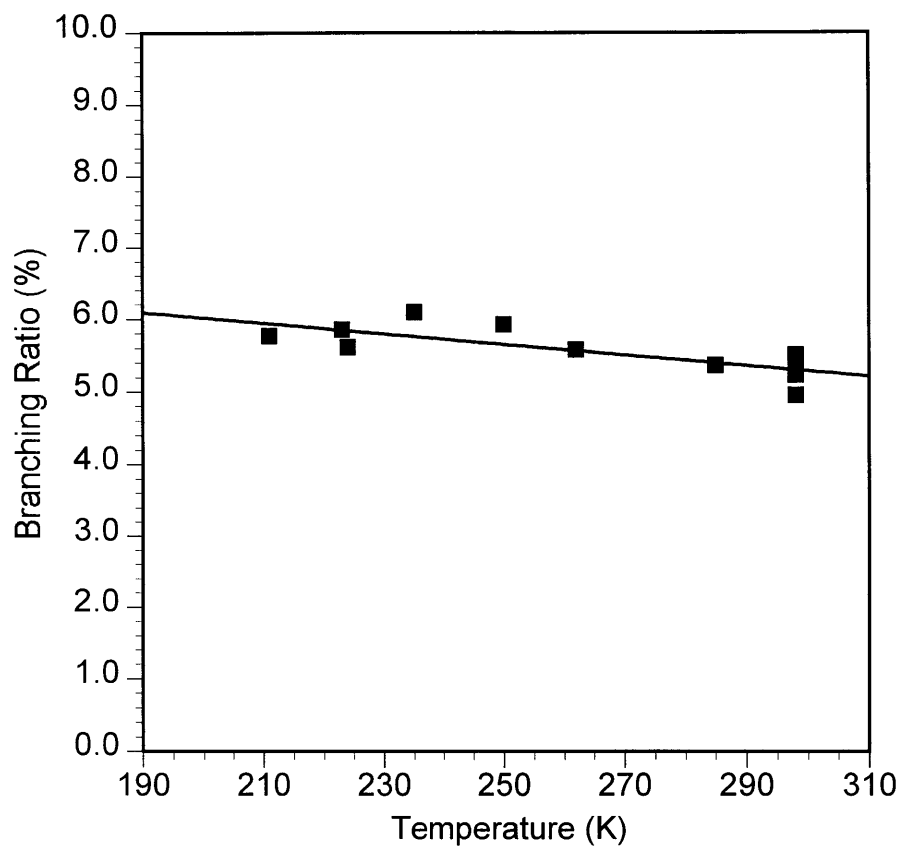


Figure 10. Plot of the branching ratio $[(k_{1b}/k_1) * 100\%]$ for the OD + ClO reaction as a function of temperature.

Table 6. Comparison of Measured Branching Ratios for the OH + ClO Reaction

Technique	T (K)	P (Torr)	Branching Ratio (k_{1b}/k_1)	Reference
DF-LF/RF	298	1.0-3.5	< 0.35	Leu and Lin [1979]
DF-LF/RF	243-298	1.0-5.0	0.15 ± 0.2	Burrows et al. [1984]
DF-LF/LMR	293	1.0	0.14 ± 0.14	Hills and Howard [1984]
DF-LF/EIMS	298	0.5-0.9	0.02 ± 0.12	Poulet et al. [1986]
DF-TF/CIMS	211-298	100	0.05 ± 0.02 at 298 K 0.06 ± 0.02 at 211 K	This work Lipson et al. [1997]

DF, discharge flow; LF, laminar flow; TF, turbulent flow; RF, resonance fluorescence detection; LMR, laser magnetic resonance detection; EIMS, electron impact mass spectrometry detection; CIMS, chemical ionization mass spectrometry detection.

self-reaction or reaction with other species in the system, *i.e.* Cl, OH and ClO. Using this indirect method, *Leu and Lin* were able to place only an upper limit on the branching ratio. *Burrows et al.* modeled the system and found that a correction of almost 50% was necessary to convert the measured HO₂/OH ratio into a branching ratio. These authors measured the branching ratio between 243 and 298 K and found no temperature dependence. However, the large uncertainties in their results probably made it difficult for them to detect the 1% change in the branching ratio that we observed over the temperature range 211-298 K. *Hills and Howard* [1984] were able to detect HO₂ directly using laser magnetic resonance; they measured the HO₂/OH ratio and then used modeling to extract the branching ratio, in a similar manner to *Burrows et al.* Of the four reported branching ratio studies, only *Poulet et al.* [1986] were able to detect the HCl product of reaction 1b directly using electron impact mass spectrometry; they determined the branching ratio by observing the HCl/OH ratio as the OH discharge was turned on and off

at a fixed injector position. However, *Poulet et al.* did not have sufficient sensitivity to observe HCl production over the reaction time. As in the other studies, the errors were too large to rule out an HCl yield of zero. Because of the indirect methods used and the large reported errors, all four previous studies were unable to positively establish the existence of the minor channel.

We have positively identified reaction 1b as a kinetically accessible product channel. In order to assess the atmospheric significance of this result, it is necessary to consider the effect of deuterium substitution on the rate of this channel. For the case of direct (*i.e.* not complex-forming) gas phase bimolecular reactions, the influence of deuterium substitution has been qualitatively understood for some time, and in many cases the effects can be quantitatively predicted using transition state theory. In general, exchanging deuterium for hydrogen lowers the zero-point energies of the species involved. H-D exchange often lowers the zero-point energies of the reactants more than the zero-point energy of the transition state, and therefore causes the activation energy of the reaction to increase. As a result, deuterium substitution tends to decrease the rates of direct bimolecular reactions [*Kaye, 1987*].

For the case of complex-forming reactions, the effect of deuterium substitution is much more complicated. In order to predict the kinetic isotope effect for a complex-mode reaction, the structure and properties of the intermediate complex and the various transition states need to be assumed or calculated by *ab initio* methods, and a full Rice-Rampsberger-Kassel-Marcus (RRKM) calculation needs to be carried out [e.g., *Mozurkewich and Benson, 1985*]. A couple of theoretical studies of the OH + ClO reaction have been conducted. However, the calculation of a reliable energy for the four-centered transition state of reaction 1b is difficult using even very advanced *ab initio* methods [*Dubey et al., 1998*]. The results of the recent theoretical studies for OH + ClO and a comparison with our experimental results will be presented in Chapter 4.

The limitations of theoretical predictions highlight the need for direct measurements

of the rate constants of complex-forming reactions such as $\text{OH} + \text{ClO}$. Because of the demonstrated atmospheric importance of the $\text{OH} + \text{ClO}$ reaction and because of the difficulty in predicting isotope effects for complex-mode reactions, it is important to have direct experimental measurements of the HCl yield from reaction 1b under pressure and temperature conditions characteristic of the stratosphere. In Chapter 4, efforts to reduce the HCl background level in the system will be presented. These efforts are aimed at making direct detection of HCl from reaction 1b possible.

3.4 Conclusions

The results presented in this chapter provide the first positive identification of a product from reaction 1b. The branching ratio involving the production of DCl was determined to be 6% under stratospheric conditions. Numerous modeling studies [e.g., *Toumi and Bekki*, 1993; *Chandra et al.*, 1993; *Michelsen et al.*, 1996; *Khosravi et al.*, 1998; *Ruhnke et al.*, 1999] have proposed that a branching ratio close to 6% would resolve discrepancies between measured and modeled chlorine partitioning and help to reduce discrepancies between measured and calculated ozone mixing ratios in the upper stratosphere. Our measurements for the overall rate constant of reaction 1 are in good agreement with the JPL recommendation at room temperature. However, we report a larger negative activation energy than the JPL recommendation by a factor of almost 2.5. Our temperature dependence is in good agreement with the work of *Hills and Howard* [1984]. In conclusion, our study has identified reaction 1b as a kinetically accessible product channel. These experiments support the theory that reaction 1b is a missing source of HCl in atmospheric models and suggest that the $\text{OH} + \text{ClO}$ reaction plays an important role in the partitioning of chlorine in the stratosphere.

References for Chapter 3

- Allen, M., and M. L. Delitsky, Inferring the abundances of ClO and HO₂ from Spacelab 3 Atmospheric Trace Molecule Spectroscopy observations, *J. Geophys. Res.*, *96*, 2913, 1991.
- Brasseur, G., A. De Rudder, and C. Tricot, Stratospheric response to chemical perturbations, *J. Atmos. Chem.*, *3*, 261, 1985.
- Burrows, J. P., T. J. Wallington, and R. P. Wayne, Kinetics of the reaction of OH with ClO, *J. Chem. Soc., Faraday Trans. 2*, *80*, 957, 1984.
- Chance, K., W. A. Traub, D. G. Johnson, K. W. Jucks, P. Ciarpallini, R. A. Stachnik, R. J. Salawitch, and H. A. Michelsen, Simultaneous measurements of stratospheric HO_x, NO_x, and Cl_x: Comparison with a photochemical model, *J. Geophys. Res.*, *101*, 9031, 1996.
- Chandra, S., C. H. Jackman, A. R. Douglass, E. L. Fleming, and D. B. Considine, Chlorine catalyzed destruction of ozone: Implications for ozone variability in the upper stratosphere, *Geophys. Res. Lett.*, *20*, 351, 1993.
- DeMore, W. B., S. P. Sander, C. J. Howard, A. R. Ravishankara, D. M. Golden, C. E. Kolb, R. F. Hampson, M. J. Kurylo, and M. J. Molina, *Chemical Kinetics and Photochemical Data for Use in Stratospheric Modeling*, JPL Publication 97-4, Jet Propulsion Laboratory, Pasadena, CA, 1997.
- Dessler, A. E., S. R. Kawa, D. B. Considine, J. W. Waters, L. Froidevaux, and J. B. Kumer, UARS measurements of ClO and NO₂ at 40 and 46 km and implications for the model "ozone deficit", *Geophys. Res. Lett.*, *23*, 339, 1996.
- Dubey, M. K., M. P. McGrath, G. P. Smith, and F. S. Rowland, HCl yield from OH + ClO: Stratospheric model sensitivities and elementary rate theory calculations, *J. Phys. Chem. A*, *102*, 3127, 1998.
- Eckman, R. S., W. L. Grose, R. E. Turner, W. T. Blackshear, J. M. Russell III, L. Froidevaux, J. W. Waters, J. B. Kumer, and A. E. Roche, Stratospheric trace constituents simulated by a three-dimensional general circulation model: Comparison with UARS data, *J. Geophys. Res.*, *100*, 13951, 1995.
- Eluszkiewicz, J., and M. Allen, A global analysis of the ozone deficit in the upper stratosphere and lower mesosphere, *J. Geophys. Res.*, *98*, 1069, 1993.
- Fritz, J. J., and C. R. Fuget, Vapor pressure of aqueous hydrogen chloride solutions, 0° to 50° C, *Chem. Eng. Data Ser.*, *1*, 10, 1956.

- Hills, A. J., and C. J. Howard, Rate coefficient temperature dependence and branching ratio for the OH + ClO reaction, *J. Chem. Phys.*, *81*, 4458, 1984.
- Huey, L. G., D. R. Hanson, and C. J. Howard, Reactions of SF₆⁻ and I⁻ with atmospheric trace gases, *J. Phys. Chem.*, *99*, 5001, 1995.
- Jucks, K. W., D. G. Johnson, K. V. Chance, W. A. Traub, R. J. Salawitch, and R. A. Stachnik, Ozone production and loss rate measurements in the middle stratosphere, *J. Geophys. Res.*, *101*, 28785, 1996.
- Kaye, J. A., Mechanisms and observations for isotope fractionation of molecular species in planetary atmospheres, *Rev. Geophys.*, *25*, 1609, 1987.
- Kegley-Owen, C. S., M. K. Gilles, J. B. Burkholder, and A. R. Ravishankara, Private communication.
- Khosravi, R., G. P. Brasseur, A. K. Smith, D. W. Rusch, J. W. Waters, and J. M. Russell III, Significant reduction in the stratospheric ozone deficit using a three-dimensional model constrained with UARS data, *J. Geophys. Res.*, *103*, 16203, 1998.
- Leu, M. T., and C. L. Lin, Rate constants for the reactions of OH with ClO, Cl₂, and Cl₂O at 298 K, *Geophys. Res. Lett.*, *6*, 425, 1979.
- Lipson, J. B., M. J. Elrod, T. W. Beiderhase, L. T. Molina, and M. J. Molina, Temperature dependence of the rate constant and branching ratio for the OH + ClO reaction, *J. Chem. Soc., Faraday Trans.*, *93*, 2665, 1997.
- Lovejoy, E. R., T. P. Murrells, A. R. Ravishankara, and C. J. Howard, Oxidation of CS₂ by reaction with OH. 2. Yields of HO₂ and SO₂ in oxygen, *J. Phys. Chem.*, *94*, 2386, 1990.
- Mallard, W. G., F. Westley, J. T. Herron, and R. F. Hampson, *NIST Chemical Kinetics Database Version 6.0*, NIST Standard Reference Data, Gaithersberg, MD, 1994.
- McElroy, M. B., and R. J. Salawitch, Changing composition of the global stratosphere, *Science*, *243*, 763, 1989.
- Michelsen, H. A., R. J. Salawitch, M. R. Gunson, C. Aellig, N. Kämpfer, M. M. Abbas, M. C. Abrams, T. L. Brown, A. Y. Chang, A. Goldman, F. W. Irion, M. J. Newchurch, C. P. Rinsland, G. P. Stiller, and R. Zander, Stratospheric chlorine partitioning: Constraints from shuttle-borne measurements of [HCl], [ClNO₃], and [ClO], *Geophys. Res. Lett.*, *23*, 2361, 1996.
- Mozurkewich, M., and S. W. Benson, Negative activation energies and curved Arrhenius plots. 1. Theory of reactions over potential wells, *J. Phys. Chem.*, *88*, 6429, 1984.

- Mozurkewich, M., and S. W. Benson, Self-reaction of HO₂ and DO₂: Negative temperature dependence and pressure effects, *Int. J. Chem. Kinet.*, *17*, 787, 1985.
- Natarajan, M., and L. B. Callis, Stratospheric photochemical studies with Atmospheric Trace Molecule Spectroscopy (ATMOS) measurements, *J. Geophys. Res.*, *96*, 9361, 1991.
- Osterman, G. B., R. J. Salawitch, B. Sen, G. C. Toon, R. A. Stachnik, H. M. Pickett, J. J. Margitan, J.-F. Blavier, and D. B. Peterson, Balloon-borne measurements of stratospheric radicals and their precursors: Implications for the production and loss of ozone, *Geophys. Res. Lett.*, *24*, 1107, 1997.
- Poulet, G., G. Laverdet, and G. Le Bras, Rate constant and branching ratio for the reaction of OH with ClO, *J. Phys. Chem.*, *90*, 159, 1986.
- Ravishankara, A. R., F. L. Eisele, and P. H. Wine, The kinetics of the reaction of OH with ClO, *J. Chem. Phys.*, *78*, 1140, 1983.
- Ruhnke, R., W. Kouker, Th. Reddmann, H. Berg, G. Hochschild, G. Kopp, R. Krupa, and M. Kuntz, The vertical distribution of ClO at Ny-Alesund during March 1997, *Geophys. Res. Lett.*, *26*, 839, 1999.
- Sandor, B. J., R. T. Clancy, D. W. Rusch, C. E. Randall, R. S. Eckman, D. S. Siskind, and D. O. Muhleman, Microwave observations and modeling of O₂(¹Δ_g) and O₃ diurnal variation in the mesosphere, *J. Geophys. Res.*, *102*, 9013, 1997.
- Seeley, J. V., J. T. Jayne, and M. J. Molina, High pressure fast-flow technique for gas phase kinetics studies, *Int. J. Chem. Kinet.*, *25*, 571, 1993.
- Seeley, J. V., R. F. Meads, M. J. Elrod, and M. J. Molina, Temperature and pressure dependence of the rate constant for the HO₂ + NO reaction, *J. Phys. Chem.*, *100*, 4026, 1996.
- Siskind, D. E., B. J. Connor, R. S. Eckman, E. E. Remsberg, J. J. Tsou, and A. Parrish, An intercomparison of model ozone deficits in the upper stratosphere and mesosphere from two data sets, *J. Geophys. Res.*, *100*, 11191, 1995.
- Smith, I. W. M., Radical-radical reactions: Kinetics, dynamics and mechanisms, *J. Chem. Soc., Faraday Trans.*, *87*, 2271, 1991.
- Stachnik, R. A., J. C. Hardy, J. A. Tarsala, and J. W. Waters, Submillimeterwave heterodyne measurements of stratospheric ClO, HCl, O₃, and HO₂: First results, *Geophys. Res. Lett.*, *19*, 1931, 1992.

Summers, M. E., R. R. Conway, D. E. Siskind, M. H. Stevens, D. Offermann, M. Riese, P. Preusse, D. F. Strobel, and J. M. Russell III, Implications of satellite OH observations for middle atmospheric H₂O and ozone, *Science*, 277, 1967, 1997.

Toumi, R., and S. Bekki, The importance of the reactions between OH and ClO for stratospheric ozone, *Geophys. Res. Lett.*, 20, 2447, 1993.

Wennberg, P. O., R. C. Cohen, R. M. Stimpfle, J. P. Koplw, J. G. Anderson, R. J. Salawitch, D. W. Fahey, E. L. Woodbridge, E. R. Keim, R. S. Gao, C. R. Webster, R. D. May, D. W. Toohey, L. M. Avallone, M. H. Proffitt, M. Loewenstein, J. R. Podolske, K. R. Chan, and S. C. Wofsy, Removal of stratospheric O₃ by radicals: In situ measurements of OH, HO₂, NO, NO₂, ClO and BrO, *Science*, 266, 398, 1994.

Chapter 4: Kinetics of the OH + ClO Reaction: Measurements of the Branching Ratio

4.1 Introduction

The branching ratio of the OH + ClO reaction is one of the largest sources of uncertainty in modeled chlorine partitioning [Dubey *et al.*, 1998]. Because models of stratospheric ozone are very sensitive to the calculated partitioning of chlorine, errors in modeled chlorine will propagate into the calculation of stratospheric ozone levels. As discussed in Chapter 3, atmospheric models have tended to overestimate the amount of active chlorine (e.g., ClO) relative to the amount of stable chlorine (e.g., HCl) in the upper stratosphere [e.g., Toumi and Bekki, 1993; Michelsen *et al.*, 1996]. The models have also tended to overpredict odd oxygen loss rates in the upper stratosphere, resulting in an underprediction of ozone mixing ratios above 35 km. This “ozone deficit” problem is at least partly due to errors in the calculated chlorine partitioning [e.g., Chandra *et al.*, 1993; Khosravi *et al.*, 1998]. The development of accurate models of stratospheric O₃ is critical to our ability to predict the consequences of future perturbations to the atmosphere, such as a proposed fleet of supersonic aircraft.

The OH + ClO reaction has long been proposed as a missing source of HCl in stratospheric models [e.g., Brasseur *et al.*, 1985; McElroy and Salawitch, 1989]. The OH + ClO reaction has two possible product channels:



Although HO₂ and Cl are the major products of reaction 1, even a relatively small branching ratio to form HCl and O₂ would have a strong impact on calculated chlorine

partitioning because the formation of HCl is a chain-terminating step in chlorine-catalyzed ozone depletion cycles. Reaction 1b is highly exothermic ($\Delta H^\circ_{298\text{ K}} = -55.8 \text{ kcal mol}^{-1}$), but kinetically unfavorable. *Ab initio* and RRKM calculations have shown that the reaction most likely proceeds through an addition-elimination mechanism via a four-centered transition state [Dubey *et al.*, 1998].

Early attempts to measure the branching ratio of the OH + ClO reaction were unable to rule out an HCl yield of zero for the minor channel due to uncertainties in the data [Leu and Lin, 1979; Burrows *et al.*, 1984; Hills and Howard, 1984; Poulet *et al.*, 1986]. As a result, no consensus had been reached on the atmospheric significance of reaction 1b, and most atmospheric models did not include this channel in their reaction set. In Chapter 3, the first direct measurements of a product from reaction 1b were presented. In these branching ratio experiments, OD was used instead of OH due to the large HCl background produced by the ClO source. Since there was virtually no DCl background in our experiments, we were able to observe the production of very small concentrations of DCl ($\sim 10^9 \text{ molecule cm}^{-3}$) over the experimental reaction time which we positively identified as coming from the minor channel of the OD + ClO reaction. The branching ratio (k_{1b}/k_1) was determined to be 0.05 ± 0.02 at 298 K and 0.06 ± 0.02 at 211 K.

In our previous study of the branching ratio for the OD + ClO reaction, we clearly demonstrated that reaction 1b is a kinetically accessible product channel. Because of the demonstrated atmospheric importance of reaction 1b and because of the possibility of an isotope effect, it is essential to have branching ratio measurements for the OH + ClO reaction. Recent improvements to the experimental technique have significantly reduced the HCl background in our system, making it possible to detect the production of very small concentrations of HCl ($\sim 10^9 \text{ molecule cm}^{-3}$) from channel 1b. In this chapter, measurements of the HCl yield and branching ratio of reaction 1 will be presented. These experiments were conducted at pressures between 100 and 200 Torr and at a range of temperatures extending to those found in the lower stratosphere using a turbulent flow

tube coupled to a high pressure chemical ionization mass spectrometer. Statistical rate theory calculations for OH + ClO have been performed by Matthias Olzmann from the Institut für Physikalische Chemie at the Universität Halle-Wittenberg in Halle, Germany in collaboration with our research group [Lipson *et al.*, 1999]. The results of this study and of another recent theoretical study by Dubey *et al.* [1998] will be presented and compared to our laboratory measurements of the branching ratio. The comparison of experimental findings with theoretical calculations is a good test of our understanding of the fundamental reaction dynamics of the OH + ClO system, as well as a test of our ability to predict kinetic isotope effects.

4.2 Experimental Section

A schematic diagram of the experimental apparatus is presented in Figure 1. The set-up is similar to that used in our previous study of the OD + ClO reaction (Chapter 3). However, several critical changes to the ClO production method have greatly reduced the HCl background in the system, as discussed in detail below. The flow tube (2.2 cm i.d., 120 cm long) was constructed of Pyrex tubing and coated with Halocarbon wax. A large flow of nitrogen carrier gas (40-75 STP L min⁻¹) was injected at the rear of the flow tube. The gases needed to generate OH were introduced through a sidearm (12 cm long, 6 mm diameter) located at the rear of the flow tube. ClO was generated in a double-nested movable injector, which consisted of an inner 6 mm alumina tube and an outer encasement made from corrugated Teflon tubing. The outer encasement was used so that the injector could be moved to various positions without breaking the vacuum seals. A Teflon device (described below) was placed at the end of the injector in order to enhance turbulent mixing. The electric discharge ion source was located between the temperature regulated flow tube and the inlet to the quadrupole mass spectrometer. A variable-sized aperture (1.2-1.8 mm diameter) was used to create a pressure drop between the flow tube and the ion-molecule region. The size of the aperture was adjusted so that the pressure in

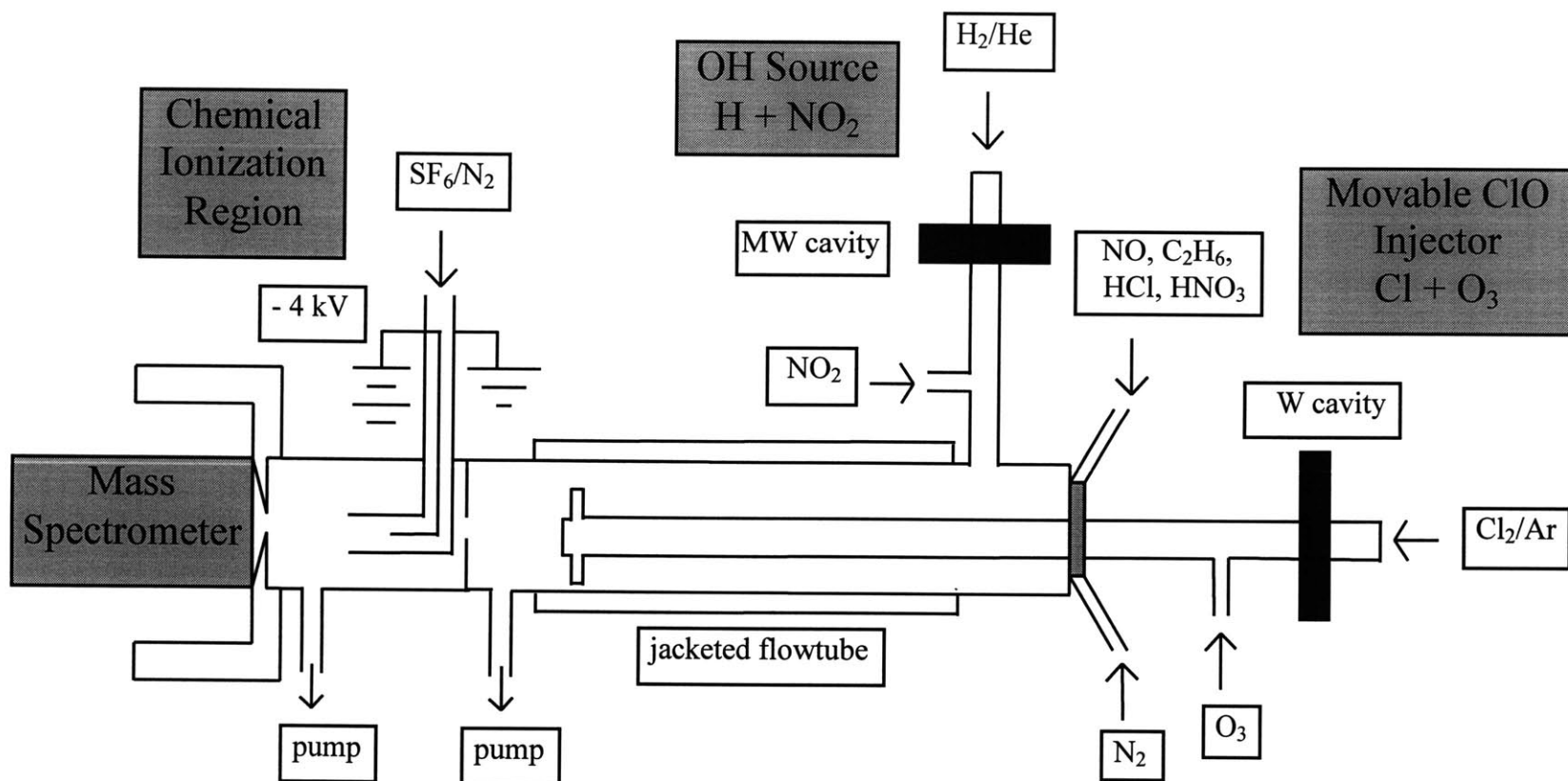


Figure 1. Schematic diagram of experimental apparatus

the ion-molecule region remained roughly constant at 15 Torr while the pressure in the flow tube was varied between 100 and 200 Torr. The pressures in the two regions were measured using MKS capacitance manometers (100 and 1000 Torr full scale). All gas flows were monitored with calibrated Tylan General mass flowmeters. For the low temperature studies, Syltherm XLT (DOW Chemical Company) was used as a coolant in the jacketed flow tube, and the nitrogen carrier gas was also precooled by passing it through a copper coil immersed in a liquid N₂ reservoir followed by resistive heating. The temperature, measured at both the entrance and exit points of the reaction region using copper-constantan thermocouples, was controlled to within 1 K.

The following gases were used as supplied or after further purification as described below: Ar (99.999%), He (99.999%), O₂ (99.994%), H₂ (99.999%), Cl₂ (>99.9%), NO₂ (99.5%), NO (>99.0%), C₂H₆ (>99.0%) and SF₆ (>99.99%).

4.2.1 Radical Production

As in our previous study of the branching ratio for the OD + ClO reaction, ClO was generated in the injector using the following reaction ($k_2 = 1.2 \times 10^{-11} \text{ cm}^3 \text{ molecule}^{-1} \text{ s}^{-1}$ [DeMore *et al.*, 1997]):



Chlorine atoms were produced by combining a ~5 STP L min⁻¹ flow of argon, which had passed through an inert gas purifier (Aeronex Gate Keeper, Model 500 K), with a ~1 STP mL min⁻¹ flow of a 1 % Cl₂/He mixture which then passed through a microwave discharge produced by a Beenakker cavity operating at 70 W. To generate ClO, the chlorine atoms were mixed with a large excess of O₃ (~ 10¹³ molecule cm⁻³) throughout the whole length of the movable alumina injector to ensure that only negligible amounts of chlorine atoms were introduced into the main flow. O₃, generated from an OREC

ozonator and stored in a silica gel trap immersed in a dry ice/methanol bath, was introduced into the system by passing a 3-20 STP mL min⁻¹ flow of N₂ through the trap. Ozone partial pressures were determined by UV absorbance at 253.7 nm in a 0.98 cm flow-through quartz cell with light provided by a Penray Hg lamp. The absorption cross section for ozone at that wavelength is $\sigma = 1.15 \times 10^{-17} \text{ cm}^2 \text{ molecule}^{-1}$ [DeMore *et al.*, 1997].

There have been several important modifications to the ClO source since our previous study that have helped to reduce the HCl background in the system by more than an order of magnitude. In our previous study, the high level of HCl background ($\sim 10^{11} \text{ molecule cm}^{-3}$) in the system was observed to be coming primarily from the ClO source. This large background made it difficult to detect small amounts of HCl produced by channel 1b over the experimental reaction time. A significant portion of the HCl background was found to come from trace impurities of H₂ in the helium sweep gas used to flush Cl₂ through the microwave discharge. Although 99.999% pure helium was used, the manufacturer specifications indicate levels of H₂ up to 1 ppm. If 1 ppm of H₂ ($\sim 10^{12} \text{ molecule cm}^{-3}$) were present and sent through the microwave discharge in the presence of chlorine, it could certainly have produced enough H atoms to create a sizable HCl background. This HCl source was significantly reduced by installing an Aeronex inert gas purifier that removes H₂ impurities to sub-ppb levels.

Another small source of HCl background came from the Cl₂ — the UHP grade Cl₂ (>99.9% pure) used in this study contains small amounts of HCl impurities. We have changed the sweep gas through the chlorine microwave discharge from helium to argon because it was found that argon increases the efficiency of Cl₂ microwave dissociation. The greater dissociation efficiency may be due to the improved energy transfer capability of the heavier argon atoms. As a result, it was possible to produce comparable amounts of ClO with lower initial Cl₂ concentrations, thereby reducing the HCl background in the system. The increased efficiency of Cl₂ microwave dissociation using argon instead of

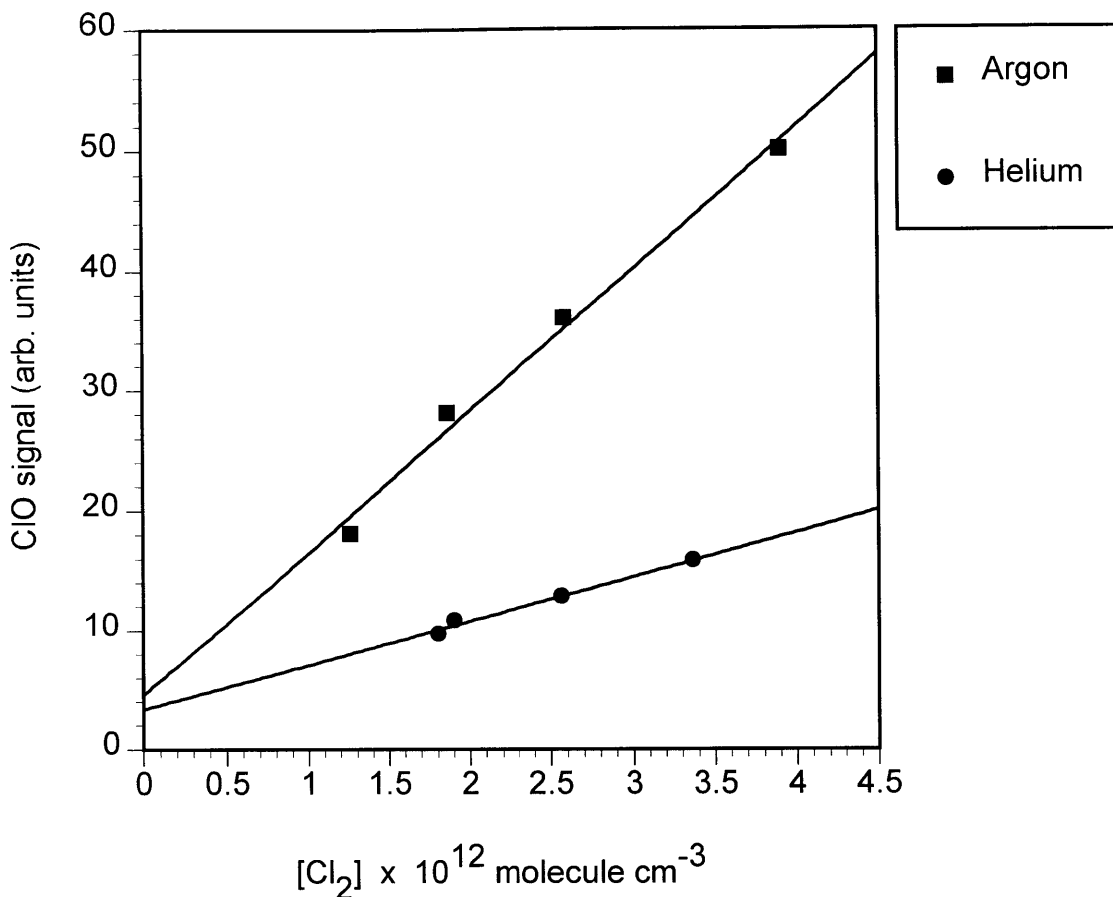


Figure 2. Comparison of Cl₂ microwave dissociation efficiencies for two different inert sweep gases: argon (■) vs. helium (●).

helium is demonstrated in Figure 2. In this figure, the ClO mass spectrometer signal is plotted versus initial Cl₂ concentration for the two different inert sweep gases. The much larger slope of the argon curve compared to the helium curve shows that, for the same initial Cl₂ concentration, greater amounts of ClO were produced using argon.

Another significant source of HCl background was identified as coming from the interaction of Cl atoms with the quartz walls of the movable injector (particularly in the few centimeters after the chlorine microwave discharge, but before the introduction of excess O₃). Dangling OH bonds on the surface of the quartz are believed to contribute to

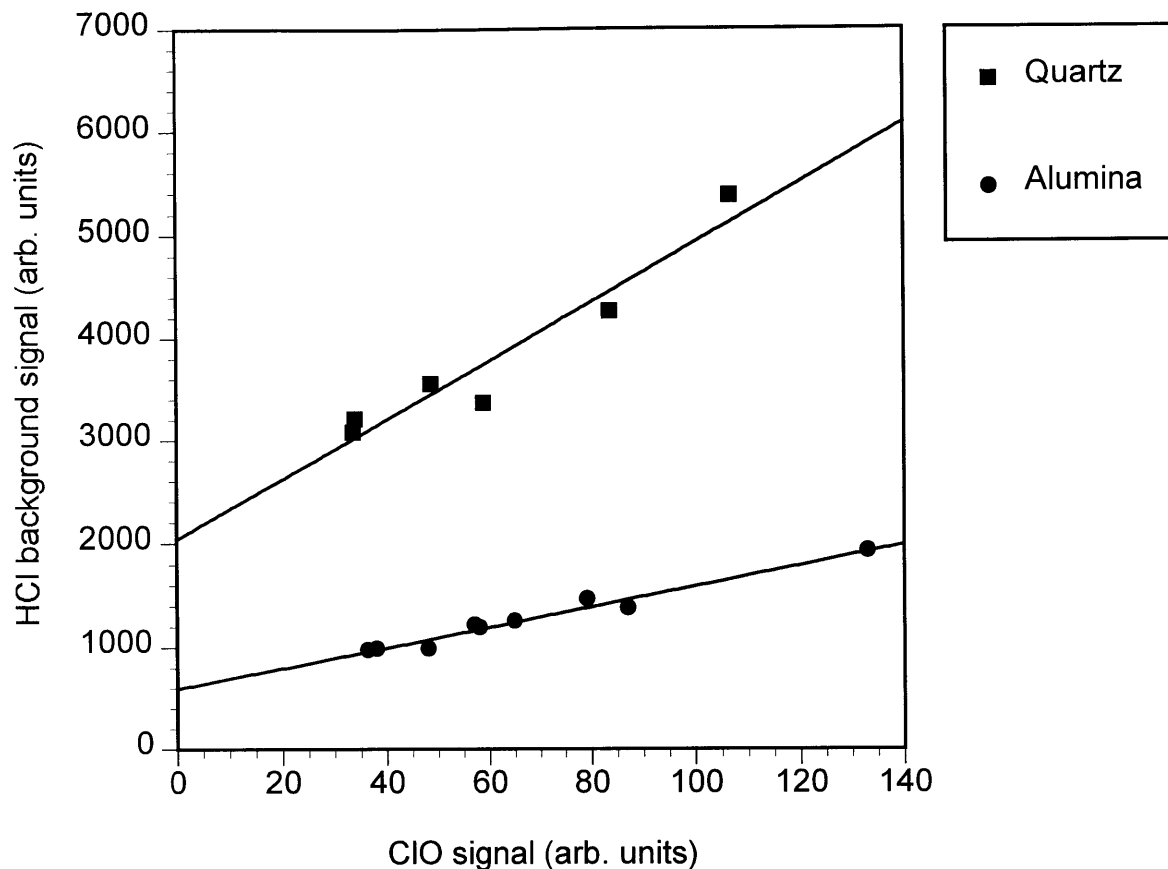


Figure 3. Comparison of HCl background levels produced by the ClO source for two different types of tubing: quartz (■) vs. alumina (●).

the formation of HCl. This source of HCl background was significantly reduced by switching to an injector made out of alumina as demonstrated in Figure 3. In this figure, the HCl background level from the ClO source is plotted versus the ClO mass spectrometer signal for the two different types of tubing. Figure 3 shows that approximately three times less HCl was produced by the ClO source when an alumina tube was used in the microwave discharge instead of a quartz tube.

A small modification to the ClO source, which ended up being important, was related to the way that O_3 was introduced into the movable injector. In our previous

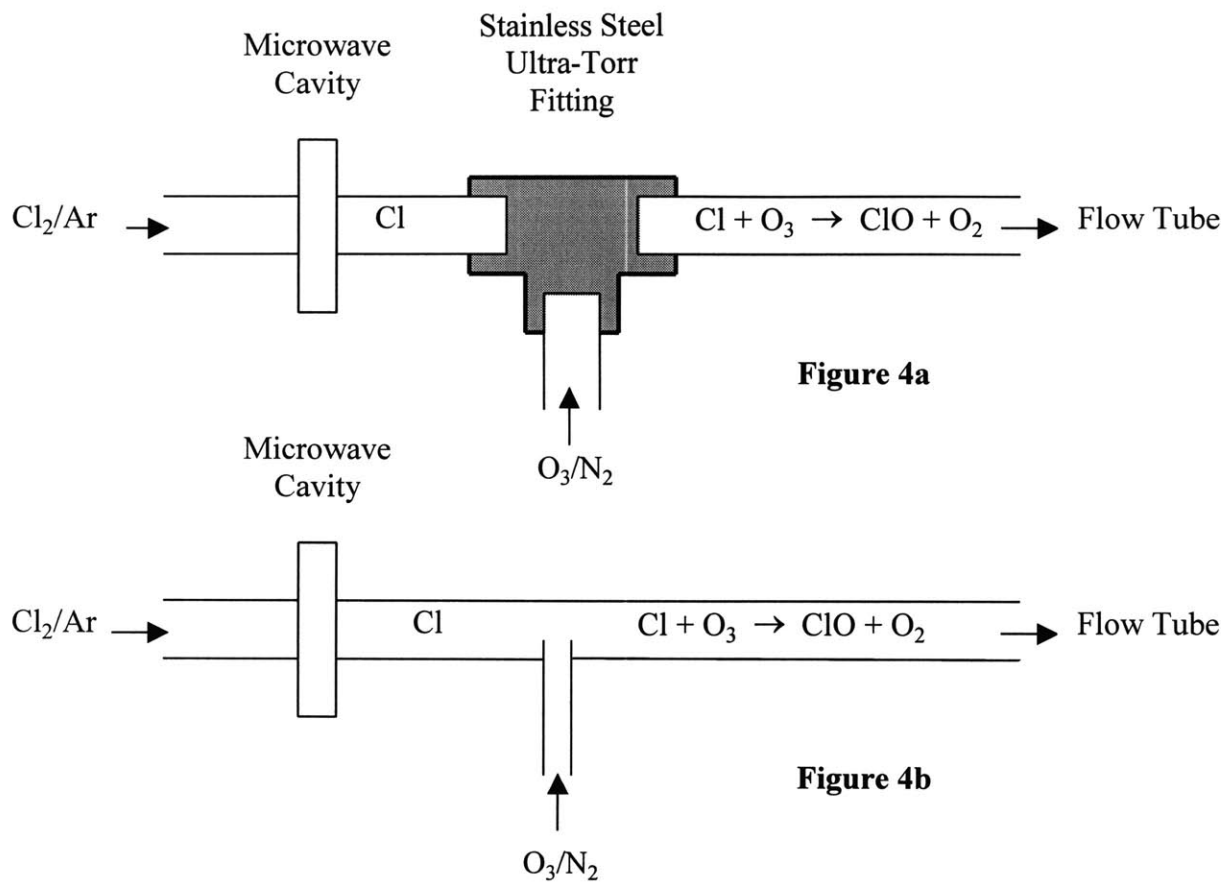


Figure 4. Schematic diagram of ClO source: 4a) old design; 4b) new design.

branching ratio experiments for the OD + ClO reaction, the O₃ was introduced into the movable injector through a T-shaped Ultra-Torr fitting as shown in Figure 4a. In the old design, the Cl atoms briefly came in contact with the stainless steel surface of the Ultra-Torr fitting before mixing with the O₃. Because of the observed reduction in HCl background when an alumina tube was used in the microwave discharge, it seemed worthwhile to try to minimize the interaction of Cl atoms with surfaces other than alumina. In the new design (Figure 4b), the injector was made out of one continuous piece of 1/4" o.d. alumina tubing, and O₃ was introduced into the injector through a 1/8"

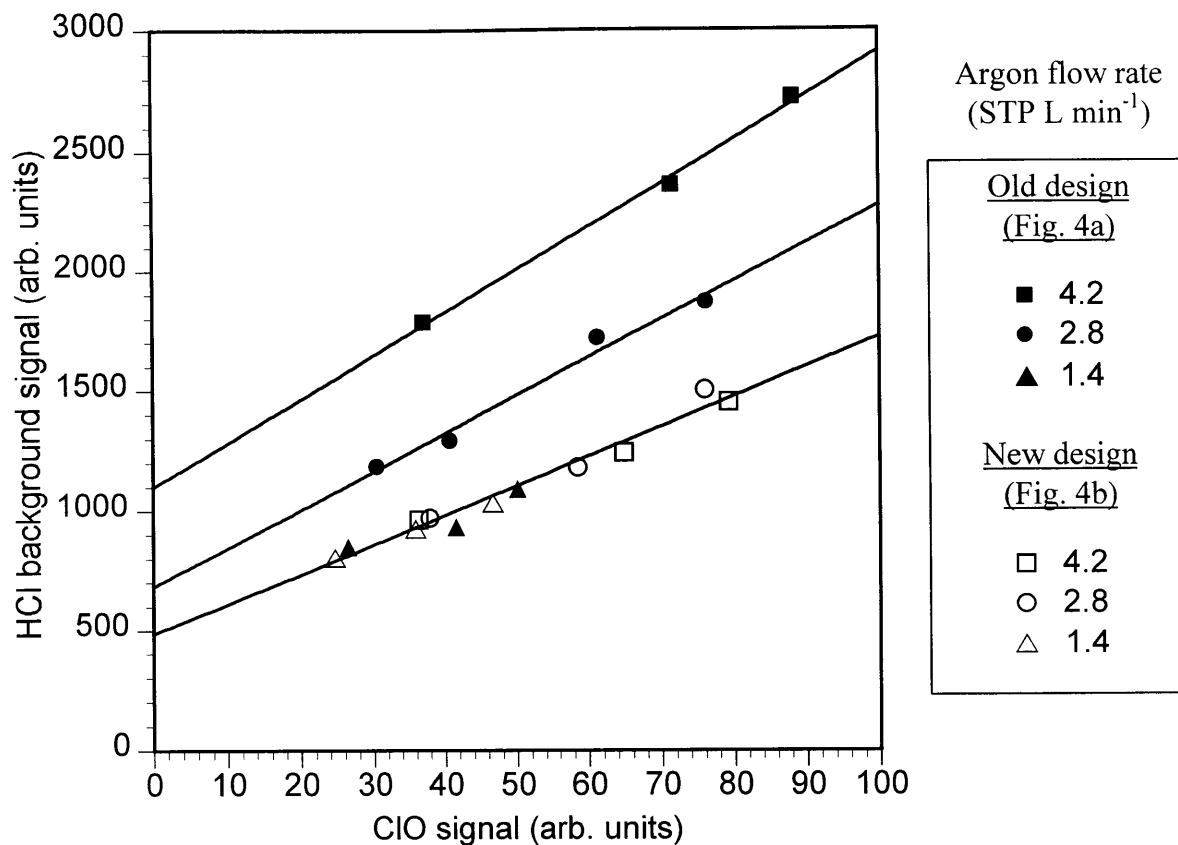


Figure 5. Comparison of HCl background levels produced by the ClO source for different argon flow rates through the microwave discharge. The dark symbols represent experiments conducted using the old design (Fig. 4a). The open symbols represent experiments conducted using the new design (Fig. 4b).

o.d. alumina side arm located a few centimeters after the chlorine microwave discharge. This design was achieved by drilling a 1/8" hole in the alumina injector and attaching a piece of 1/8" alumina tubing to the injector using Torr-Seal in order to create a vacuum-tight connection. In this design, the 1/8" alumina tubing was purposely allowed to protrude into the flow of Cl atoms in order to improve mixing. This small modification turned out to be an important improvement to the ClO source. With the old design, it was found that the HCl background level from the ClO source varied with the flow rate of argon sweep gas through the injector. As demonstrated in Figure 5, the HCl background

level (dark symbols) increased at the higher argon flows. However, a higher argon flow rate was preferable because it reduced the ClO self-reaction time in the injector. When the new design was implemented, it was found that the HCl background level (open symbols) was no longer a function of argon flow, as shown in Figure 5. Therefore, it was possible to go to higher argon flow rates without increasing the HCl background level in the system. The optimal flow rate for ClO production was determined to be ~ 5 STP L min^{-1} .

Overall, modifications to the ClO source have reduced the HCl background in the system by more than an order of magnitude (from $\sim 5 \times 10^{11}$ to $< 4 \times 10^{10}$ molecule cm^{-3}), making it possible to observe production of very small amounts of HCl from reaction 1b. The modifications to the ClO source have been described in detail because decreasing the HCl background was critical to our ability to make accurate measurements of the branching ratio for the OH + ClO reaction. The background level was very stable during each experiment, but it varied somewhat from run to run as conditions, such as the initial ClO concentration, were changed.

In addition to the sources of HCl mentioned above, the production of HCl background by secondary reactions in the main flow tube was also a concern. For example, the products of the main channel of the OH + ClO reaction are HO₂ and Cl, which can react further to form HCl ($k_3 = 3.2 \times 10^{-11}$ cm³ molecule⁻¹ s⁻¹ [DeMore *et al.*, 1997]):



Since reaction 3 is relatively fast, and HO₂ and Cl are the major products of reaction 1, reaction 3 was found to be the largest potential source of HCl background due to secondary chemistry. However, the large excess of O₃ ($\sim 10^{13}$ molecule cm^{-3}) used in the production of ClO also helped to scavenge Cl atoms produced by reaction 1a, and

therefore, helped to minimize HCl background production from side reactions such as reaction 3.

As described in our previous study of the branching ratio for the OD + ClO reaction (Chapter 3), absolute ClO concentrations were determined by the titration reaction ($k_4 = 1.7 \times 10^{-11} \text{ cm}^3 \text{ molecule}^{-1} \text{ s}^{-1}$ [DeMore *et al.*, 1997]):



and subsequent calibration of the NO₂ mass spectrometer signal. The NO was purified, using the method described in Chapter 3, in order to reduce the background NO₂ contribution. An excess of ethane ($\sim 5 \times 10^{13} \text{ molecule cm}^{-3}$), injected at the rear of the flow tube, scavenged the Cl atoms produced by the titration reaction in order to prevent regeneration of ClO due to the excess of O₃ used in the experiments. Modeling was used to correct for a slight underestimation of ClO concentration ($\leq 15\%$) caused by the secondary reaction of C₂H₅ with NO₂. In Chapter 3, we demonstrated that our ClO titration technique yields linear calibration curves. For this study, ClO concentrations ranged from $5\text{-}9 \times 10^{11} \text{ molecule cm}^{-3}$.

For the branching ratio studies, OH was generated in the side arm of the flow tube by the following reaction ($k_5 = 1.3 \times 10^{-10} \text{ cm}^3 \text{ molecule}^{-1} \text{ s}^{-1}$ [DeMore *et al.*, 1997]):



H atoms were generated by combining $\sim 2 \text{ STP L min}^{-1}$ flow of helium with $\sim 0.5 \text{ STP mL min}^{-1}$ flow of a 3 % H₂/He mixture, which then passed through a molecular sieve trap immersed in liquid nitrogen and finally through a microwave discharge produced by a Beenakker cavity. The H atoms were then mixed with excess NO₂ to ensure that practically no hydrogen atoms were introduced into the main flow. The excess NO₂

helped to minimize production of background HCl from the following side reaction ($k_6 = 2.5 \times 10^{-11} \text{ cm}^3 \text{ molecule}^{-1} \text{ s}^{-1}$ [Mallard *et al.*, 1994]):



Because OH was introduced through the side arm, where the corresponding concentrations are ~ 30 times higher than in the main flow tube, the secondary reaction with NO_2 ($k_7 = 3.3 \times 10^{-12} \text{ cm}^3 \text{ molecule}^{-1} \text{ s}^{-1}$ at 100 Torr [DeMore *et al.*, 1997]):



was a concern in the production of OH by reaction 5. This difficulty was surmounted by using a relatively high flow of helium sweep gas through the H_2 microwave discharge in order to decrease the reaction time in the side arm. Experimental conditions in the side arm were optimized to ensure that reaction 5 went virtually to completion without significant loss of OH due to reaction 7. Although reaction 7 was minimized in the production of OH, this reaction provided a convenient titration method for determining absolute concentrations of OH. A large excess of NO_2 was used to convert all of the OH into HNO_3 followed by calibration of the HNO_3 mass spectrometer signal using a bubbler containing 60 wt % $\text{HNO}_3/\text{H}_2\text{O}$ solution maintained at 0°C . In Chapter 3, we demonstrated that our OH titration technique yields linear calibration curves. OH concentrations used in this study ranged from $1\text{-}4 \times 10^{11} \text{ molecule cm}^{-3}$.

Absolute HCl concentrations were determined by calibrating the HCl mass spectrometer signal using a bubbler containing 20 wt % $\text{HCl}/\text{H}_2\text{O}$ solution kept at 0°C . For the low temperature experiments, the HCl from the bubbler took a long time to equilibrate. For reasons of convenience, calibrations of the HCl signal at low temperatures were also made by reacting H atoms with a known amount of Cl_2 . The H

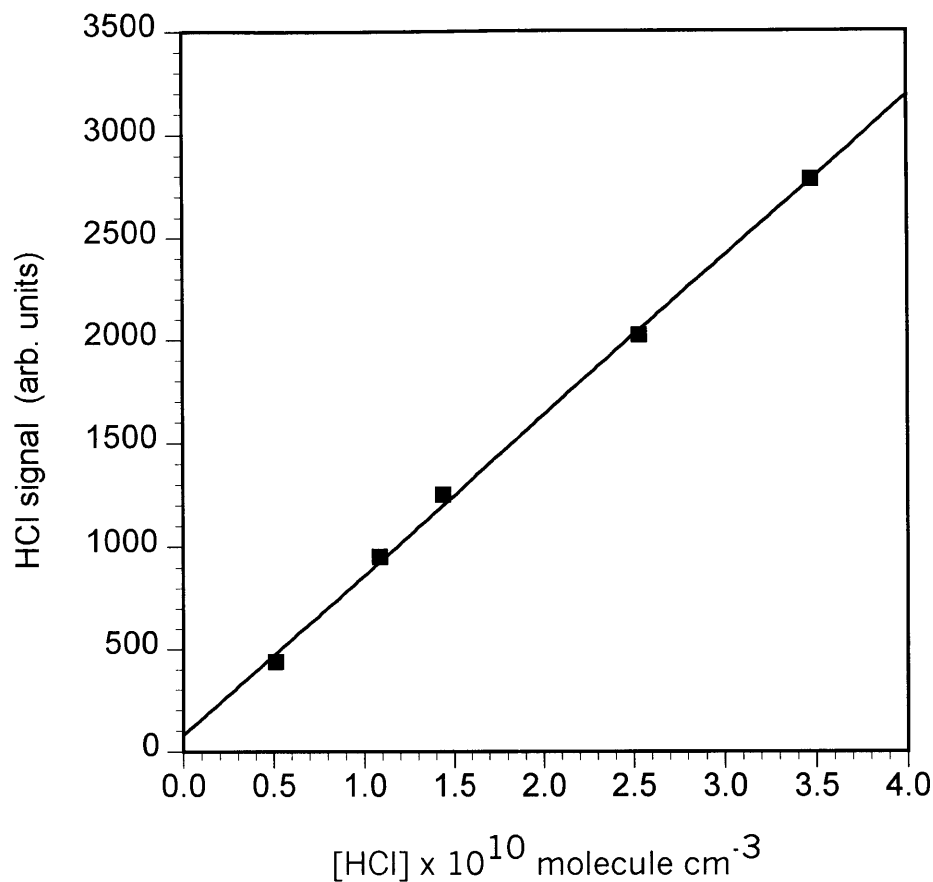


Figure 6. HCl calibration plot

atoms from the OH source were introduced through the side arm, and the Cl₂ from the ClO source was introduced through the movable injector. The Cl₂ and HCl mass spectrometer signals were monitored as the hydrogen microwave discharge was turned on and off. The concentration of HCl was determined by calculating the concentration of Cl₂ lost. As demonstrated in Figure 6, this method yielded linear calibration curves. The two methods of HCl calibration were in very good agreement.

4.2.2 Detection of Reactants and Products

Most of the chemical species relevant to this study (OH, ClO, HO₂, HCl, Cl₂, O₃, NO₂, and HNO₃) were chemically ionized with the SF₆⁻ reagent ion and then detected

with the quadrupole mass spectrometer. SF_6^- was produced in the ion source by combining ~ 2 STP L min^{-1} flow of nitrogen with a 0.2 STP mL min^{-1} flow of a 5% SF_6/N_2 mixture which then passed over the electric discharge. In order to confine the ionization process to SF_6 alone and to control the ion-molecule reaction time, another piece of Pyrex tubing (of variable length) was used to direct the SF_6^- downstream into the main flow tube effluent. More extensive descriptions of the ion source, ion lenses and the quadrupole mass spectrometer are given in Chapter 2.

In the chemical ionization scheme employed here, OH, ClO, Cl_2 , O_3 and NO_2 were detected as their parent negative ions by charge-transfer reactions with SF_6^- . For example, OH was detected as OH^- through the following reaction:



HCl and HNO_3 were detected as FHCl^- and FHNO_3^- through fluoride-transfer reactions with SF_6^- :



HO_2 was detected as SF_4O_2^- , generated presumably through a multi-step pathway. The rate constants of many of the relevant ion-molecule reactions have been measured by Huey *et al.* [1995]. The ion-molecule region was kept at a lower pressure (15 Torr) than the flow tube (100-200 Torr). The drop in pressure lowered the concentrations of the neutrals in the ion-molecule region, thus decreasing the rates of potential ion-molecule side reactions. The lower neutral concentrations in the ion-molecule region also helped to prevent depletion of the SF_6^- reagent ions due to reaction with species in large excess such as O_3 .

4.3 Results and Discussion

4.3.1 Branching Ratio Experiments

Because of the improvements to the experimental apparatus described in the Experimental Section, the HCl background level from the ClO source was significantly reduced in these experiments. As a result, we were able to observe production of very small concentrations of HCl ($\sim 10^9$ molecule cm^{-3}) over the reaction time (~ 20 ms) which we have positively identified as coming from reaction 1b. Figure 7 shows that the rise of HCl is easily observed above the background noise. In Figure 7, the HCl rise (dark squares) has been overlaid on the background signal (open squares) in order to demonstrate that the HCl rise is much larger than the $\pm 2\sigma$ level of the background noise. Under the optimal experimental conditions ($[\text{ClO}] \sim 1 \times 10^{12}$ molecule cm^{-3} and $[\text{OH}] \sim 1 \times 10^{11}$ molecule cm^{-3}), modeling shows that side reactions can only produce concentrations of HCl that are less than the detection limit of the instrument ($\sim 10^8$ molecule cm^{-3}). Table 1 contains a list of the reactions used in the modeling. The following side reactions can produce HCl in our system:



In the branching ratio experiments, the source conditions for OH and ClO were optimized in order to prevent stray H and Cl atoms from entering the main flow tube. Furthermore, reaction 11 is too slow to be important in our system ($k_{11} = 1.6 \times 10^{-14}$ cm^3 molecule $^{-1}$ s $^{-1}$ [Mallard *et al.*, 1994]). Reaction 3 is more difficult to avoid because HO₂ and Cl are the products of reaction 1a, the main channel of the OH + ClO reaction. However, modeling shows that the large excess of O₃, used to generate ClO, is efficient in scavenging Cl

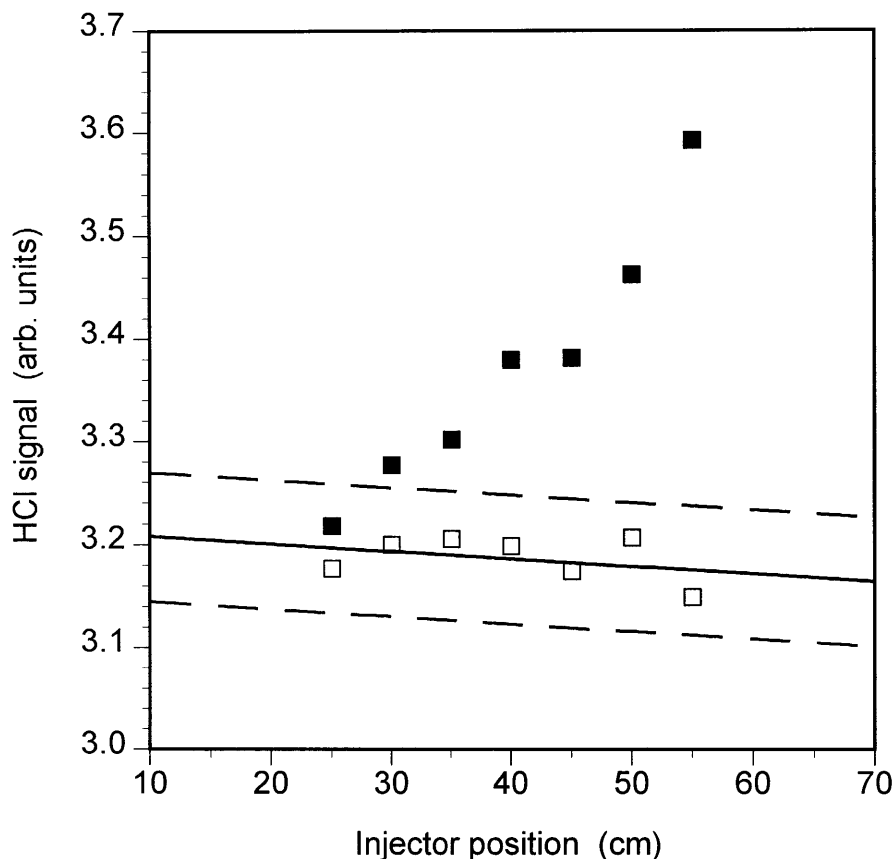


Figure 7. Observed production of HCl ($[\text{HCl}] = 2.7 \times 10^9 \text{ molecule cm}^{-3}$) from reaction 1b (■) above the HCl background level (□) as a function of injector position. A least-squares fit to the HCl background data was performed, and the dotted lines represent the $\pm 2\sigma$ level. This data set was obtained under the following conditions: $P = 97 \text{ Torr}$, $T = 298\text{K}$, average velocity = 1800 cm s^{-1} , Reynolds number = 5000, $[\text{OH}]_0 = 1.8 \times 10^{11} \text{ molecule cm}^{-3}$, $[\text{ClO}]_0 = 8.3 \times 10^{11} \text{ molecule cm}^{-3}$.

Table 1. Chemical Reactions Used in Computer Simulations for the Branching Ratio Studies of the OH + ClO Reaction

Reaction	k (cm ³ molecule ⁻¹ s ⁻¹)
OH + ClO → HO ₂ + Cl	1.46 x 10 ⁻¹¹
OH + ClO → HCl + O ₂	see text
Cl + HO ₂ → HCl + O ₂	3.2 x 10 ⁻¹¹
Cl + HO ₂ → OH + ClO	9.1 x 10 ⁻¹²
Cl + O ₃ → ClO + O ₂	1.2 x 10 ⁻¹¹
Cl + H ₂ → HCl + H	1.6 x 10 ⁻¹⁴
Cl + H ₂ O ₂ → HCl + HO ₂	4.1 x 10 ⁻¹³
Cl + NO ₂ + M → ClONO + M	3.3 x 10 ⁻¹²
H + Cl ₂ → HCl + Cl	2.5 x 10 ⁻¹¹
H + O ₃ → OH + O ₂	2.9 x 10 ⁻¹¹
H + NO ₂ → OH + NO	1.3 x 10 ⁻¹⁰
OH + O ₃ → HO ₂ + O ₂	6.8 x 10 ⁻¹⁴
OH + Cl ₂ → HOCl + Cl	6.7 x 10 ⁻¹⁴
OH + OH → H ₂ O + O	1.9 x 10 ⁻¹²
OH + OH + M → H ₂ O ₂ + M	1.4 x 10 ⁻¹²
OH + HO ₂ → H ₂ O + O ₂	1.1 x 10 ⁻¹⁰
OH + NO ₂ + M → HNO ₃ + M	3.3 x 10 ⁻¹²
OH + NO + M → HONO + M	1.7 x 10 ⁻¹²
OH + HCl → H ₂ O + Cl	8.0 x 10 ⁻¹³
ClO + ClO → products	7.7 x 10 ⁻¹⁴
ClO + HO ₂ → HOCl + O ₂	5.0 x 10 ⁻¹²
ClO + NO → NO ₂ + Cl	1.7 x 10 ⁻¹¹
ClO + NO ₂ + M → ClONO ₂ + M	4.6 x 10 ⁻¹³
HO ₂ + HO ₂ → H ₂ O ₂ + O ₂	1.9 x 10 ⁻¹²
HO ₂ + NO ₂ + M → HO ₂ NO ₂ + M	3.8 x 10 ⁻¹³
HO ₂ + NO → NO ₂ + OH	8.1 x 10 ⁻¹²

Rate constants are from *DeMore et al.* [1997] and *Mallard et al.* [1994] at 298 K and 100 Torr. The rate constant for the reaction OH + ClO → HO₂ + Cl is from measurements of this reaction reported in Chapter 3.

Table 2. Summary of Experimental Conditions and Results for the Branching Ratio Studies of the OH + ClO Reaction

Expt. #	T (K)	P (Torr)	[OH] ₀ (10 ¹¹ molecule cm ⁻³)	[ClO] ₀ (10 ¹¹ molecule cm ⁻³)	k _{1b} (10 ⁻¹³ cm ³ molecule ⁻¹ s ⁻¹)	Branching Ratio (k _{1b} /k ₁)
1	298	98	3.5	6.0	10.2	0.070
2	298	94	2.2	6.1	9.5	0.065
3	298	97	1.8	8.3	10.4	0.071
4	298	96	1.4	7.9	8.6	0.059
5	298	96	1.9	4.9	10.2	0.070
6	298	94	1.2	8.2	9.1	0.062
7	298	191	2.2	7.0	8.3	0.057
8	298	201	1.3	5.7	9.1	0.062
9	298	203	1.9	6.6	10.2	0.070
10	275	171	2.2	6.9	10.2	0.064
11	259	152	1.5	5.8	10.5	0.062
12	246	157	1.4	6.2	12.2	0.068
13	233	152	1.8	5.6	13.1	0.068
14	217	140	1.7	6.6	15.1	0.071
15	207	127	2.5	6.5	14.5	0.064

atoms produced in the main flow tube. Under optimal experimental conditions, reaction 3 can only produce levels of HCl ($\sim 10^8$ molecule cm⁻³) that are below the detection limit of our instrument. In theory, Cl atoms from reaction 1a could also react with H₂O₂, from the self-reaction of OH, to form HCl and HO₂. However, this reaction is relatively slow ($k = 4.1 \times 10^{-13}$ cm³ molecule⁻¹ s⁻¹ [DeMore *et al.*, 1997]), and the concentrations of H₂O₂ and Cl in the flow tube are low enough that this reaction can only produce levels of HCl that are far below the detection limit of the instrument under our experimental conditions.

Computer modeling was used to extract a rate constant for reaction 1b by fitting the observed HCl production. The model input included the initial concentrations of ClO, OH, and of all precursors. Table 2 contains a list of the initial conditions and calculated rate constants (k_{1b}) for the branching ratio experiments. The observed HCl signal was found to increase linearly over the experimental reaction time as can be seen in Figure 7.

Modeling confirms that the HCl signal is practically linear and does not approach its equilibrium level under typical experimental conditions and reaction times. In Figure 8, the observed HCl rise from Figure 7 (minus the HCl background) has been plotted versus the experimental reaction time. For this experiment, a rate constant of $k_{1b} = 1.04 \times 10^{-12} \text{ cm}^3 \text{ molecule}^{-1} \text{ s}^{-1}$ was found to give the best fit to the data as shown in Figure 8. For comparison, the model was also run assuming the same initial conditions, but varying k_{1b} in order to demonstrate the sensitivity of the modeling procedure. The model HCl signal and the least-squares fit to the data have been plotted in Figure 8 for the case where k_{1b} was doubled and the case where k_{1b} was halved. These model HCl curves are clearly not consistent with the observed HCl production, and therefore these values of the rate constant ($k_{1b} = 2.08 \times 10^{-12}$ and $5.2 \times 10^{-13} \text{ cm}^3 \text{ molecule}^{-1} \text{ s}^{-1}$) are easily excluded by the data. Figure 8 demonstrates that accurate determinations of the rate constant for the minor channel could be made using the modeling procedure described above.

The branching ratio for the OH + ClO reaction was measured at room temperature and at a pressure of 100 Torr under a variety of conditions to ensure that the results were independent of the initial concentrations. In experiment 5, close to optimal initial concentrations for OH and ClO were used, such that the observed HCl production was due to reaction 1b only. In experiment 1, the initial OH concentration was increased by 85% compared to experiment 5. Under these conditions, modeling shows that ~20% of the observed HCl production was due to the side reaction $\text{HO}_2 + \text{Cl}$. Despite the different initial conditions and the differing amounts of HCl production from side reactions, experiments 1 and 5 yielded the same rate constant for the minor channel ($k_{1b} = 10.2 \times 10^{-13} \text{ cm}^3 \text{ molecule}^{-1} \text{ s}^{-1}$). Therefore, the modeling approach appears to correctly simulate the chemistry in our system, yielding branching ratio results which are independent of the initial conditions.

As expected, the fitting procedure used to calculate k_{1b} is sensitive to the initial concentrations of OH and ClO and to the observed concentration of HCl produced over a

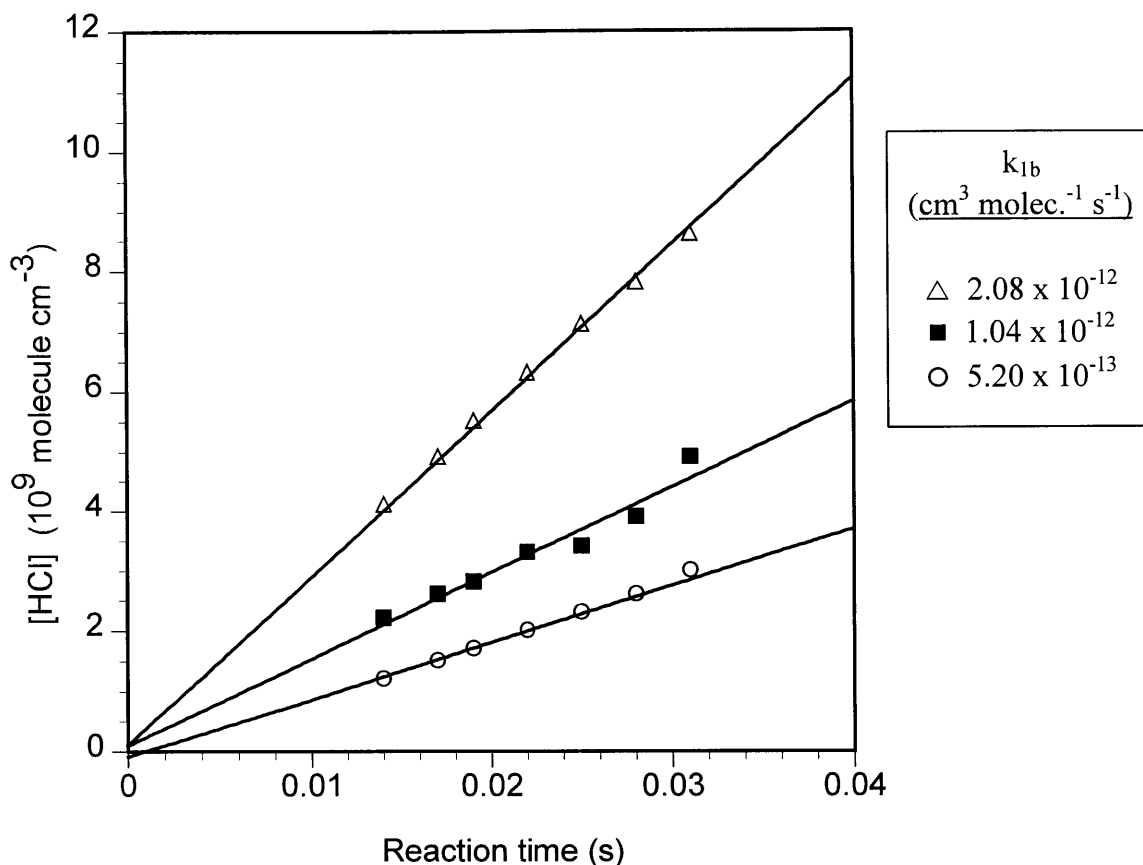


Figure 8. Comparison of measured and modeled HCl production for different model inputs for k_{1b} : Observed HCl rise (minus the HCl background) (■); this data was obtained under the same conditions as listed in Figure 7. The best fit to the data yields $k_{1b} = 1.04 \times 10^{-12} \text{ cm}^3 \text{ molecule}^{-1} \text{ s}^{-1}$. Modeled HCl rise when k_{1b} is doubled (△) and when k_{1b} is halved (○).

specific reaction time. These concentrations were measured to better than 30% accuracy; we found that these errors propagate linearly into the calculated branching ratio. The fitting procedure used to calculate k_{1b} is also affected by the other rate constants used in the model. For example, increasing the rate constant k_3 for the reaction $\text{Cl} + \text{HO}_2 \rightarrow \text{HCl} + \text{O}_2$ increases the proportion of HCl production coming from side reactions, and therefore decreases k_{1b} ; however, a 50% increase in k_3 leads to only a 20% decrease in the calculated value of k_{1b} . Furthermore, the fitting procedure is not very sensitive to

changes in the rate constant k_{1a} for the major channel of the OH + ClO reaction. For example, changing k_{1a} by 50% leads to less than a 15% change in the calculated value of k_{1b} . In the modeling procedure we assumed that $k_{1a} = k_1$. This assumption was necessary in the initial analysis of the data when the value of k_{1b} was unknown. However, a reanalysis of one data set using $k_{1a} = k_1 - k_{1b}$ verified that our initial assumption introduced negligible error into the branching ratio measurements.

Although modeling shows that for optimal initial conditions the observed HCl production cannot be due to homogeneous side reactions, the possibility exists that the HCl could be a result of heterogeneous reactions on the wall of the flow tube. In our previous study of OD + ClO (Chapter 3), we performed two experiments to demonstrate that the observed DCl production was not due to heterogeneous processes. First, we checked that an uncoated tube gave results in very good agreement with those obtained with the Halocarbon wax-coated tube, indicating that the observed DCl production was not due to reactions on the wall of the flow tube. Second, the total pressure in the flow tube was increased by almost a factor of two. As discussed in Chapter 3, the effects of heterogeneous processes are reduced at higher pressures [Seeley *et al.*, 1993], and yet the branching ratio did not decrease when the pressure was increased. These experiments provided further evidence that the observed DCl production was not due to heterogeneous processes. In fact, the branching ratio for OD + ClO was observed to increase by ~35% at the higher pressure (180 vs. 95 Torr). Considering experimental uncertainties, we were not able to draw any definite conclusions about the pressure dependence of the branching ratio. There are many examples of radical-radical reactions that proceed through an intermediate complex which is stabilized at higher pressures. However, in the case of OD + ClO, theoretical calculations indicate that the intermediate complex (DOOCl*) is not long-lived enough to be stabilized by collisions under atmospheric conditions [Dubey *et al.*, 1998]. This point will be discussed in more detail below in the section describing the statistical rate theory calculations.

In this study, we have conducted a more thorough investigation of the pressure dependence of the OH + ClO branching ratio, and the results are presented in Table 2. The measured rate constants for the minor channel at 200 Torr are clearly within the range of the values for the 100 Torr experiments. In these experiments we did not see any evidence for a pressure effect on the rate constant of reaction 1b. Furthermore, in our previous measurements we found the overall rate constant of the OH + ClO reaction (k_1) to be independent of pressure as demonstrated by the good agreement between our measurements at 100 Torr and previous measurements at low pressure (~ 1 Torr) [Hills and Howard, 1984]. We therefore conclude that the branching ratio of the OH + ClO reaction is independent of pressure for conditions relevant to the stratosphere. Two important modifications to the experimental apparatus have been made for these measurements, which might help to explain the slight discrepancy between the DCl and HCl experiments. The first modification was that the diameter of the aperture between the flow tube and ion-molecule region was varied in order to maintain a constant pressure in the ion-molecule region for the HCl measurements at 200 Torr. In the DCl experiments, the aperture size was kept constant even at higher pressures. Thus, the doubling of pressure in the flow tube from 95 to 180 Torr also created a doubling of pressure in the ion-molecule region. This doubling of neutral concentrations in the ion-molecule region may have contributed to an increase in secondary ion-molecule reactions which could have affected the DCl experiments at 180 Torr. The second modification to the experimental apparatus was that the shape of the turbulizer, on the end of the movable injector, was redesigned to better enhance turbulent mixing in the flow tube at increased pressures. In our DCl experiments, an open, fan-shaped turbulizer (Figure 9a) was used for the measurements at both 95 and 180 Torr. However, in recent mixing tests we found that a modified turbulizer design (Figure 9b) helped to improve mixing at 200 Torr. In the new design, the gas in the movable injector is forced through a series of small holes punched in several pieces of Teflon tubing that protrude into the flow tube perpendicular

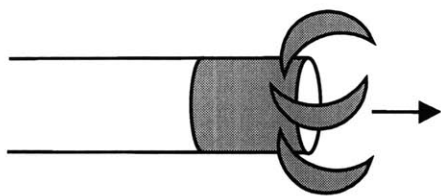


Figure 9a

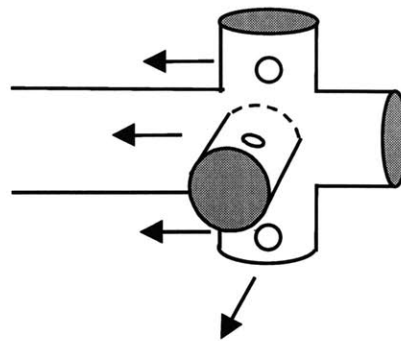


Figure 9b

Figure 9. Comparison of old design (9a) and new design (9b) for the turbulizer, placed on the end of the movable injector in order to enhance turbulent mixing. In the new design, the gas from the movable injector is forced through a series of holes that are perpendicular or opposite to the direction of the main flow.

to the direction of the main flow. All of the branching ratio studies for the OH + ClO reaction were conducted using this modified turbulizer design. In the DCl experiments at 180 Torr, insufficient mixing may have contributed to error in the measurement of the branching ratio. Overall, the discrepancy between the HCl and DCl measurements at higher pressures is certainly within the reported errors of the measurements. However, we believe that these two recent improvements to the apparatus have produced more accurate measurements of the branching ratio for the OH + ClO reaction at 200 Torr.

We performed several measurements of the branching ratio for OH + ClO at temperatures between 207 and 298 K in order to establish the temperature dependence of the rate constant k_{1b} for conditions relevant to the stratosphere. From the data listed in Table 2 and plotted in Figure 10, we obtain the Arrhenius expression $k_{1b}(T) = (3.2 \pm 0.8) \times 10^{-13} \exp [(325 \pm 60) / T] \text{ cm}^3 \text{ molecule}^{-1} \text{ s}^{-1}$. The uncertainty represents the two standard deviation statistical error in the data and is not an estimate of systematic errors. The negative temperature dependence of k_{1b} indicates that reaction 1b most likely

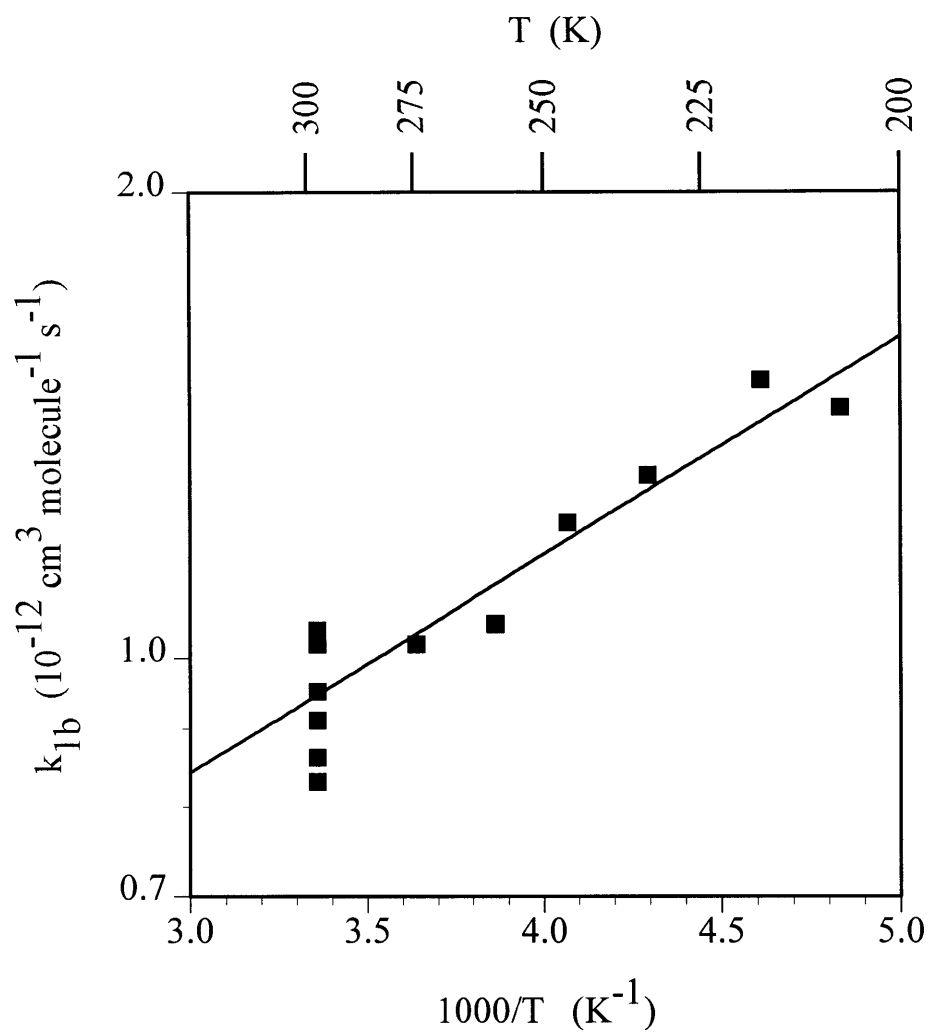


Figure 10. Arrhenius plot for the reaction $\text{OH} + \text{ClO} \rightarrow \text{HCl} + \text{O}_2$, the least-squares fit to the data yields the expression $k_{1b}(T) = (3.2 \pm 0.8) \times 10^{-13} \exp [(325 \pm 60) / T] \text{ cm}^3 \text{ molecule}^{-1} \text{ s}^{-1}$.

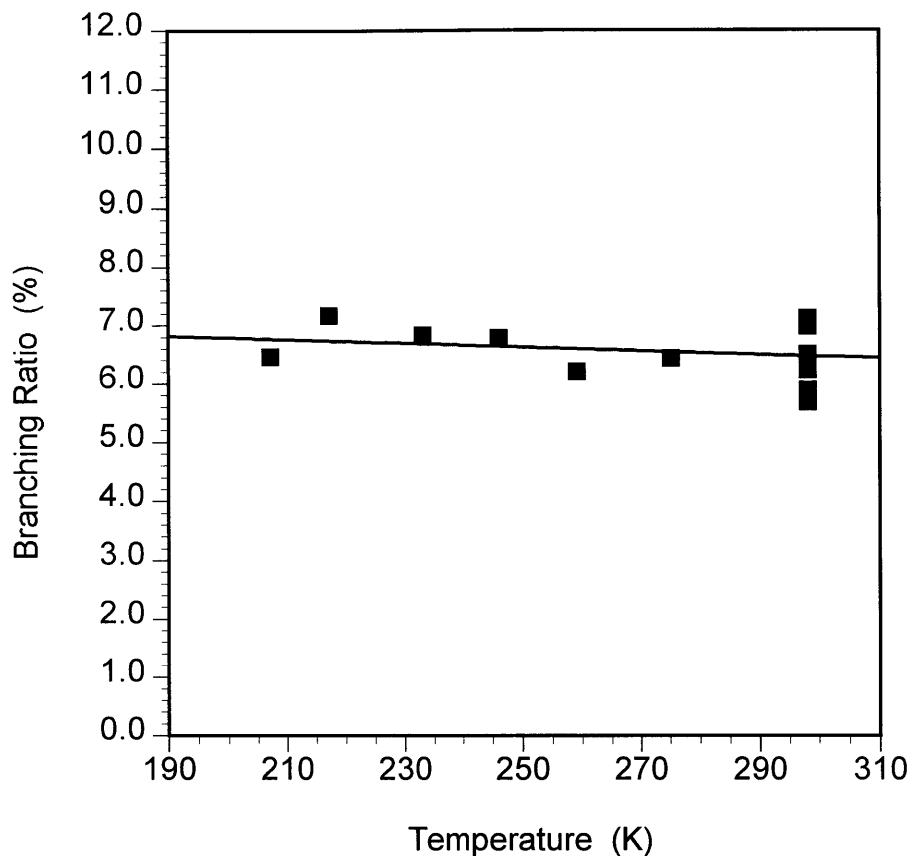


Figure 11. Plot of the branching ratio $[(k_{1b}/k_1) * 100\%]$ for the OH + ClO reaction as a function of temperature.

proceeds through an intermediate complex [Trope, 1994]. The fundamental reaction dynamics of the OH + ClO system will be discussed in more detail in the next section describing the statistical rate theory calculations. The branching ratios (k_{1b}/k_1) reported in Table 2 were calculated using the measured Arrhenius expression for the overall rate constant of the OH + ClO reaction from Chapter 3: $k_1(T) = (5.5 \pm 1.6) \times 10^{-12} \exp[(292 \pm 72)/T] \text{ cm}^3 \text{ molecule}^{-1} \text{ s}^{-1}$. The branching ratio for the OH + ClO reaction has been determined to be 0.07 ± 0.03 . Within the error of the measurement, the branching ratio does not appear to have a strong temperature dependence, as can be seen in Figure 11. The reported error for the branching ratio is an estimate of the systematic error and the

uncertainty of the model fitting procedure based on a sensitivity analysis. In our previous study of the OD + ClO reaction, we found that the branching ratio to form DCI ranged from 0.05 ± 0.02 at 298 K to 0.06 ± 0.02 at 211 K. In the OH + ClO branching ratio studies at low temperatures, there may exist a slight trend toward increasing branching ratios at lower temperatures. However, within the error of the OH + ClO branching ratio measurements, it is difficult to identify a trend of less than 1%. Therefore, we conclude that the branching ratio is essentially independent of temperature under conditions relevant to the atmosphere. Overall, the isotope effect on the branching ratio appears to be small. The observed isotope effect and its agreement with theoretical predictions will be discussed further in the next section describing the statistical rate theory calculations.

Our results for the branching ratio of reaction 1 are consistent with the results of previous studies, which are presented in Table 3. As discussed in Chapter 3, previous attempts to measure the branching ratio were unsuccessful in ruling out an HCl yield of zero for the minor channel due to uncertainties in the results. The laboratory studies were not able to directly observe a product from reaction 1b due to either the inability to detect HCl and O₂ [*Leu and Lin, 1979; Burrows et al., 1984; Hills and Howard, 1984*] or due to insufficient sensitivity for HCl [*Poulet et al., 1986*]. Because of the indirect methods used and the large reported errors, all four previous studies were unable to positively establish the existence of the minor channel. In contrast, our direct measurements of HCl production from reaction 1b over the experimental reaction time have positively established the existence and kinetic significance of the minor channel under atmospherically relevant conditions.

Our measurements of the branching ratio for the OH + ClO reaction should help to improve models of stratospheric chlorine partitioning. As mentioned in the Introduction, atmospheric models have tended to overestimate the ClO/HCl ratio in the upper stratosphere. Numerous modeling studies have proposed that including a small branching ratio for reaction 1 would resolve discrepancies between measured and calculated

Table 3. Comparison of Measured Branching Ratios for the OH + ClO Reaction

Technique	T (K)	P (Torr)	Branching Ratio (k_{1b}/k_1)	Reference
DF-LF/RF	298	1.0-3.5	< 0.35	Leu and Lin [1979]
DF-LF/RF	243-298	1.0-5.0	0.15 ± 0.2	Burrows et al. [1984]
DF-LF/LMR	293	1.0	0.14 ± 0.14	Hills and Howard [1984]
DF-LF/EIMS	298	0.5-0.9	0.02 ± 0.12	Poulet et al. [1986]
DF-TF/CIMS	211-298	100	0.06 ± 0.02 at 211 K 0.05 ± 0.02 at 298 K	Lipson et al. [1997] OD + ClO
DF-TF/CIMS	207-298	100-200	0.07 ± 0.03	This work Lipson et al. [1999]

DF, discharge flow; LF, laminar flow; TF, turbulent flow; RF, resonance fluorescence detection; LMR, laser magnetic resonance detection; EIMS, electron impact mass spectrometry detection; CIMS, chemical ionization mass spectrometry detection.

chlorine partitioning. Some very recent studies have already incorporated the results of our DCI experiments (Chapter 3) into their models [*Khosravi et al.*, 1998; *Ruhnke*, 1999], and have been able to more accurately reproduce measurements of ClO and HCl mixing ratios in the upper stratosphere. The direct measurements of HCl production from reaction 1 presented in this chapter should help to further refine modeled chlorine partitioning.

Because of the demonstrated kinetic significance of the minor channel for the OH + ClO reaction, it is interesting to consider whether this channel might also be accessible in the analogous bromine reaction. There has only been one experimental study of the OH + BrO reaction [*Bogan et al.*, 1996], and the overall rate constant was determined to be

$(7.5 \pm 4.2) \times 10^{-11} \text{ cm}^3 \text{ molecule}^{-1} \text{ s}^{-1}$ at 300 K and 1 Torr. *Bogan et al.* proposed that the reaction most likely proceeds through the formation of the HOOBr intermediate complex, similar to the proposed mechanism for the OH + ClO reaction (discussed in more detail below). Similar to OH + ClO, the OH + BrO reaction has two possible exothermic product channels: $\text{HO}_2 + \text{Br}$ ($\Delta H_{\text{R}} = -10 \text{ kcal mol}^{-1}$) and $\text{HBr} + \text{O}_2$ ($\Delta H_{\text{R}} = -48 \text{ kcal mol}^{-1}$). *Bogan et al.* were unable to put any limits on the product distribution from OH + BrO due to interfering side reactions in their system. However, two recent modeling studies have proposed that including a small branching ratio for HBr production (1-3%) in their models would help to improve the agreement between measured and calculated HBr mixing ratios in the upper stratosphere [*Chipperfield et al.*, 1997; *Chartrand and McConnell*, 1998]. Further experimental and theoretical studies are needed to determine if HBr formation is feasible from the OH + BrO reaction.

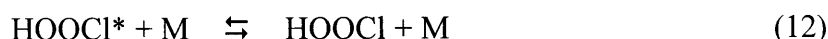
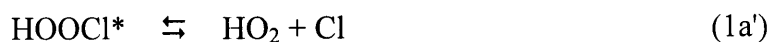
4.3.2 Statistical Rate Theory Calculations

As already outlined above, the overall reaction of OH + ClO is assumed to proceed via an addition-elimination mechanism [*Weissman et al.*, 1981; *Burrows et al.*, 1984; *Dubey et al.*, 1998]. In order to verify and rationalize the experimentally determined branching ratios and to characterize the influence of isotopic substitution, a detailed modeling using master equations and statistical rate theory was performed by Matthias Olzmann in collaboration with our research group [*Lipson et al.*, 1999]. The temperature and pressure dependence of the overall rate constant was also examined, because an adequate description of these different quantities by a common model could provide additional evidence for the postulated mechanism.

Within this model, the reactions



correspond to the following microscopic steps, where an asterisk denotes vibrational and rotational excitation:



Because the electronic ground state of the intermediate, HOOCI, is most likely a singlet state, reaction 1b' is assumed to yield $\text{O}_2(^1\Delta)$ due to spin conservation [Weissman *et al.*, 1981; Burrows *et al.*, 1984; Lee and Rendell, 1993; Dubey *et al.*, 1998]. The thermochemistry of the system is characterized by using the following heats of formation, $\Delta_f H^\circ_{0K}$ (in kcal mol⁻¹): ClO, 24.4; OH, 9.32; Cl, 28.59 [Atkinson *et al.*, 1992]; HO₂, 4.18 [Howard, 1980; Atkinson *et al.*, 1992]; HOOCI, 1.5 [Lee and Rendell, 1993].

An *ab initio* study by Francisco *et al.* [1994] investigated the structures and energetics of possible intermediate complexes formed by reaction 1. They identified three stable isomers: HOOCI, HOCIO and HClO₂. Of these three isomers, HOOCI was found to be the lowest energy structure. Their calculated heat of formation for HOOCI was in good agreement with the earlier study by Lee and Rendell [1993] and a more recent study by Dubey *et al.* [1998]. The equilibrium geometries for HOOCI determined by these three studies were also in good agreement. The minimum energy structure of HOOCI is a skewed conformation, as shown in Figure 12. Approximate values are given for the bond lengths and angles based on the results of the three theoretical studies.

The kinetic quantities of a chemical activation system can be derived by solving the appropriate master equation [e.g., Forst, 1972; Gilbert and Smith, 1990], which describes

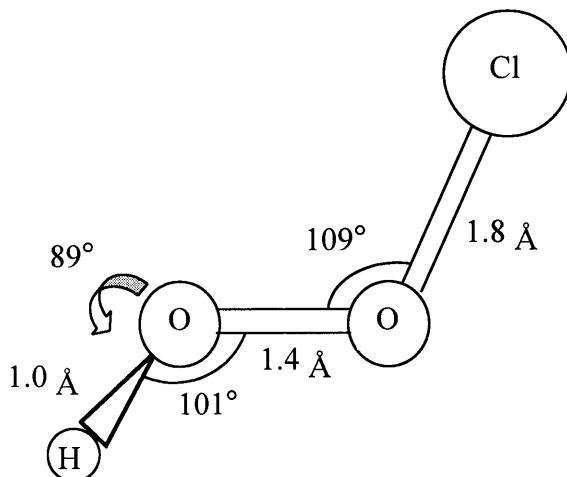


Figure 12. Equilibrium geometry for HOOCI. Approximate values for the bond lengths and angles are based on the *ab initio* calculations of *Lee and Rendell* [1993], *Francisco et al.* [1994], and *Dubey et al.* [1998].

the balance over all gain and loss processes for a given energy level, E_i , of the intermediate, i.e., in our case of HOOCI:

$$\frac{dn_i}{dt} = R_{\text{form}} f_i - \omega n_i + \omega \sum_j P_{ij} n_j - (k_{-1,i} + k_{1a',i} + k_{1b',i}) n_i \quad (13)$$

Here, $n_i = n(E_i)$ is the concentration of the intermediate with an internal energy E_i . R_{form} represents the overall rate of its formation and $f_i = f(E_i)$ its normalized nascent distribution function as generated by this formation reaction. The second and third terms characterize the collisional depopulation and population, respectively, of the energy level in question with ω being the collision frequency and P_{ij} the probability for a transition $E_i \leftarrow E_j$. Finally, the last term describes the unimolecular reaction steps of the energized adduct with the specific rate constants $k_{r,i} = k_r(E_i)$ for the reaction pathway r . The energy, in general, is counted from the rovibrational ground state of HOOCI.

Equation 13 can be cast into matrix form [Robinson and Holbrook, 1972], and, assuming steady-state conditions [Schranz and Nordholm, 1984], $dn_i/dt = 0$, one obtains

$$\mathbf{R}_{\text{form}} \underline{\mathbf{F}} = \left[\omega (\underline{\mathbf{I}} - \underline{\mathbf{P}}) + \sum_r \underline{\mathbf{K}}_r \right] \underline{\mathbf{N}}^s \equiv \underline{\mathbf{J}} \underline{\mathbf{N}}^s \quad (14)$$

where the vector/matrix symbols correspond to the symbols in eq 13, and $\underline{\mathbf{I}}$ denotes the unit matrix. The steady-state population $\underline{\mathbf{N}}^s$ can be calculated by inversion of the matrix $\underline{\mathbf{J}}$, and then the rate of the r -th unimolecular step, D_r , can be obtained by averaging the rate constants $k_{r,i}$ over the steady-state distribution. Using the principle of mass conservation, $R_{\text{form}} = D_{-1} + D_{1a'} + D_{1b'} + S$, the yield of the stabilized intermediate (S) can be obtained as follows:

$$\frac{S}{R_{\text{form}}} = 1 - \sum_r \frac{D_r}{R_{\text{form}}} \quad (15)$$

In this way, all branching ratios of interest can be calculated.

The measurable bimolecular rate constant at a given temperature and pressure, $k_1(T,P)$, can be related to the corresponding capture or high-pressure limiting value, $k_1^\infty(T)$, by the relation:

$$k_1(T,P) = k_1^\infty(T) \left[1 - \frac{D_{-1}(T,P)}{R_{\text{form}}(T)} \right] \quad (16)$$

Here, k_1 is expressed as the product of the pressure independent capture rate constant and a yield factor, which characterizes the fraction of the intermediates that does not

redissociate [e.g., *Troe*, 1994]. One should note that the temperature dependence of k_1 is a combined effect of the temperature dependence of both k_1^∞ and the yield factor, whereas the pressure dependence is only governed by the latter. The quantity R_{form} does not need to be specified, because it only implicitly appears within the ratios D_r/R_{form} . For $\text{ClO} + \text{OH}$, it would follow that $R_{\text{form}} = k_1^\infty(T)[\text{ClO}][\text{OH}]$, and because this represents a capture rate, it is not pressure dependent.

The methods applied for the calculation of the different quantities in eq 13 and 14 are briefly described next. The nascent population of HOOC1 , $f(E)$, is approximated by a shifted thermal distribution, and the specific unimolecular rate constants are calculated by statistical rate theory [e.g., *Forst*, 1972; *Gilbert and Smith*, 1990]:

$$k_r(E) = \frac{W_r(E - E_{0(r)})}{h \rho_{\text{HOOC1}}(E)} \quad (17)$$

where W_r denotes the sum of states, $E_{0(r)}$ represents the reaction threshold energy, ρ_{HOOC1} is the density of states of the intermediate, and h is Planck's constant. For the number of open reaction channels W_r , one has to distinguish between two different cases. Reactions -1 and 1a' are simple bond fissions and W_r is calculated by the statistical adiabatic channel model (SACM) in its simplified version [*Troe*, 1983]. Reaction 1b', on the other hand, proceeds via a well-defined transition-state configuration [*Weissman et al.*, 1981; *Dubey et al.*, 1998], and, accordingly, $W_{1b'}$ is identified with its sum of states (RRKM model) [*Marcus*, 1952].

All densities and sums of states are determined by direct counting procedures [*Troe*, 1983; *Olzmann and Troe*, 1994] for a total angular momentum quantum number $J = 15$. This value corresponds to an average, which can be estimated from the angular momenta of the reactants and the orbital angular momentum associated with the capture process [*Olzmann*, 1997]. It turns out that the influence of J on the branching ratios is very weak

Table 4. Rotational Constants and Frequencies Used in the Modeling Calculations

Species	A, B, C (cm ⁻¹)	ν_i (cm ⁻¹)
OH	18.91 ^a	3738 ^a
OD	10.02 ^b	2721 ^b
ClO	0.623 ^a	854 ^a
HO ₂	20.82, 1.154, 1.097 ^c	3459, 1370, 1161 ^c
DO ₂	11.40, 1.087, 0.993 ^c	2548, 1173, 1009 ^c
HOCl	1.606, 0.201, 0.182 ^d	3589, 1372, 851, 610, 407, 353 ^d
DOCl	1.454, 0.193, 0.175 ^d	2615, 1013, 850, 609, 361, 292 ^d
HCl-O ₂ ^e	1.213, 0.139, 0.125 ^d	3154, 1494, 972, 443, 189 ^d
DCl-O ₂ ^e	1.117, 0.138, 0.124 ^d	2299, 1129, 928, 396, 185 ^d

^aRadzig and Smirnov, 1985. ^bHerzberg, 1950. ^cCalculated *ab initio* at UMP2/6-311+G(d,p) level with Gaussian 94 (Frisch *et al.*, 1995), frequencies scaled by a factor of 0.943 (Scott and Radom, 1996). ^dDubey *et al.*, 1998. ^eTransition state of reaction 1b'.

within the range accessible at temperatures between 200 and 300 K ($5 \leq J \leq 25$). The molecular geometries and frequencies employed in our calculations are compiled in Table 4.

For the transition probabilities P_{ij} , a stepladder model obeying detailed balancing is used [e.g., Robinson and Holbrook, 1972; Gilbert and Smith, 1990]. For the step size, we assume $\Delta E_{SL} = 100 \text{ cm}^{-1}$, which corresponds to an average energy transferred per collision of about -20 cm^{-1} [Snider, 1985]. This is a reasonable value compared to other molecules of similar excitation energy and size [e.g., Heymann *et al.*, 1988]. Moreover, it turns out that the calculated branching ratios are again quite insensitive to this quantity (see below). The collision frequency of HOCl in air, ω , is based on a Lennard-Jones

collision number of $1 \times 10^7 \text{ Torr}^{-1} \text{ s}^{-1}$ at 300 K [Reid *et al.*, 1987]. The inversion of the tridiagonal matrix \underline{J} is achieved by standard procedures with a grain size of 10 cm^{-1} .

The relative branching fraction (yield) for the channel leading to $\text{HCl} + \text{O}_2$ is expressed as

$$Y_{1b'} = \frac{D_{1b'}}{D_{1a'} + D_{1b'} + S} \quad (18)$$

It is accessible *via* eq 15, where the rate of formation, R_{form} , cancels. One should note that D_{-1} is missing in the denominator, because it merely represents the reaction back to $\text{OH} + \text{ClO}$ and, therefore, must not be included in the balance governing $Y_{1b'}$.

As already mentioned, the specific rate constants for the dissociation reactions -1 and 1a' are calculated by the statistical adiabatic channel model. With the molecular data for the reactants and reaction products from Table 4 and the thermochemical data given above, there remains one parameter to be fixed, the so called anisotropy ratio α/β [Troe, 1983]. In principle, this quantity could be adjusted to thermal high-pressure limiting rate constants for the corresponding association reactions. However, obviously the measured rate constants for $\text{OH} + \text{ClO}$ and $\text{HO}_2 + \text{Cl}$ do not represent high-pressure limits but are decreased by falloff effects (see below). Hence, we generally employ a value of $\alpha/\beta = 0.5$ in our calculations. It has been shown that in many cases, specific as well as the corresponding thermally averaged dissociation and recombination rate constants can be predicted reasonably well by using this "standard" value [Cobos and Troe, 1985]. The specific rate constants obtained in this way for the reactions -1 and 1a' are shown in Figure 13.

Reaction 1b', which proceeds through a tight transition state, is described by RRKM theory. The molecular parameters used are compiled in Table 4. The $\text{TS}_{(1b')}$ molecular parameters in Table 4 are from the *ab initio* calculations reported by Dubey *et al.* [1998].

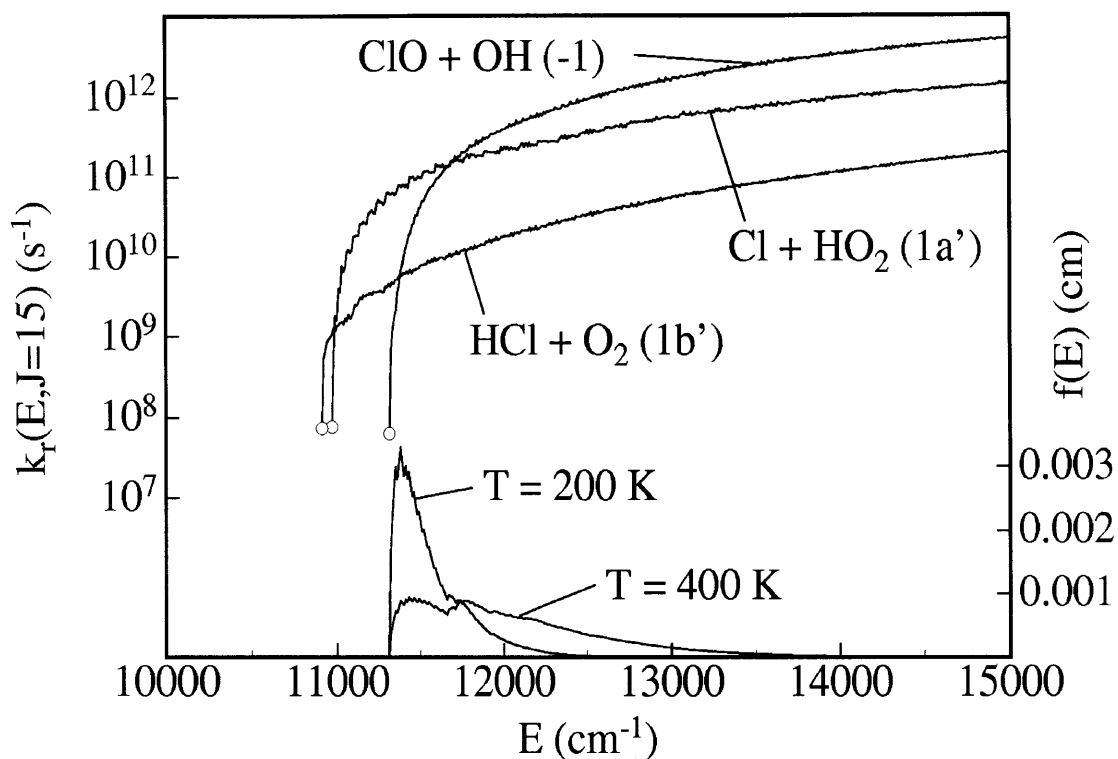


Figure 13. Specific rate constants for the different decomposition pathways and nascent molecular distribution functions for HOOC1 generated from OH + ClO at two different temperatures. The open circles mark the threshold rate constants $k_r(E_{0(r)})$

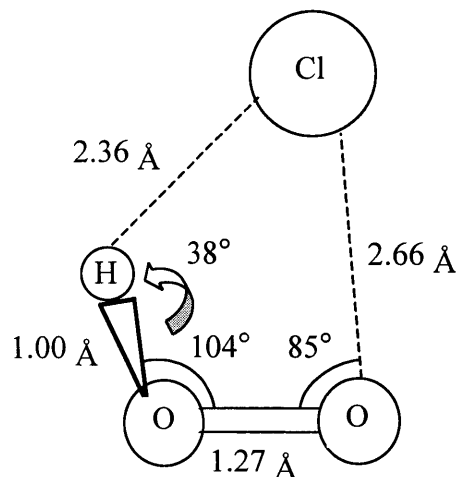


Figure 14. Optimized geometry for the 4-center transition state leading to the products $\text{HCl} + \text{O}_2$ in the $\text{OH} + \text{ClO}$ reaction from the *ab initio* calculations of *Dubey et al.* [1998].

As already discussed in the work of *Dubey et al.* [1998], the calculation of a reliable barrier height for the 4-center transition state involved is not without problems. In their study, *ab initio* calculations were performed to determine the structure and energetics of the 4-center transition state. The optimized geometry determined by their calculations is shown in Figure 14. For comparison, the height of the 4-center transition state energy barrier was calculated using several different *ab initio* methods and several different basis sets. The calculated electronic energy barriers ranged from 19.7 to 34.8 kcal mol⁻¹. The energy of the barrier tended to increase as more complete basis sets were used. A value of 30.6 kcal mol⁻¹ was determined using the cc-pVQZ basis set and the multireference CISD method corrected for size inconsistency, which they believe to be the best estimate of the electronic barrier. Including zero point contributions, the energy of the 4-center transition state was found to lie 2.3 ± 3 kcal mol⁻¹ below the $\text{OH} + \text{ClO}$ entrance channel at 0 K. However, *Dubey et al.* point out that the calculated branching ratio is very sensitive to the height of the 4-center transition state barrier, and computation of the

barrier height with sufficient accuracy ($\pm 0.3 \text{ kcal mol}^{-1}$) to predict the branching ratio to two digits after the decimal is impractical. As a result, the height of the barrier was treated as a variable parameter in their RRKM calculations. According to their calculations, a branching ratio of 7% requires that the 4-center transition state lie $2.5 \text{ kcal mol}^{-1}$ below the entrance channel, which is in good agreement with their best estimate of the energy from the *ab initio* calculations. Because of the difficulty in determining the height of the 4-center transition state barrier, we also treat $E_{0(1b')}$ as an adjustable parameter, which is fitted so as to reproduce the observed relative yield $Y_{1b'} = 0.07 \pm 0.03$ at $T = 300 \text{ K}$. A value of $(31.1 \pm 0.6) \text{ kcal mol}^{-1}$ is obtained. This lies $\sim 1.2 \text{ kcal mol}^{-1}$ below the thermochemical limit at 0 K for $\text{OH} + \text{ClO}$ and essentially agrees with the results of the calculations by *Dubey et al.* The corresponding specific rate constants are also shown in Figure 13.

The calculated branching fractions and the relative yields ($Y_{1b'}$) are compiled in Table 5. It is evident that the temperature dependence of $Y_{1b'}$ is very weak, which is in agreement with the experimental findings. The reason becomes clear by inspection of Figure 13. The curves of the specific rate constants for the two product channels, $\text{HCl} + \text{O}_2$ and $\text{Cl} + \text{HO}_2$, do not cross and are nearly parallel in the energy range, where the main part of the HOOC1 population is located. Consequently, a shift of this population to higher energies by increasing the temperature will hardly change the branching ratio. Whether the ratio is slightly decreasing (as might be suggested by the branching ratio experiments for the $\text{OD} + \text{ClO}$ reaction, *cf.* also Table 5) or increasing (as suggested by the present calculations) can not be decided unambiguously. Here, much more detailed information on the properties of $\text{TS}_{(1b')}$ and on the adiabatic channel pattern for reaction $1a'$ is required, where especially the latter is beyond the capabilities of current quantum chemical calculations.

Table 5 also shows that the influence of deuteration on the branching ratio turns out to be very weak. The calculated yields $Y_{1b'}$ for $\text{OD} + \text{ClO}$ are, on an absolute scale, only

Table 5. Relative Branching Fractions for HOOCI (DOOCI) formed from OH (OD) + ClO, P = 100 Torr, $\Delta E_{SL} = 100 \text{ cm}^{-1}$

T (K)	D_{-1}/R_{form}	D_{1a}/R_{form}	D_{1b}/R_{form}	$Y_{1b'}$	$Y_{1b'}(\text{exp})$	$Y_{1b'}$	$Y_{1b'}(\text{exp})^a$
	HOOCI				DOOCI		
200	0.3010	0.6506	0.0484	0.0693	0.07 ± 0.03	0.0588	0.06 ± 0.02 ^b
250	0.3733	0.5831	0.0436	0.0695		0.0599	
300	0.4362	0.5241	0.0396	0.0703		0.0613	0.05 ± 0.02
400	0.5341	0.4319	0.0340	0.0730		0.0647	

^aLipson *et al.*, 1997 (Chapter 3). ^bT = 211 K. exp: experimental values.

~1% lower than those for OH + ClO. This is again in agreement with the experimental findings.

By averaging the specific rate constants over the molecular distributions, a lifetime of ~ 5 ps can be estimated for the vibrationally excited HOOCI* generated from ClO + OH. Therefore, collisional stabilization is negligible under atmospheric conditions, and the branching ratios are virtually independent of pressure, in agreement with our measurements of the branching ratio at 100 and 200 Torr. For instance, at P = 100 Torr, the relative fraction of stabilized HOOCI lies between 1×10^{-6} and 1×10^{-7} in the temperature range 200-400 K, and at T = 300 K, the HCl + O₂ yield increases from 0.07030 at 1 Torr to 0.07035 at 760 Torr. This general picture is also not influenced by a change of the energy-transfer parameter of the stepladder model.

Equation 16 and the values for D_{-1}/R_{form} from Table 5 reveal that the overall rate constant for OH + ClO under atmospheric conditions is not in its high-pressure limit, since ~30 to ~45% redissociation occurs, depending on the temperature. Consequently, a

comparison of the predicted and observed overall rate constants is useful in order to evaluate the quality of our model and to derive additional information on the reaction mechanism. Furthermore, it can be shown from eq 16 that the pressure dependence of the rate constant k_1 is governed solely by the relative branching fraction D_{-1}/R_{form} . The latter, however, proves nearly independent of pressure. For example, at $T = 300$ K, it varies from 0.4359 to 0.4363 upon increasing the pressure from 1 to 760 Torr (see the discussions above). Thus, the pressure dependence of k_1 is negligible in this range. As discussed in Chapter 3, our measurements of the overall rate constant for the OH + ClO reaction at 100 Torr were found to be in good agreement with previous measurements made at low pressures (~ 1 Torr) [e.g., *Hills and Howard*, 1984]. The experimental results confirm that the overall rate constant does not have a significant pressure dependence.

Whereas the yield factor in eq 16 follows from the master equation, the high-pressure limiting rate constant, $k_1^\infty(T)$, is calculated directly from the canonical version of the SACM [*Cobos and Troe*, 1985]. For reaction 1, $\text{OH} + \text{ClO} \rightarrow \text{HOOCI}^*$, it can be written as

$$k_1^\infty(T) = k_1^{\text{PST}}(T) f_1^{\text{rigid}}(T) \quad (19)$$

Here, the first factor,

$$k_1^{\text{PST}}(T) = \frac{k_B T}{h} \left(\frac{h^2}{2\pi \mu k_B T} \right)^{3/2} \frac{Q_{\text{el}}(\text{HOOCI})}{Q_{\text{el}}(\text{OH})Q_{\text{el}}(\text{ClO})} Q_{\text{cent}} \quad (20)$$

represents the rate constant in the loose or phase-space limit, i.e., in a purely isotropic potential, and a rigidity factor, $f_1^{\text{rigid}} \leq 1$, globally accounts for the anisotropy [*Cobos and*

Troe, 1985]. In eq 20, μ denotes the reduced mass of OH and ClO and Q_{el} the corresponding electronic partition functions. For the discussion of the temperature dependence of k_1^∞ , one can essentially concentrate on k_1^{PST} , since the rigidity factors are often only slightly temperature dependent. Thus, provided the electronic partition functions are known, the main task remaining is the determination of the centrifugal partition function Q_{cent} . It can be calculated from the maxima, $E_{0(l)}(J)$, of the effective potential

$$V_{eff}(q) = V(q) + B_{cent}(q)J(J+1) \quad (21)$$

as follows:

$$Q_{cent}(T) = \sum_{J=0}^{\infty} (2J+1) \exp\left(-\frac{E_{0(l)}(J) - E_{0(l)}(J=0)}{k_B T}\right) \quad (22)$$

where q is the interfragment distance between OH and ClO. In the original version of the simplified SACM [*Troe*, 1983], a Morse potential was adopted for $V(q)$ and approximate expressions for the effective rotational constant, B_{cent} , were employed. In our calculations, we used the quasitriatomic model for the latter [*Troe*, 1981], and the rigidity factors as given by *Cobos and Troe* [1985] (formally multiplied by a factor Q_{cent}^*/Q_{cent} , because eq 20 contains Q_{cent} instead of Q_{cent}^* used in the work of *Cobos and Troe*). All electronic partition functions were set identical to the corresponding ground-state degeneracy with the exception of OH/OD, for which the partition function was calculated with a spin-orbit splitting of 139.7 cm^{-1} [*Herzberg*, 1950].

The results of the calculations are shown in Figure 15. One can realize that the predicted rate constants based on a Morse potential and a value of $\alpha/\beta = 0.5$, k_1^{MO} , are

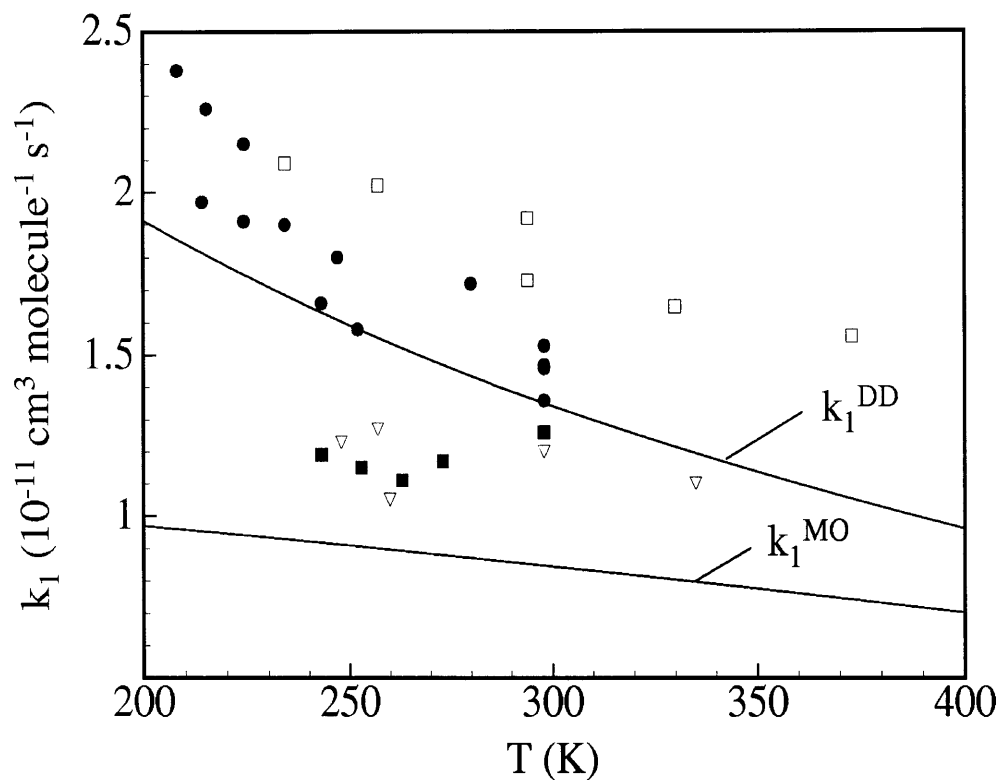


Figure 15. Calculated and reported experimental rate constants for the reaction $\text{OH} + \text{ClO}$. Experiments: \blacksquare *Burrows et al.* [1984]; \square *Hills and Howard* [1984]; \bullet *Lipson et al.* [1997]; ∇ *Ravishankara et al.* [1983]. The calculated values are based on a Morse (k_1^{MO}) and a dipole-dipole (k_1^{DD}) potential for k_1^∞ , respectively (see text).

likely to be somewhat too small, and their temperature dependence is probably too weak. The latter is a known deficiency of this simple approximation, and the situation can be improved by using a more adequate interfragment potential [Trope, 1986].

Because both OH and ClO have comparably large dipole moments ($\mu_{\text{OH}} = 1.66$ D, $\mu_{\text{ClO}} = 1.24$ D [Radzig and Smirnov, 1985]), the corresponding long-range electrostatic interaction is a better description of the potential range that governs the capture process. From the isotropic part of the dipole-dipole interaction, it follows $V(q) = -2\mu_{\text{OH}}\mu_{\text{ClO}}/q^3$ and the centrifugal rotational constant becomes $B_{\text{cent}}(q) = \hbar^2/(2\mu q^2)$ [Trope, 1985; Levine and Bernstein, 1987]. For such types of effective potentials, the evaluation of Q_{cent} is straightforward, because the maxima, $E_{0(1)}(J)$, can be calculated analytically [Levine and Bernstein, 1987]. It turns out that in the temperature range from 200 to 400 K, the average (Boltzmann weighted) J in Q_{cent} varies from 49 to 55. The corresponding maxima of the effective potential, $E_{0(1)}(J = 49)$ and $E_{0(1)}(J = 55)$, are located at interfragment distances of 9.6 and 7.7×10^{-10} m, respectively. That is, the main part of Q_{cent} is indeed sampled over a range, where the dipole-dipole interaction is likely to provide the dominating contribution to the potential energy, and where valence forces to a first approximation can be neglected. The rate constants, k_1^{DD} , obtained in this way are also shown in Figure 15. Here, a rigidity factor $f_1^{\text{rigid}} \approx 0.354$ was used [Maergoiz et al., 1996], which is independent of temperature for a pure dipole-dipole interaction. The agreement with the experimental data is reasonable, and we note again that the only adjustable parameter is $E_{0(1b)}$. Because the dipole-dipole potential is probably more adequate than the Morse potential, our calculations favor the experimental rate constants with the stronger temperature dependence.

The influence of deuteration on the recombination rate is potentially underestimated by the calculations. In the experiments presented in Chapter 3, an isotope effect of $k_1(\text{OH} + \text{ClO})/k_1(\text{OD} + \text{ClO}) \approx 1.4$ was determined experimentally in the temperature range 200-300 K. From our model, based on the dipole-dipole potential, a value of \approx

1.03 is obtained. However, it is important to note that the uncertainty in the experimental determination is large, since it involves independent measurements of OH and OD decays. Considering the reported experimental errors, a value of 1.03 is not excluded by the measurements. Considering furthermore the uncertainties in the calculations, the predicted isotope effect and the measured isotope effect for k_1 are in reasonable agreement. Nonetheless, it is interesting to raise the question of whether the rather small isotope dependence of the branching ratio $Y_{1b'}$ given above can be correctly predicted (*cf.* Table 5). The situation is most conveniently analyzed in terms of eq 16. Here, one has to distinguish between the influence of the isotopic substitution on the capture rate constant, k_1^∞ , and on the yield factor, $(1-D_{-1}/R_{\text{form}})$. From our model, the respective ratios due to isotopic substitution are ≈ 1.02 and ≈ 1.01 . Because the influence on k_1^∞ is mainly governed by the mass difference of the two isotopomers, the effect is small and probably reproduced in the correct order of magnitude by the SACM approach. The main influence on the yield factor, on the other hand, is caused by the shift of the threshold energies relative to each other due to the different zero-point energies of the isotopomers. Inspection of Figure 13 reveals that the location of the crossing point of the two curves $k_{-1}(E)$ and $k_{1a'}(E)$ sensitively governs the yield D_{-1}/R_{form} for HOOC1 formed from OH + ClO, and in this way affects the recombination rate constant k_1 . Small uncertainties in the threshold energies would lead to slightly different energy dependencies of $k_r(E)$, as becomes obvious from eq 17. Because of the similar slopes of $k_{-1}(E)$ and $k_{1a'}(E)$ near the crossing point, the location of the latter could be considerably shifted even by these small uncertainties, and, therefore, the rate constant k_1 is strongly influenced. On the other hand, the branching between Cl + HO₂ and HCl + O₂ is much less sensitive to variations in $E_{0(r)}$, because at the relevant energies above $E_{0(-1)}$, the corresponding curves, $k_{1a'}(E)$ and $k_{1b'}(E)$, are nearly parallel. Therefore, small uncertainties in the differences of the zero-point energies for the two isotopomers may have a stronger influence on the rate constant k_1 than on the branching fraction $Y_{1b'}$.

4.4 Conclusions

The results presented in this chapter have established the kinetic significance of the minor channel for the OH + ClO reaction. The branching ratio involving the production of HCl was determined to be 7% under stratospheric conditions. Statistical rate theory calculations have demonstrated that theoretical predictions are in good agreement with the experimental results. Numerous atmospheric modeling studies have proposed that a branching ratio close to 7% would resolve discrepancies between measured and calculated chlorine partitioning in the upper stratosphere and help to resolve some of the discrepancies between measured and calculated O₃ concentrations, especially near 40 km. This work should help to improve modeling of O₃ levels in the upper stratosphere by placing more stringent constraints on the partitioning of stratospheric chlorine.

References for Chapter 4

- Atkinson, R., D. L. Baulch, R. A. Cox, R. F. Hampson, Jr., J. A. Kerr, and J. Troe, Evaluated kinetic and photochemical data for atmospheric chemistry supplement-IV – IUPAC subcommittee on gas kinetic data evaluation for atmospheric chemistry, *J. Phys. Chem. Ref. Data*, *21*, 1125, 1992.
- Bogan, D. J., R. P. Thorn, F. L. Nesbitt, and L. J. Stief, Experimental 300 K measurement of the rate constant of the reaction $\text{OH} + \text{BrO} \rightarrow \text{products}$, *J. Phys. Chem.*, *100*, 14383, 1996.
- Brasseur, G., A. De Rudder, and C. Tricot, Stratospheric response to chemical perturbations, *J. Atmos. Chem.*, *3*, 261, 1985.
- Burrows, J. P., T. J. Wallington, and R. P. Wayne, Kinetics of the reaction of OH with ClO, *J. Chem. Soc., Faraday Trans. 2*, *80*, 957, 1984.
- Chandra, S., C. H. Jackman, A. R. Douglass, E. L. Fleming, and D. B. Considine, Chlorine catalyzed destruction of ozone: Implications for ozone variability in the upper stratosphere, *Geophys. Res. Lett.*, *20*, 351, 1993.
- Chartrand, D. J., and J. C. McConnell, Evidence for HBr production due to minor channel branching at mid-latitudes, *Geophys. Res. Lett.*, *25*, 55, 1998.
- Chipperfield, M. P., D. E. Shallcross, and D. J. Lary, A model study of the potential role of the reaction $\text{BrO} + \text{OH}$ in the production of stratospheric HBr, *Geophys. Res. Lett.*, *24*, 3025, 1997.
- Cobos, C. J., and J. Troe, Theory of thermal unimolecular reactions at high-pressures. 2. Analysis of experimental results, *J. Chem. Phys.*, *83*, 1010, 1985.
- DeMore, W. B., S. P. Sander, C. J. Howard, A. R. Ravishankara, D. M. Golden, C. E. Kolb, R. F. Hampson, M. J. Kurylo, and M. J. Molina, *Chemical Kinetics and Photochemical Data for Use in Stratospheric Modeling*, JPL Publication 97-4, Jet Propulsion Laboratory, Pasadena, CA, 1997.
- Dubey, M. K., M. P. McGrath, G. P. Smith, and F. S. Rowland, HCl yield from $\text{OH} + \text{ClO}$: Stratospheric model sensitivities and elementary rate theory calculations, *J. Phys. Chem. A*, *102*, 3127, 1998.
- Forst, W., *Theory of Unimolecular Reactions*, Academic Press, New York, 1972.
- Francisco, J. S., S. P. Sander, T. J. Lee, and A. P. Rendell, Structures, relative stabilities, and spectra of isomers of HClO_2 , *J. Phys. Chem.*, *98*, 5644, 1994.

Frisch, M. J., G. W. Trucks, H. B. Schlegel, P. M. W. Gill, B. G. Johnson, M. A. Robb, J. R. Cheeseman, T. Keith, G. A. Petersson, J. A. Montgomery, K. Raghavachari, M. A. Al-Laham, V. G. Zakrzewski, J. V. Ortiz, J. B. Foresman, J. Cioslowski, B. B. Stefanov, A. Nanayakkara, M. Challacombe, C. Y. Peng, P. Y. Ayala, W. Chen, M. W. Wong, J. L. Andres, E. S. Replogle, R. Gomperts, R. L. Martin, D. J. Fox, J. S. Binkley, D. J. Defrees, J. Baker, J. P. Stewart, M. Head-Gordon, C. Gonzalez, and J. A. Pople, *Gaussian 94*, Revision D.2, Gaussian Inc., Pittsburgh PA, 1995.

Gilbert, R. G., and S. C. Smith, *Theory of Unimolecular and Recombination Reactions*, Blackwell, Oxford, 1990.

Herzberg, G., *Molecular Spectra and Molecular Structure, Vol. I, Spectra of Diatomic Molecules*, van Nostrand, Princeton, 1950.

Heymann, M., H. Hippler, D. Nahr, H. J. Plach, and J. Troe, UV absorption study of collisional energy transfer in vibrationally highly excited SO₂ molecules, *J. Phys. Chem.*, *92*, 5507, 1988.

Hills, A. J., and C. J. Howard, Rate coefficient temperature dependence and branching ratio for the OH + ClO reaction, *J. Chem. Phys.*, *81*, 4458, 1984.

Howard, C. J., Kinetic study of the equilibrium HO₂ + NO ⇌ OH + NO₂ and the thermochemistry of HO₂, *J. Am. Chem. Soc.*, *102*, 6937, 1980.

Huey, L. G., D. R. Hanson, and C. J. Howard, Reactions of SF₆⁻ and I⁻ with atmospheric trace gases, *J. Phys. Chem.*, *99*, 5001, 1995.

Khosravi, R., G. P. Brasseur, A. K. Smith, D. W. Rusch, J. W. Waters, and J. M. Russell III, Significant reduction in the stratospheric ozone deficit using a three-dimensional model constrained with UARS data, *J. Geophys. Res.*, *103*, 16203, 1998.

Lee, T. J., and A. P. Rendell, *Ab initio* characterization of ClOOH: Implications for atmospheric chemistry, *J. Phys. Chem.*, *97*, 6999, 1993.

Leu, M. T., and C. L. Lin, Rate constants for the reactions of OH with ClO, Cl₂, and Cl₂O at 298 K, *Geophys. Res. Lett.*, *6*, 425, 1979.

Levine, R. D., and R. B. Bernstein, *Molecular Reaction Dynamics and Chemical Reactivity*, Oxford University Press, Oxford, 1987.

Lipson, J. B., M. J. Elrod, T. W. Beiderhase, L. T. Molina, and M. J. Molina, Temperature dependence of the rate constant and branching ratio for the OH + ClO reaction, *J. Chem. Soc., Faraday Trans.*, *93*, 2665, 1997.

Lipson, J. B., T. W. Beiderhase, L. T. Molina, M. J. Molina, and M. Olzmann, Production of HCl in the OH + ClO reaction: Laboratory measurements and statistical rate theory calculations, submitted to *J. Phys. Chem. A*, 1999.

Maergoiz, A. I., E. E. Nikitin, J. Troe, and V. G. Ushakov, Classical trajectory and adiabatic channel study of the transition from adiabatic to sudden capture dynamics. 3. Dipole-dipole capture, *J. Chem. Phys.*, *105*, 6277, 1996.

Mallard, W. G., F. Westley, J. T. Herron, and R. F. Hampson, *NIST Chemical Kinetics Database Version 6.0*, NIST Standard Reference Data, Gaithersberg, MD, 1994.

Marcus, R. A., Unimolecular dissociations and free radical recombination reactions, *J. Chem. Phys.*, *20*, 359, 1952.

McElroy, M. B., and R. J. Salawitch, Changing composition of the global stratosphere, *Science*, *243*, 763, 1989.

Michelsen, H. A., R. J. Salawitch, M. R. Gunson, C. Aellig, N. Kämpfer, M. M. Abbas, M. C. Abrams, T. L. Brown, A. Y. Chang, A. Goldman, F. W. Irion, M. J. Newchurch, C. P. Rinsland, G. P. Stiller, and R. Zander, Stratospheric chlorine partitioning: Constraints from shuttle-borne measurements of [HCl], [ClNO₃], and [ClO], *Geophys. Res. Lett.*, *23*, 2361, 1996.

Olzmann, M., and J. Troe, Approximate determination of rovibrational densities of states $\rho(E,J)$ and numbers of states $W(E,J)$, *Ber. Bunsenges. Phys. Chem.*, *98*, 1563, 1994.

Olzmann, M., On nascent angular-momentum distributions in complex-forming bimolecular reactions, *Ber. Bunsenges. Phys. Chem.*, *101*, 533, 1997.

Poulet, G., G. Laverdet, and G. Le Bras, Rate constant and branching ratio for the reaction of OH with ClO, *J. Phys. Chem.*, *90*, 159, 1986.

Radzig, A. A., and B. M. Smirnov, *Reference Data on Atoms, Molecules, and Ions*, Springer Series in Chemical Physics 31, Springer-Verlag, Berlin, 1985.

Ravishankara, A. R., F. L. Eisele, and P. H. Wine, The kinetics of the reaction of OH with ClO, *J. Chem. Phys.*, *78*, 1140, 1983.

Reid, R. C., J. M. Prausnitz, and B. E. Poling, *The Properties of Gases and Liquids*, McGraw-Hill, New York 1987.

Robinson, P. J., and K. A. Holbrook, *Unimolecular Reactions*, Wiley, New York, 1972.

Ruhnke, R., W. Kouker, Th. Reddmann, H. Berg, G. Hochschild, G. Kopp, R. Krupa, and M. Kuntz, The vertical distribution of ClO at Ny-Alesund during March 1997, *Geophys. Res. Lett.*, *26*, 839, 1999.

Schranz, H. W., and S. Nordholm, Theory of chemically activated unimolecular reactions – weak collisions and steady-states, *Chem. Phys.*, *87*, 163, 1984.

Scott, A. P., and L. Radom, Harmonic vibrational frequencies: An evaluation of Hartree-Fock, Moller-Plesset, quadratic configuration interaction, density functional theory, and semiempirical scale factors, *J. Phys. Chem.*, *100*, 16502, 1996.

Seeley, J. V., J. T. Jayne, and M. J. Molina, High pressure fast-flow technique for gas phase kinetics studies, *Int. J. Chem. Kinet.*, *25*, 571, 1993.

Snider, N., Theory of chemical activation in the high-pressure limit, *J. Phys. Chem.*, *89*, 1257, 1985.

Toumi, R., and S. Bekki, The importance of the reactions between OH and ClO for stratospheric ozone, *Geophys. Res. Lett.*, *20*, 2447, 1993.

Troe, J., Theory of thermal unimolecular reactions at high pressures, *J. Chem. Phys.*, *75*, 226, 1981.

Troe, J., Specific rate constants $k(E,J)$ for unimolecular bond fissions, *J. Chem. Phys.*, *79*, 6017, 1983.

Troe, J., Statistical adiabatic channel model of ion neutral dipole capture rate constants, *Chem. Phys. Lett.*, *122*, 425, 1985.

Troe, J., Relation between potential and rate parameters for reactions on attractive potential-energy surfaces – application to the reaction $\text{HO} + \text{O} \rightleftharpoons \text{HO}_2^* \rightarrow \text{H} + \text{O}_2$, *J. Phys. Chem.*, *90*, 3485, 1986.

Troe, J., The colourful world of complex-forming bimolecular reactions, *J. Chem. Soc., Faraday Trans.*, *90*, 2303, 1994.

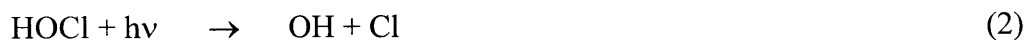
Weissman, M., L. G. S. Shum, S. P. Heneghan, and S. W. Benson, Thermochemical considerations regarding the reactions $\text{HO}_2 + \text{Cl}$ and $\text{OH} + \text{Cl}$, *J. Phys. Chem.*, *85*, 2863, 1981.

Chapter 5: Kinetics of the HO₂ + ClO Reaction: Current Research

5.1 Introduction

The HO₂ + ClO reaction plays an important role in stratospheric ozone depletion.

This reaction is the rate-limiting step in an important catalytic cycle that destroys ozone:

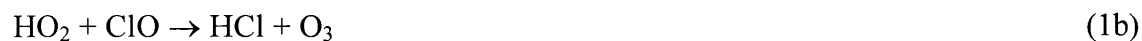


In a study of the various catalytic cycles that contribute to ozone depletion, *Wennberg et al.* [1994] found that this cycle accounts for ~ 30% of halogen-controlled ozone loss at midlatitudes. There have been several measurements of the overall rate constant of the HO₂ + ClO reaction at room temperature [*Reimann and Kaufman*, 1978; *Leck et al.*, 1980; *Burrows and Cox*, 1981; *Cattell and Cox*, 1986]. However, there has only been one study of the temperature dependence of this reaction [*Stimpfle et al.*, 1979]. In this study, *Stimpfle et al.* found that the rate constant varied very little with temperature at the higher temperatures, but increased significantly with temperature at the lower temperatures. The curvature of the Arrhenius plot for the HO₂ + ClO reaction lead *Stimpfle et al.* to conclude that the reaction must proceed by two different mechanisms. At higher temperatures (T > 370 K), direct H atom abstraction was proposed to be the dominant mechanism. At lower temperatures (T < 270 K), it was assumed that intermediate complex formation was dominant. A more recent *ab initio* study by *Buttar*

and Hirst [1994], supports the theory that the HO₂ + ClO reaction proceeds via two different reaction pathways.

Because of the atmospheric significance of reaction 1, further studies of the temperature dependence of this reaction are necessary. The lowest temperature attained in the study by *Stimpfle et al.* was 235 K, due to limitations inherent in the conventional low pressure laminar discharge flow method. As discussed in Chapter 1, the turbulent flow tube technique has significantly reduced wall loss effects at low temperatures compared to the laminar flow tube technique. The studies presented in Chapters 2-4 have demonstrated that the turbulent flow tube technique can be used to study the kinetics of radical-radical reactions at temperatures as low as 200 K. The experiments of *Stimpfle et al.* were also restricted to low pressures (1-3 Torr). However, at low temperatures intermediate complex formation may be enhanced by collisional stabilization. Therefore, measurements of the rate constant at low temperatures and higher pressures are clearly needed. As *Wennberg et al.* [1994] have pointed out, the interpretation of field measurements and the development of accurate atmospheric models have been hindered by uncertainties in the laboratory-measured rate constants. These uncertainties are largely due to the fact that many studies have not been conducted under pressure and temperature conditions characteristic of the stratosphere.

Although the major products of the HO₂ + ClO reaction are HOCl and O₂, the reaction may also have a thermodynamically feasible minor channel to form HCl ($\Delta H^\circ_{298\text{ K}} = -15\text{ kcal mol}^{-1}$):



Similar to the minor channel of the OH + ClO reaction, discussed in Chapters 3 and 4, this reaction represents a chain-terminating step in catalytic ozone depletion cycles.

Reaction 1b converts an active form of chlorine (ClO) into a more stable reservoir species

(HCl), and therefore this reaction could have an impact on the partitioning of chlorine in the stratosphere. As discussed in Chapters 3 and 4, stratospheric models have tended to overestimate the ClO/HCl ratio in the upper stratosphere. Our measurements of the branching ratio for the OH + ClO reaction have helped to resolve the discrepancies between measured and modeled chlorine partitioning. However, a small HCl yield from reaction 1b would be an additional refinement to chlorine partitioning calculations.

Several previous attempts to measure the branching ratio of the HO₂ + ClO reaction have only been able to put an upper limit on the branching ratio of ~1% at room temperature [Leu, 1980; Leck *et al.*, 1980; Burrows and Cox, 1981; Finkbeiner *et al.*, 1995]. However, at 210 K Finkbeiner *et al.* have observed the formation of O₃ using matrix-isolation/FTIR spectroscopy and determined the branching ratio to be 5 ± 2%. Additional measurements of reaction 1b are needed to better quantify the contribution of this reaction to HCl production in the stratosphere.

This chapter will present current research on the HO₂ + ClO reaction. The production, detection and titration schemes for both HO₂ and ClO have already been developed in our previous studies of HO₂ + BrO (Chapter 2) and OH + ClO (Chapters 3 and 4). Furthermore, our previous study of the OH + ClO reaction has clearly demonstrated our ability to measure small branching ratios using the turbulent flow tube technique coupled with high pressure chemical ionization mass spectrometry. Measurements of the kinetics and product distribution of the HO₂ + ClO reaction under pressure and temperature conditions characteristic of the stratosphere should help to place more stringent constraints on the partitioning of chlorine in the stratosphere and to improve modeling of stratospheric ozone levels, especially at midlatitudes.

5.2 Experimental Section

A schematic diagram of the experimental apparatus is presented in Figure 1. The flow tube (2.2 cm i.d., 120 cm long) was constructed of Pyrex tubing and coated with

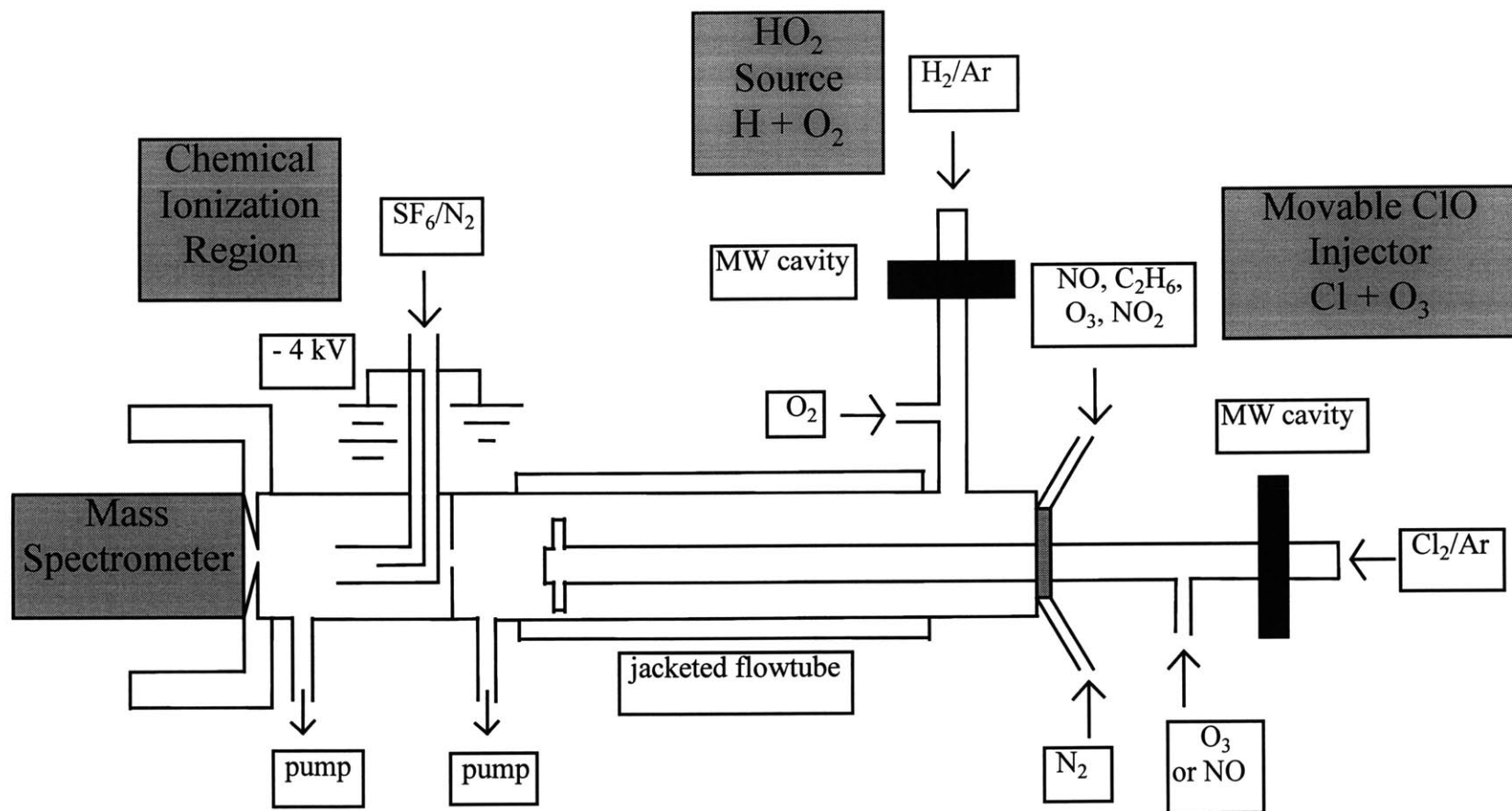


Figure 1. Schematic diagram of experimental apparatus

Halocarbon wax. A large flow of nitrogen carrier gas (~ 35 STP L min^{-1}) was injected at the rear of the flow tube. The gases needed to generate HO₂ were introduced through a sidearm (12 cm long, 6 mm diameter) located at the rear of the flow tube. ClO was generated in a double-nested movable injector, which consisted of an inner 6 mm alumina tube and an outer encasement made from corrugated Teflon tubing. The outer encasement was used so that the injector could be moved to various positions without breaking the vacuum seals. A Teflon device (see Figure 9b in Chapter 4) was placed at the end of the injector in order to enhance turbulent mixing. The corona ion source was located between the flow tube and the inlet to the quadrupole mass spectrometer. An aperture between the flow tube and the ion-molecule region created a pressure drop from 200 Torr in the flow tube to 50 Torr in the ion-molecule region. The pressures in the two regions were measured using MKS capacitance manometers (100 and 1000 Torr full scale). All gas flows were monitored with calibrated Tylan General mass flowmeters.

The following gases were used as supplied or after further purification as described below: Ar (99.999%), He (99.999%), O₂ (99.994%), H₂ (99.999%), Cl₂ (>99.9%), NO₂ (99.5%), NO (>99.0%), C₂H₆ (>99.0%) and SF₆ (>99.99%).

5.2.1 Radical Production

Bimolecular rate constants were measured using the pseudo-first-order approximation method with HO₂ as the excess reagent. HO₂ was generated using the following reaction:



($k_5 = 3.4 \times 10^{-13} \text{ cm}^3 \text{ molecule}^{-1} \text{ s}^{-1}$ at 200 Torr [*DeMore et al.*, 1997]). H atoms were produced by combining a ~ 4.0 STP L min^{-1} flow of argon, which had passed through an inert gas purifier (Aeronex Gate Keeper, Model 500 K), with a 0.1-1.0 STP mL min^{-1}

flow of a 40% H₂/He mixture which then passed through a molecular sieve trap immersed in liquid nitrogen and finally through a microwave discharge produced by a Beenakker cavity operating at 15 W. The H atoms were then mixed with O₂ in order to form HO₂ via reaction 5. A large excess of O₂ ($\sim 10^{17}$ molecule cm⁻³) was used in order to minimize the concentration of stray H atoms entering the main flow. The production of OH in the microwave discharge due to impurities was a concern in these experiments. However, it was found that sending the argon sweep gas through both an inert gas purifier and a molecular sieve trap immersed in liquid nitrogen, before the microwave discharge, greatly reduced the observed OH production from the HO₂ source. This point will be discussed in more detail later.

Absolute HO₂ concentrations were routinely determined by the titration reaction:



($k_6 = 8.1 \times 10^{-12}$ cm³ molecule⁻¹ s⁻¹ [*DeMore et al.*, 1997]) and subsequent calibration of the NO₂ mass spectrometer signal. Purified NO/N₂ mixtures (the purification process is described in Chapter 3) were passed through a silica gel trap immersed in a dry ice/ethanol bath to further reduce the background NO₂ contribution. During the titrations, loss of NO₂ due to reaction with OH (produced by reaction 6):



($k_7 = 4.9 \times 10^{-12}$ cm³ molecule⁻¹ s⁻¹ at 200 Torr [*DeMore et al.*, 1997]) could have introduced error into the titration procedure. However, this problem was avoided by using a very large excess of NO ($\sim 5 \times 10^{14}$ molecule cm⁻³) such that OH was driven to react with NO to form HONO:

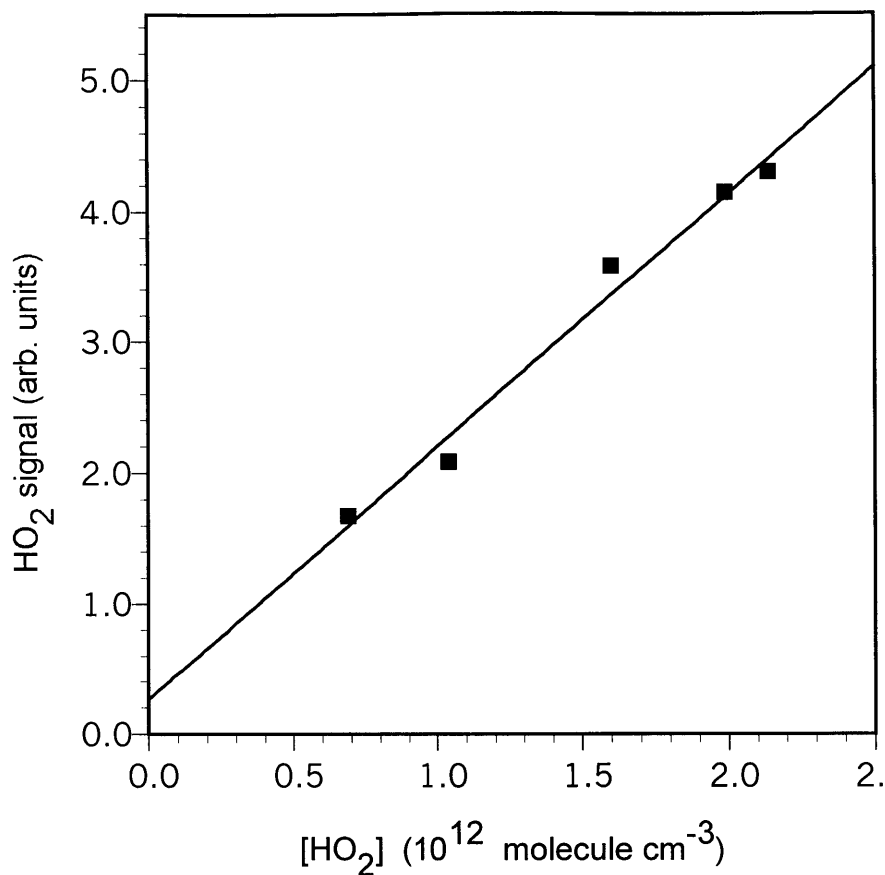


Figure 2. HO₂ calibration plot



($k_8 = 3.1 \times 10^{-12} \text{ cm}^3 \text{ molecule}^{-1} \text{ s}^{-1}$ at 200 Torr [DeMore *et al.*, 1997]) instead of reacting with NO₂ to form HNO₃. During the HO₂ titrations, both HONO and HNO₃ were monitored to ensure that OH was preferentially being converted to HONO instead of HNO₃. A sample HO₂ calibration curve is shown in Figure 2. For this study HO₂ concentrations ranged from 0.9 to 3.0 × 10¹² molecule cm⁻³.

As discussed in Chapter 2 (HO₂ + BrO reaction), the concentration of HO₂ in the flow tube is affected by self-reaction:



($k_9 = 2.0 \times 10^{-12} \text{ cm}^3 \text{ molecule}^{-1} \text{ s}^{-1}$ [DeMore *et al.*, 1997]) and by wall loss. In our measurements of the overall rate constant for the $\text{HO}_2 + \text{BrO}$ reaction, HO_2 was also the excess reagent. In these experiments, the *mean* HO_2 concentration present in the reaction zone was used to determine the bimolecular rate coefficient. It was found that under typical experimental conditions, this approximation resulted in values accurate to within 5% of the true rate constant. As a result, this method was also used in the determination of the overall rate constant for the $\text{HO}_2 + \text{ClO}$ reaction. As described above, HO_2 was formed in a side arm in the back of the flow tube. In order to determine the mean concentration of HO_2 it was necessary to titrate HO_2 at the beginning and end of the reaction zone. This was achieved by introducing NO through the movable injector for the titrations. In this way, the concentration of HO_2 in the flow tube was directly determined via reaction 6 at the beginning of the reaction zone (injector pushed in) and at the end of the reaction zone (injector pulled out). The very large excess of NO used in the titrations converted the HO_2 to NO_2 very rapidly, essentially preventing HO_2 self-reaction and wall loss from occurring downstream of the titration point. This was particularly important for the titrations of HO_2 at the end of the reaction zone (injector pulled out). For typical experimental conditions, wall loss of HO_2 on the surface of the movable injector was found to be significant. As the injector was pulled back, the HO_2 was exposed to less injector surface area. Therefore, wall loss of HO_2 on the movable injector decreased as the injector was pulled back. As a result, the HO_2 mass spectrometer signal was observed to increase as the injector was pulled out. Typically, the loss of HO_2 on the movable injector over the experimental reaction zone was on the order of 10% at 298 K, as shown in Figure 3.

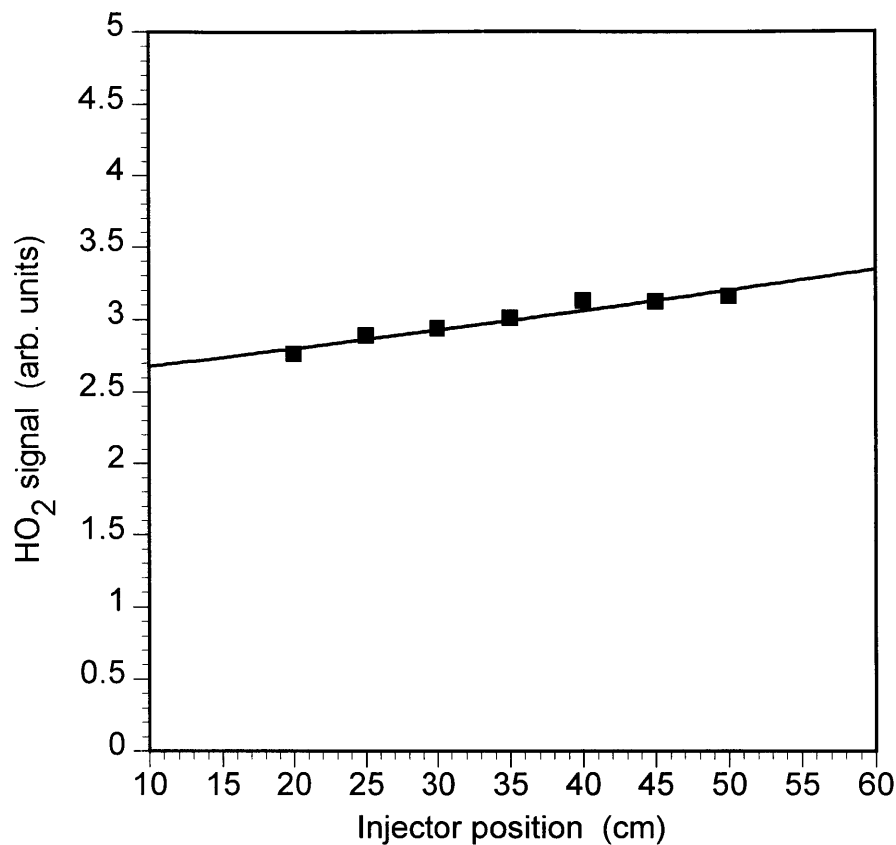
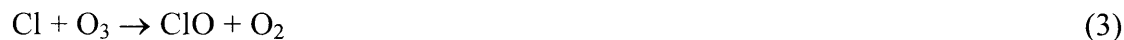


Figure 3. Observed wall loss of HO₂ on the movable injector at 298 K

ClO was generated in the injector using the following reaction:



($k_3 = 1.2 \times 10^{-11} \text{ cm}^3 \text{ molecule}^{-1} \text{ s}^{-1}$ [DeMore *et al.*, 1997]). Chlorine atoms were produced by combining a $\sim 4.0 \text{ STP L min}^{-1}$ flow of argon, which had passed through an inert gas purifier (Aeronex Gate Keeper, Model 500 K), with a $\sim 0.1 \text{ STP mL min}^{-1}$ flow of a 1% Cl₂/He mixture which then passed through a microwave discharge produced by a Beenakker cavity operating at 70 W. To generate ClO, the chlorine atoms were mixed with an excess of O₃ throughout the whole length of the movable alumina injector to

ensure that only negligible amounts of chlorine atoms were introduced into the main flow. O₃, generated from an OREC ozonator and stored in a silica gel trap immersed in a dry ice/methanol bath, was introduced into the system by passing a 1-5 STP mL min⁻¹ flow of N₂ through the trap. Ozone partial pressures were determined by UV absorbance at 253.7 nm (Penray Hg lamp) in a 0.98 cm flow-through quartz cell.

Absolute ClO concentrations were determined by the titration reaction:



($k_{10} = 1.7 \times 10^{-11} \text{ cm}^3 \text{ molecule}^{-1} \text{ s}^{-1}$ [DeMore *et al.*, 1997]) and subsequent calibration of the NO₂ mass spectrometer signal. As discussed in Chapters 3 and 4, the Cl atoms produced by reaction 10 can lead to regeneration of ClO via reaction 3. An excess of ethane, injected at the rear of the flow tube, was used to scavenge the Cl atoms in order to prevent regeneration of ClO. Modeling of the titration system was used to correct for a slight underestimation of ClO concentration caused by the secondary reaction of C₂H₅ with NO₂. In Chapter 3, we demonstrated that this ClO titration technique yields linear calibration curves.

For reasons of convenience, ClO titrations have also been performed using a second method. In this second method, ClO concentrations were determined by reacting Cl atoms from the movable injector with a known amount of O₃, injected at the rear of the flow tube. The O₃ and ClO mass spectrometer signals were monitored as the chlorine microwave discharge was turned on and off. The concentration of ClO was determined by calculating the concentration of O₃ lost. This procedure is similar to the HCl calibration method described in Chapter 4, in which H atoms were reacted with a known amount of Cl₂ to produce HCl. For the ClO titrations, it was very important that the O₃ was introduced in the back of the flow tube, and not in the injector (where O₃ normally enters during the kinetics experiments in order to produce ClO). In the injector, the

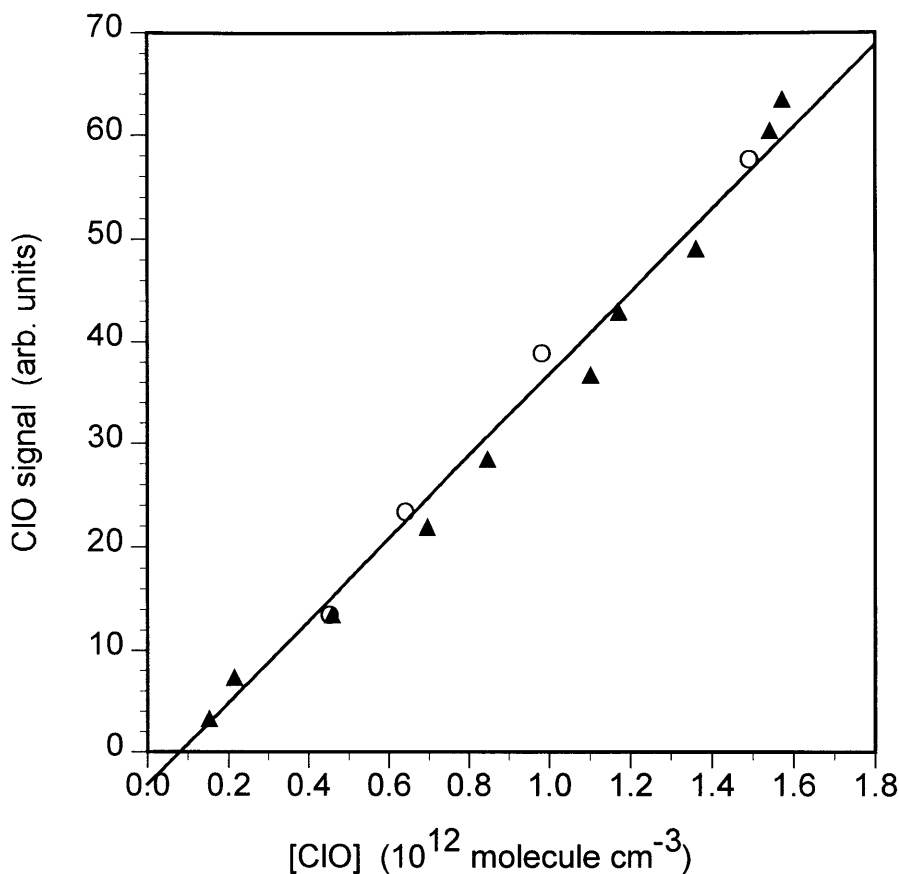


Figure 4. Comparison of ClO calibration plots for the two different ClO titration methods described in the text: ClO + NO method (○) and Cl + O₃ method (▲).

reaction time between Cl and O₃ is very long. Furthermore, the concentration of ClO in the injector is high compared to the flow tube, where ClO is diluted by the large flow of the main nitrogen carrier gas. As a result, secondary processes in the injector, such as ClO self-reaction and wall loss, would introduce error into the ClO titration procedure. However, when O₃ is injected at the rear of the flow tube and Cl atoms are introduced through the movable injector, the Cl + O₃ reaction time can be controlled by changing the position of the movable injector. Furthermore, the concentrations of ClO used in this experiment ($< 10^{12}$ molecule cm⁻³) are low enough that secondary reactions in the main

flow tube are unimportant and do not affect the determination of ClO concentrations. A sample ClO calibration curve is shown in Figure 4. Figure 4, also contains a comparison of the two ClO titration methods, demonstrating that the methods are in very good agreement. The main advantage of the second method (Cl + O₃) is that computer modeling is not necessary. In order to ensure pseudo-first-order kinetic conditions, the concentration of ClO was kept at most one-tenth as large as [HO₂].

5.2.2 Detection of Reactants and Products

Most of the chemical species relevant to this study (HO₂, ClO, HOCl, O₃, OH, HCl, Cl₂, NO₂, HNO₃ and HONO) were chemically ionized with the SF₆⁻ reagent ion and then detected with the quadrupole mass spectrometer. SF₆⁻ was produced in the ion source by combining ~ 10 STP L min⁻¹ flow of nitrogen with a ~ 1.0 STP mL min⁻¹ flow of a 15 % SF₆/N₂ mixture which then passed over the corona discharge. In order to confine the ionization process to SF₆ alone and to control the ion-molecule reaction time, another piece of Pyrex tubing (of variable length) was used to direct the SF₆⁻ downstream into the main flow tube effluent. More extensive descriptions of the ion source, ion lenses and the quadrupole mass spectrometer are given in Chapter 2.

In the chemical ionization scheme employed here, OH, ClO, Cl₂, O₃ and NO₂ were detected as their parent negative ions by charge-transfer reactions with SF₆⁻. For example, OH was detected as OH⁻ through the following reaction:



HCl, HNO₃ and HONO were detected as FHCl⁻, FHNO₃⁻ and FHNO₂⁻ through fluoride-transfer reactions with SF₆⁻. For example:



HO₂ was detected as SF₄O₂⁻ and HOCl was detected as SF₅O⁻, generated presumably through multi-step pathways. The ion-molecule region was kept at a lower pressure (~ 50 Torr) than the flow tube (~ 200 Torr). The drop in pressure lowered the concentrations of the neutrals in the ion-molecule region, thus decreasing the rates of potential ion-molecule side reactions.

5.3 Preliminary Results and Discussion

5.3.1 Overall Rate Constant Measurements

Bimolecular rate constants were obtained via the usual pseudo-first-order approximation method, using HO₂ as the excess reagent. Typical ClO decay curves as a function of injector position are shown in Figure 5. The first-order rate constants obtained from fitting the ClO decay curves were plotted against [HO₂] in order to determine the bimolecular rate constant, as shown in Figure 6. This approach for determining bimolecular rate constants assumes that deviations from the plug flow approximation are negligible. Under the conditions present in our turbulent flow tube, *Seeley et al.* [1996] estimated that these deviations result in apparent rate constants which are at most 8 % below the actual values. Hence, the flow corrections were neglected as they are smaller than the sum of the other likely systematic errors in the measurements of gas flows, temperature, detector signal, pressure and absolute HO₂ concentrations. Indeed, we consider the major source of error in our experiments to arise from the determination of [HO₂] from the titration procedure outlined above. Considering such sources of error, we estimate that rate constants can be determined with an accuracy of $\pm 30\%$ (2σ).

The overall rate constant for the HO₂ + ClO reaction at 298 K, determined from the data in Figures 5 and 6, is $4.0 \times 10^{-12} \text{ cm}^3 \text{ molecule}^{-1} \text{ s}^{-1}$. This value is in fairly good

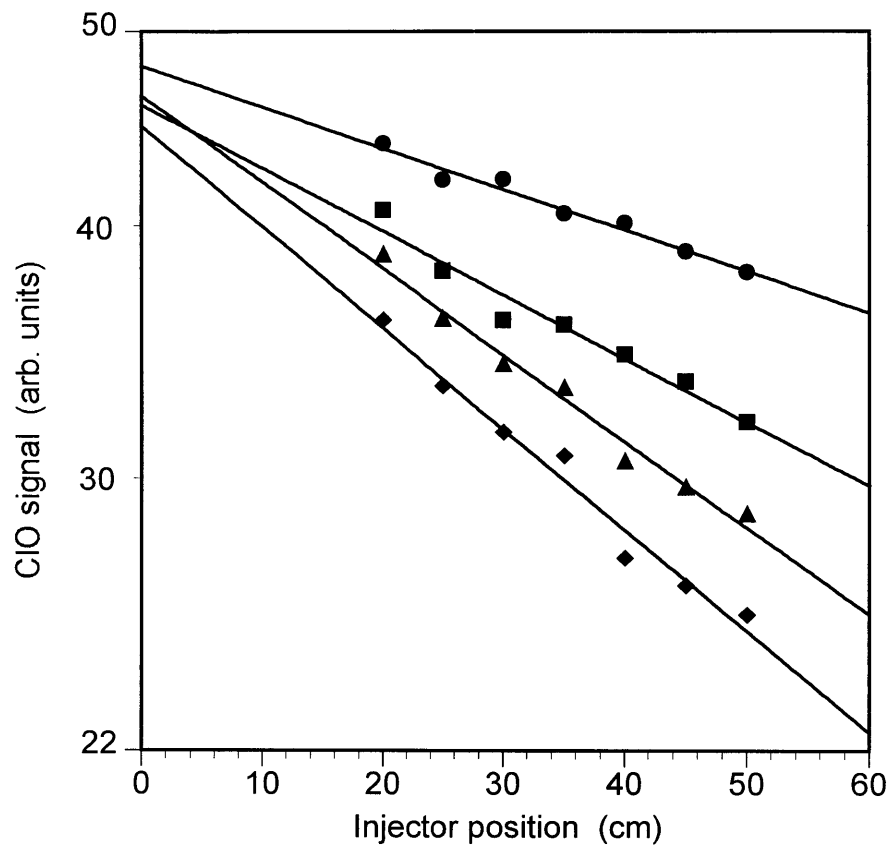


Figure 5. Set of CIO signals as a function of injector distance. This data set was obtained under the following conditions: $P = 195$ Torr; $T = 298$ K; average velocity = 1000 cm s^{-1} ; Reynolds number = 2900.

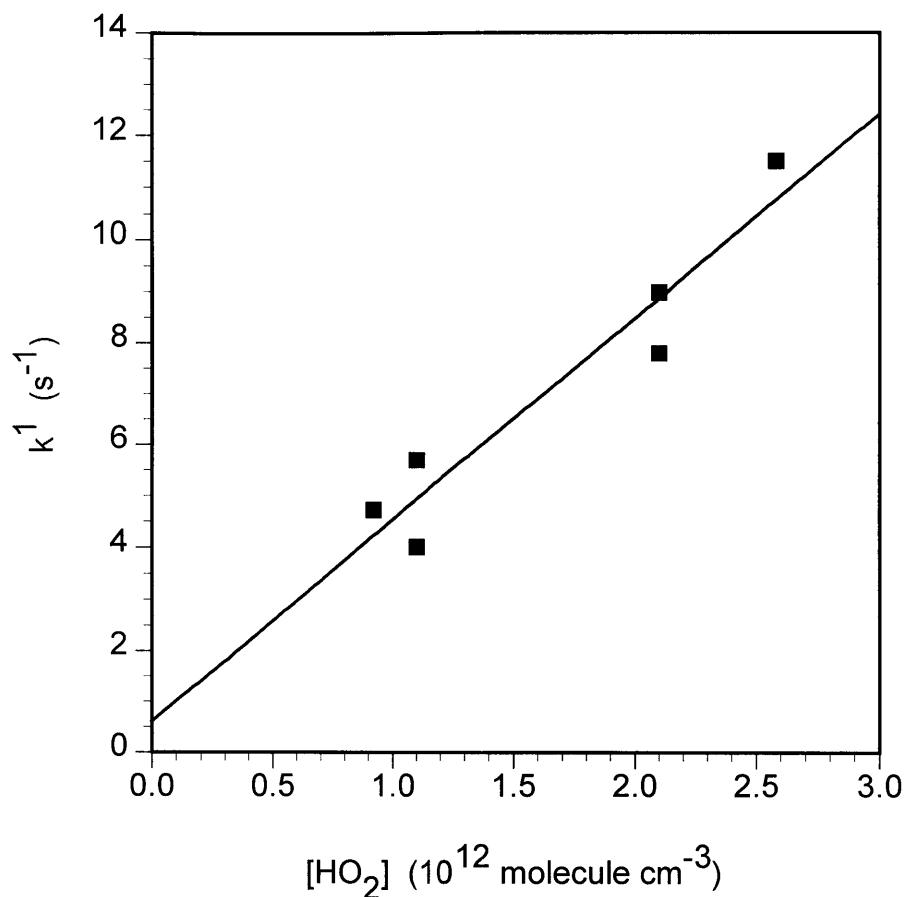


Figure 6. Plot of k^1 as a function of $[\text{HO}_2]$. This plot was obtained under the same conditions as listed in Figure 5.

agreement with the results of previous measurements of the rate constant at room temperature, which are listed in Table 1. Additional measurements of the overall rate constant at room temperature are necessary in order to verify this initial experimental result. Furthermore, the temperature dependence of the overall rate constant for the $\text{HO}_2 + \text{ClO}$ reaction will be investigated. The experiment is already set-up to perform measurements at low temperatures, and our previous studies of the $\text{HO}_2 + \text{BrO}$ and $\text{OH} + \text{ClO}$ reactions have demonstrated our ability to determine rate constants of radical-radical reactions at temperatures as low as 200 K. As discussed in the Introduction, there has

Table 1. Comparison of Measured Rate Constants Near Room Temperature for the HO₂ + ClO Reaction

Technique	P (Torr)	T (K)	$k_{298\text{ K}}$ (10^{-12} cm ³ molecule ⁻¹ s ⁻¹)	Reference
DF-LF/RF, LIF	2-3	298	3.8 ± 0.5	Reimann and Kaufman [1978]
DF-LF/LMR	0.8-3.4	235-393	6.3 ± 1.3	Stimpfle et al. [1979]
DF-LF/EIMS	2-6	298	4.5 ± 0.9	Leck et al. [1980]
MM/UV	760	300	$5.4 \pm \frac{4}{2}$	Burrows and Cox [1981]
MM/UV	50-760	308	6.2 ± 1.5	Cattell and Cox [1986]

DF, discharge flow; LF, laminar flow; MM, molecular modulation; RF, resonance fluorescence detection; LIF, laser-induced fluorescence detection; LMR, laser magnetic resonance detection; EIMS, electron impact mass spectrometry detection; UV, ultraviolet spectroscopy detection.

only been one published study of the temperature dependence of the HO₂ + ClO reaction [Stimpfle et al., 1979]. In this study, experiments were conducted at temperatures between 235 and 393 K, and the data was fit to the following complex expression: $k(T) = [3.3 \times 10^{-11} \exp(-850/T)] + [4.5 \times 10^{-12} * (T/300)^{-3.7}]$ cm³ molecule⁻¹ s⁻¹. The curvature in the Arrhenius plot lead Stimpfle et al. to conclude that the HO₂ + ClO reaction must proceed via two separate reaction pathways. At high temperatures ($T > 370$ K) direct H atom abstraction was proposed to be the dominant mechanism, and at low temperatures ($T < 270$ K) intermediate complex formation was assumed to be dominant. The Stimpfle et al. data for temperatures between 235 and 298 K can be fit by an Arrhenius expression

as follows: $k(T) = 4.8 \times 10^{-13} \exp(700/T) \text{ cm}^3 \text{ molecule}^{-1} \text{ s}^{-1}$. This expression is the current JPL recommendation for the temperature dependence of the $\text{HO}_2 + \text{ClO}$ reaction [DeMore *et al.*, 1997]. Because of the atmospheric importance of reaction 1, additional studies of the temperature dependence of this reaction are needed.

Measurements of the pressure dependence of reaction 1, particularly at low temperatures are also needed. A study of the pressure dependence of reaction 1 at room temperature found the rate constant to be independent of pressure over the range 50 to 760 Torr [Cattell *et al.*, 1986]. As can be seen in Table 1, the lack of a pressure dependence is also demonstrated by the good agreement between the results of independent studies conducted at very different pressures. Stimpfle *et al.* [1979] proposed that reaction 1 proceeds through the formation of an intermediate complex at low temperatures. *Ab initio* calculations by Buttar and Hirst [1994] have determined that intermediate complex formation is energetically feasible in the $\text{HO}_2 + \text{ClO}$ reaction. They also found that this pathway must proceed through a singlet potential surface in which the O_2 product is formed in the excited singlet state. In the only study of the temperature dependence of reaction 1, all of the experiments were conducted at low pressures (~ 1 Torr) [Stimpfle *et al.*, 1979]. However, intermediate complex formation at low temperatures may be collisionally stabilized at higher pressures. The studies of the $\text{HO}_2 + \text{BrO}$ and $\text{OH} + \text{ClO}$ reactions presented in this thesis have demonstrated that the turbulent flow tube technique coupled with chemical ionization mass spectrometry is ideally suited for investigating the rate constants of radical-radical reactions at low temperatures and high pressures.

5.3.2 Branching Ratio Experiments

Although the major products of the $\text{HO}_2 + \text{ClO}$ reaction are HOCl and O_2 , reaction 1 may also have a thermodynamically feasible minor channel to form HCl and O_3 (reaction 1b). The results of previous studies have only been able to put an upper limit on the

Table 2. Comparison of Measured Branching Ratios for the HO₂ + ClO Reaction

Technique	P (Torr)	T (K)	Branching Ratio (k _{1b} /k ₁) x 100%	Reference
DF-LF/ EIMS, RF	2-3	298 248	< 1.5 < 3.0	Leu [1980]
DF-LF/EIMS	2-6	298	< 2	Leck et al. [1980]
MM/UV	760	300	< 0.3	Burrows and Cox [1981]
MI/FTIR	700	300 240 210	< 1 2 ± 1 5 ± 2	Finkbeiner et al. [1995]

DF, discharge flow; LF, laminar flow; MM, molecular modulation; MI, matrix isolation; EIMS, electron impact mass spectrometry detection; RF, resonance fluorescence detection; UV, ultraviolet spectroscopy detection; FTIR, Fourier transform infrared spectroscopy detection.

branching ratio of ~ 1 % at room temperature, as shown in Table 2. However, a study by *Finkbeiner et al.* [1995] observed the formation of O₃ at 210 K using matrix-isolation/FTIR spectroscopy. In this study the branching ratio of reaction 1 was determined to be 5 ± 2 % at 210 K. *Finkbeiner et al.* also observed O₃ formation at room temperature. However, some of the O₃ formation was attributed to secondary chemistry involving the photolysis of OCIO in their flow system to produce O atoms. (According to their modeling, the production of OCIO in their system was greatly reduced at low temperatures, and so this secondary process was not a concern at 210 K.) Because of the large concentration of O₂ used in their experiments, the O atoms produced by the photolysis of OCIO were rapidly converted to O₃, creating a significant background level

at room temperature. As a result, *Finkbeiner et al.* were only able to place an upper limit on the branching ratio at room temperature, similar to the other studies listed in Table 2.

In Chapter 4, we positively identified production of HCl from the minor channel of the OH + ClO reaction. This study clearly demonstrated our ability to measure small branching ratios using the turbulent flow tube technique coupled with chemical ionization mass spectrometry. Therefore, this technique seems well suited to study the branching ratio of the HO₂ + ClO reaction. In Chapter 4, we demonstrated that the HCl background level in the system had been significantly reduced by several key improvements to the ClO source. As a result, it was possible to detect the production of very small quantities of HCl ($\sim 10^9$ molecule cm⁻³) over the experimental reaction time. The branching ratio of the OH + ClO reaction was determined by fitting the observed HCl production using a computer model of the chemical reaction system. In theory this same approach could be used to study the branching ratio of the HO₂ + ClO reaction. The sensitive detection of very small amounts of O₃ is not possible using our current ClO source, although alternative ClO production methods could be explored. Nonetheless, the best approach is probably to try to look for the production of HCl from reaction 1b. As in the OH + ClO experiments, it is important to identify possible side reactions that could contribute to HCl production in the system. The formation of OH due to impurities in the hydrogen microwave discharge would certainly be a concern in these experiments. Based on our measurements of the rate constant of the minor channel for the OH + ClO reaction, this reaction is a potential source of HCl production in the flow tube. However, this problem has potentially been avoided by improvements to the HO₂ source. The OH background produced by the HO₂ source has been significantly reduced by sending the argon sweep gas through an inert gas purifier and then through a molecular sieve trap immersed in liquid nitrogen before the argon is sent through the hydrogen microwave discharge. Formal titrations of the OH produced by the HO₂ source are necessary in order to better quantify the importance of this side reaction.

In addition to identifying possible side reactions that could contribute to HCl formation, it is also worthwhile to consider what level of HCl sensitivity would be necessary to observe HCl production from a 1% branching ratio for reaction 1. (Most of the previous studies have set an upper limit of $\sim 1\%$ for the branching ratio at room temperature.) Assuming an overall rate constant of $5.0 \times 10^{-12} \text{ cm}^3 \text{ molecule}^{-1} \text{ s}^{-1}$ at 298 K (based on the current JPL recommendation for the $\text{HO}_2 + \text{ClO}$ reaction [DeMore *et al.*, 1997]), a 1% branching ratio would yield a rate constant of $5.0 \times 10^{-14} \text{ cm}^3 \text{ molecule}^{-1} \text{ s}^{-1}$. This rate constant is more than an order of magnitude slower than the rate constant of the minor channel for the $\text{OH} + \text{ClO}$ reaction ($\sim 1.0 \times 10^{-12} \text{ cm}^3 \text{ molecule}^{-1} \text{ s}^{-1}$ at 298 K) measured in Chapter 4. As a result, it might be difficult to detect HCl production from the minor channel of the $\text{HO}_2 + \text{ClO}$ reaction at 298 K if the rate constant is really as slow as suggested by previous measurements. However, experiments by Finkbeiner *et al.* [1995] suggest that the branching ratio increases at lower temperatures. As a result, measurements of the branching ratio for the $\text{HO}_2 + \text{ClO}$ reaction may be more feasible at low temperatures. In order to determine the branching ratio of reaction 1, it is first necessary to complete our measurements of the temperature dependence of the overall rate constant for the $\text{HO}_2 + \text{ClO}$ reaction.

5.4 Preliminary Conclusions

An initial measurement of the overall rate constant for the $\text{HO}_2 + \text{ClO}$ reaction at 298 K and 200 Torr has been presented. A study of the temperature dependence of the overall rate constant is currently being conducted using radical production, detection and titration schemes developed in our previous studies of the $\text{HO}_2 + \text{BrO}$ and $\text{OH} + \text{ClO}$ reactions. The feasibility of measuring the branching ratio of reaction 1 has also been discussed. These experiments should help to improve models of stratospheric ozone by placing more stringent constraints on the partitioning of stratospheric chlorine.

References for Chapter 5

- Burrows, J. P., and R. A. Cox, Kinetics of chlorine oxide radical reactions using modulated photolysis, *J. Chem. Soc., Faraday Trans. 1*, 77, 2465, 1981.
- Buttar, D., and D. M. Hirst, *Ab initio* quantum chemistry study of the gas-phase reaction of ClO with HO₂, *J. Chem. Soc., Faraday Trans.*, 90, 1811, 1994.
- Cattell, F. C., and R. A. Cox, Pressure dependence of the reactions of HO₂ with Cl and ClO, *J. Chem. Soc., Faraday Trans. 2*, 82, 1413, 1986.
- DeMore, W. B., S. P. Sander, C. J. Howard, A. R. Ravishankara, D. M. Golden, C. E. Kolb, R. F. Hampson, M. J. Kurylo, and M. J. Molina, *Chemical Kinetics and Photochemical Data for Use in Stratospheric Modeling*, JPL Publication 97-4, Jet Propulsion Laboratory, Pasadena, CA, 1997.
- Finkbeiner, M., J. N. Crowley, O. Horie, R. Müller, G. K. Moortgat, and P. J. Crutzen, Reaction between HO₂ and ClO: Product formation between 210 and 300 K, *J. Phys. Chem.*, 99, 16264, 1995.
- Leck, T. J., J. L. Cook, and J. W. Birks, Studies of reactions of importance in the stratosphere. III. Rate constant and products of the reaction between ClO and HO₂ radicals at 298 K, *J. Chem. Phys.*, 72, 2364, 1980.
- Leu, M. T., Product distribution for the reaction of HO₂ with ClO, *Geophys. Res. Lett.*, 7, 173, 1980.
- Reimann, B., and F. Kaufman, Rate constant of the reaction HO₂ + ClO → HOCl + O₂, *J. Chem. Phys.*, 69, 2925, 1978.
- Seeley, J. V., R. F. Meads, M. J. Elrod, and M. J. Molina, Temperature and pressure dependence of the rate constant for the HO₂ + NO reaction, *J. Phys. Chem.*, 100, 4026, 1996.
- Stimpfle, R. M., R. A. Perry, and C. J. Howard, Temperature dependence of the reaction of ClO and HO₂ radicals, *J. Chem. Phys.*, 71, 5183, 1979.
- Wennberg, P. O., R. C. Cohen, R. M. Stimpfle, J. P. Koplów, J. G. Anderson, R. J. Salawitch, D. W. Fahey, E. L. Woodbridge, E. R. Keim, R. S. Gao, C. R. Webster, R. D. May, D. W. Toohey, L. M. Avallone, M. H. Proffitt, M. Loewenstein, J. R. Podolske, K. R. Chan, and S. C. Wofsy, Removal of stratospheric O₃ by radicals: In situ measurements of OH, HO₂, NO, NO₂, ClO and BrO, *Science*, 266, 398, 1994.

Chapter 6: Conclusions and Future Directions

This thesis has presented experimental kinetics studies of several important gas phase halogen reactions involved in stratospheric ozone depletion. These experiments have demonstrated the ability of the turbulent flow tube technique (TF) to measure rate constants of radical-radical reactions under pressure and temperature conditions characteristic of the stratosphere. Furthermore, chemical ionization mass spectrometry (CIMS) has been used to detect many of the reactants, products and precursors in these experiments with high sensitivity. This high sensitivity was especially important in the branching ratio measurements for the OH + ClO reaction. In these experiments, HCl production from the minor channel of the OH + ClO reaction was positively identified for the first time. The results of these branching ratio experiments have helped to resolve a long-standing discrepancy between measured and modeled chlorine partitioning in the upper stratosphere. This study has clearly demonstrated the advantages of the TF-CIMS technique for measuring very small branching ratios. Overall, our measurements of the rate constants for the HO₂ + BrO, OH + ClO and HO₂ + ClO reactions should help to improve models of stratospheric ozone by placing more stringent constraints on the partitioning of bromine and chlorine in the stratosphere.

The TF-CIMS technique is suitable to study a wide range of reactions, and there are many other important reactions that have not been investigated under atmospheric conditions. The O + HO₂ and OH + HO₂ reactions are believed to play an important role in the partitioning of HO_x in the stratosphere. Uncertainties in the rate constants of these reactions are a significant source of error in current models of the upper stratosphere, and therefore these reactions are strong candidates for future work. Hopefully, the studies presented in this thesis have contributed to a better understanding of complex-mode radical-radical reactions, as well as a better understanding of the homogeneous mechanisms of stratospheric ozone depletion.